INFN – Istituto Nazionale di Fisica Nucleare
Sezione di Roma 2

INFN/AE–97/53
10 Ottobre 1997

WIZARD Collaboration

Papers presented at the XXIV International Cosmic Ray Conference July 30 – August 6, Durban, South Africa

CONTENTS

SH 4.5.1

THE TELESCOPE NINA TO INVESTIGATE NUCLEAR FLUXES IN THE NEAR-EARTH SPACE

A. Vacchi[1] on behalf of the WiZard-RIM1 collaboration
[1] *Dept. of Physics, Univ. of Trieste and INFN, Italy*

ABSTRACT
The mission NINA is conceived to make extensive studies of the Anomalous Component and the isotopic composition of the Cosmic Rays from H to Fe, in the energy range 10-100 MeV/nuc. NINA, briefly described in this article, is a silicon detector going to fly on the Russian Resource 01 n.4 satellite, by the end of 1997.

INTRODUCTION

In the frame of primary cosmic ray investigations, the Italian National Institute of Nuclear Physics (INFN) and the Moscow Engineering Physics Institute (MEPhI) are developing a program of observations with detectors on board of satellites, named WiZard-RIM.
First step of the WiZard-RIM program is the development of the small-size silicon telescope NINA (WiZard-RIM1) able to detect cosmic ray nuclei, from H to Fe, between 10 and 100 MeV/n. The experiment will be carried out on board of the Russian satellite Resource-01, to be launched on a 98° inclination orbit by the end of 1997 and flying at 835 km of altitude.
The technology adopted for the mission is a development of the silicon calorimeter corrently used in various WiZard balloon flights with the New Mexico Balloon Facility (Golden 1990, Aversa 1995, Bocciolini 1996, "The WiZard collaboration", this conference).

SCIENTIFIC TASKS

A very attractive problem still open in astrophysics is the determination of the isotopic composition of ACR's, SCR's and GCR's, as well as of their energetic, temporal and spatial distributions.
Anomalous Cosmic Rays were discovered at the beginning of 1970 observing energetic spectra of GCR nuclei (Webber, 1975); for energies lower than 50 MeV/n, in fact, the registered abundances of several nuclei (He, O, N, Ne) turned out to be higher than the expected.
ACR's are nowadays identified as singly-charged interplanetary nuclei originated from interstellar neutral particles swept into the heliosphere, ionized by solar UV rays or charge exchange with the solar wind, convected into the outer heliosphere and finally accelerated.
ACR nuclei were afterwards discovered in the near-Earth space (Dutta, 1991, Adams, 1991, Bobrovskaia, 1993, Cummings, 1993); it was shown, in particular, that those trapped by the Earth's geomagnetic field form radiation belts.
Starting from July 1992, and still in progress, a full-scale study of the nuclear component of Cosmic Rays from H to Ni, in a wide energy range, has being carried out by SAMPEX satellite (Baker, 1993). Despite the large number of experiments dealing with ACR's realized so far, anyway, a detailed study of their physical processes is still limited by the absence of a complete and statistically reliable set of experimental data, in different periods of the solar activity cycle. The problem of nuclear production, propagation and penetration into the Earth's

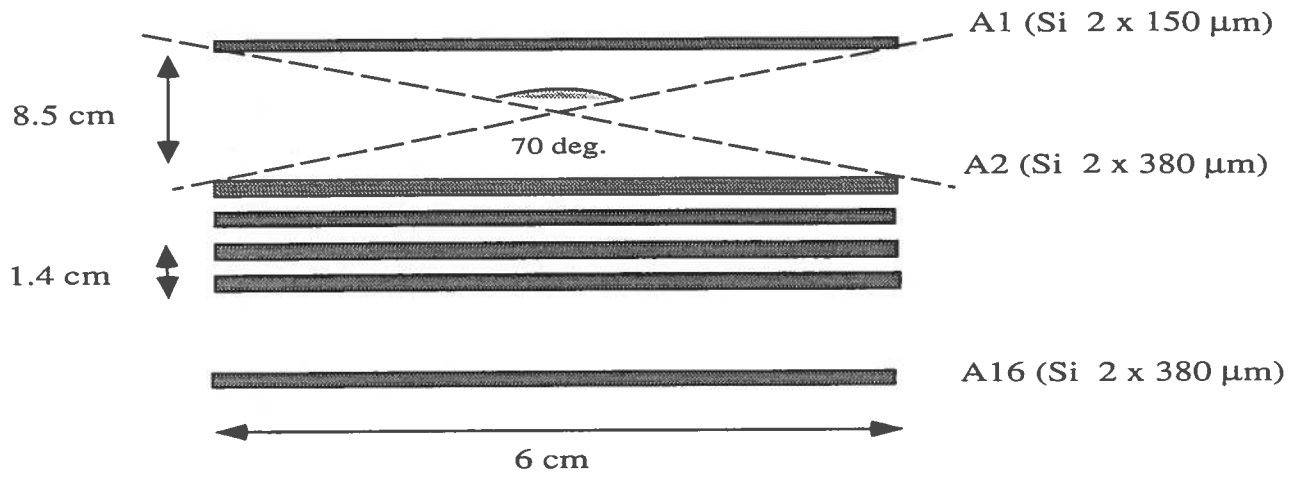

Figure 1: Geometric configuration of Nina detector. A1...A16 are the silicon planes, with orthogonal strips.

conditions they can strongly depend on the intensity and type flare and therefore can change from flare to flare as well as during a single event. As an example, the ratio between proton and helium fluxes for energies greater than 20 MeV/n can vary from 1 till 300. Another peculiarity of some solar flares is a heavy element enrichment (Iron group) in relation to the composition of the solar atmosphere as well as a changing in the $^3He/^4He$ ratio from 10^{-2} up to 1-8.
In order to clarify the physical processes related to flares, it is necessary to carry out more detailed investigations of the charge and isotopic composition of SCR's.
Finally, a detailed study of the nuclear and isotopic composition of *Galactic Cosmic Rays*, as well as of their dynamics, is always of great interest in astrophysics, due to the variations of GCR's fluxes with the solar activity.
Long-term and continuos observations of GCR's and SCR's will allow us to find out which effects, in the temporal and energetic particle flux parameters, are definitely connected to the heliosphere modulation induced by the solar activity.

THE INSTRUMENT NINA

The telescope NINA consists of four parts: the *detector* $D1$, located on a lateral side of the spacecraft service module, the *on board processors* for data handling $D2$, the *computer interface* with the satellite E and finally the *power supply* P, these all placed in the lower part of the spacecraft. Mass and electric power for all the telescope parts are respectively 40 kg and 40 W. The interaction between the Ground Station and NINA during the flight is driven by 22 telecommands. Some are dedicated to operations like power switching ON/OFF, data transferring, memory cleaning; others act on the trigger logic or on the storage model, having therefore a direct effect on the data collection.

The Silicon detector

The active part $D1$ of NINA instrument is composed by a 16 silicon planes telescope. Each sensitive element consists of two n-type silicon detectors, 60×60 mm^2, attached to a supporting ceramic frame leaving only Silicon on the particle path. The 16 strips of the two views are ortogonal in order to measure x,y coordinates of the detected particle. The thickness of the

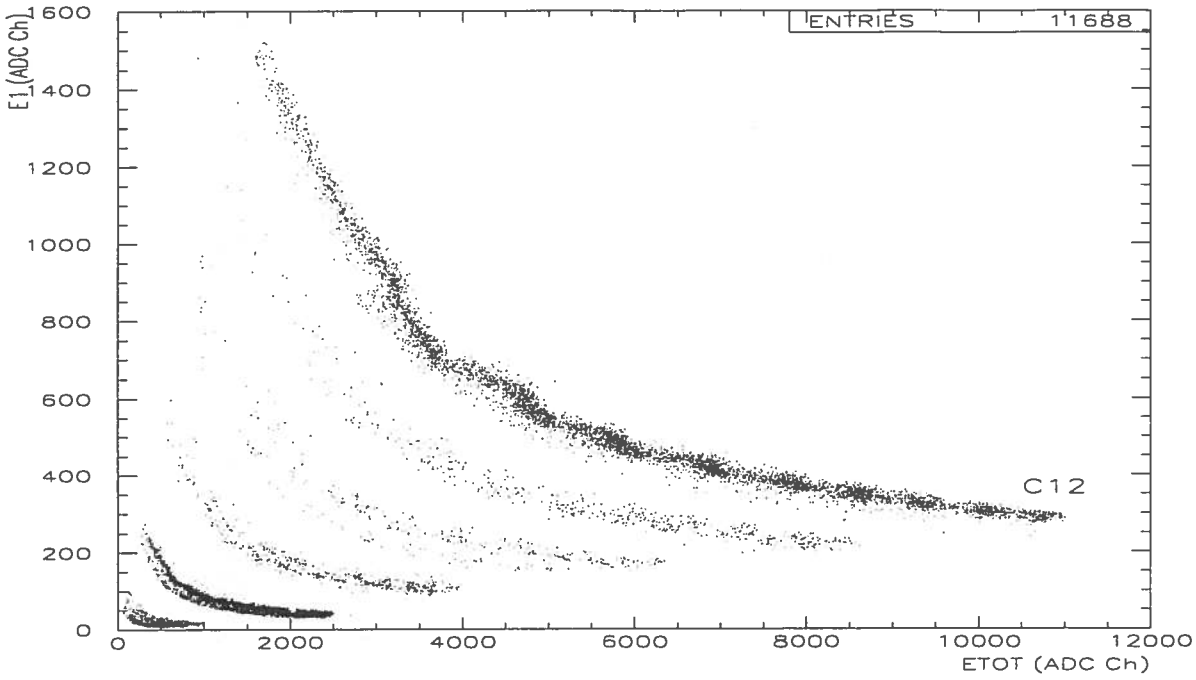

Figure 2: E_1 vs. E_{tot} for several nuclei in NINA obtained by ^{12}C fragmentation (data taken on a beam test at GSI).

by 8.5 cm, for a better measurement of the particle incident angle. NINA geometrical factor, therefore, is 8.3 cm^2sr for particles stopping in the second plane, and decreases till 1 cm^2sr for longer tracks. Finally, the detector is covered by 300 μm of Aluminum.

Trigger logic

The veto system, rejecting particles not stopping inside the calorimeter, is performed setting in anticoincidence the strips 1 and 16 of the planes from 2 up to 15 (lateral AC), and all the plane 16 strips (bottom AC). The basic operating trigger of the acquisition system (TRG1) asks therefore the particle not to hit the lateral and bottom anticoincidence strips, having at the same time released a detectable signal in the first 3 silicon detectors, i.e. a signal over threshold but below the saturation limit of the ADC.

In particular data taking configurations, or in case of failure of the first plane, it is possible to switch, via telecommand, to a second trigger logic (TRG2) which asks instead a signal in the second and third planes of the detector. In case of hardware malfunctioning of the lateral AC, it can be removed from the trigger via a dedicated ground command. Finally, to study particles crossing the whole telescope it is possible to exclude the bottom veto, again via telecommand. The default threshold for the trigger is set at 250 KeV to eliminate all relativistic particles. A 10 times higher threshold, in order to select Z>1 nuclei, has also been foreseen.

Acquisition modes

The particle rate changes very fast along the orbit so that the operation mode has to be adapted to the local conditions. In automatic operation, 3 data acquisition and storage modes

$D2$ calculates the total energy released in the first plane (E_1) and in the whole detector (E_{tot}) by the crossing particle and transmits only such information (E_1 - E_{tot} *mode*).
3. Rate meter rate (above 100 Hz). If the trigger rate rises above 100 Hz, only the counting rates of certain planes, chosen at different depths of the telescope, are stored (*rate-meter mode*).

NINA PERFORMANCES
Nina energy window for the most aboundant chemical elements is reported in Table 1. Last two columns present the acceptable energy limit in MeV/n.

Table 1

Particle	Z	A	E_{min} (MeV/n)	E_{max} (MeV/n)
H	1	1	10.0	48.0
He	2	4	9.25	47.2
B	5	10	16.0	79.0
C	6	12	17.5	87.5
N	7	14	18.6	95.0
O	8	16	20.0	103.1
Ca	20	40	38.5	174.5
Fe	26	56	58.2	194.6

NINA has been tested at the Cyclotron of the PSI Laboratory at Villigen (Zurich) in 1996 and at the SIS Synchrotron of the GSI Laboratory at Darmstadt in 1997.
At GSI Laboratory, tests of the detector in its final space configuration, using therefore all the devices to be finally installed on the Resource satellite, have been made. A ^{12}C beam at energies of 65, 80, 100 and 300 MeV/n was available for the measurements. Some results on NINA isotopic discrimination, from GSI data, are shown in Figure 2 and reported elsewhere (cfr. R. Sparvoli, this conference).

CONCLUSIONS
The NINA silicon telescope, developed for deepening our knowledge on the solar and galactic compositions of CR's between 10-100 MeV/n, has been already constructed and calibrated and will be integrated on the Russian Resource satellite in July 1997.
The window launch from the space base of Baikonour in Kazakistan is fixed for the period September-November 1997.

REFERENCES
Adams, J. H., et al., Proc. 22nd Int. Cosmic Ray Conference, Dublin, 3, 358 (1991).
Aversa, F., et al., NIM, A360, 17 (1995).
Baker, D. N., et al., IEEE Transactions on geoscience and remote sensing, 31, 3, 531 (1993).
Blake, J. B., STEP, 2, 8, 1 (1992).
Bobrovskaya, V. V. , et al., Proc. 23rd Int. Cosmic Ray Conference, Calgary, 3, 432 (1993).
Bocciolini, M., et al., NIM, A370, 403 (1996).
Cummings, J. R., et al., Proc. 23rd Int. Cosmic Ray Conference, Calgary, 3, 428 (1993).
Dutta, A., and Goswami, J. N., Proc. 22nd Int. Cosmic Ray Conference, Dublin, 3, 385 (1991).

SH 4.5.3

ISOTOPE DISCRIMINATION WITH THE EXPERIMENT NINA

R. Sparvoli[1] on behalf of the WiZard-RIM1 collaboration
[1] *Dept. of Physics, Univ. of Rome "Tor Vergata" and INFN, Italy*

ABSTRACT

NINA is a detector going to fly on the Russian Resource-01 satellite by the end of 1997. By means of the signal released in its silicon strips, the telescope is able to perform nuclear and isotope discrimination, from H to Fe, in the energy range 10-100 MeV/n.
In this article we present some theoretical and experimental results on NINA mass recognition.

INTRODUCTION

First step of the WiZard-RIM program, proposed by an Italian (INFN) - Russian (MePhI) collaboration and aiming to make observations with satellite-borne detectors, is the development of the small-size silicon telescope NINA (RIM-1). NINA will be sensitive to cosmic ray nuclei between 10 and 100 MeV/n; the experiment will be carried out on board of the satellite Resource-01 n.4, developed by the Russian Space Company VNIIEM, to be launched on a polar orbit by the end of 1997 and to take data for three years.

NINA will give the possibility to deepen our knowledge on the Anomalous Cosmic Rays (ACR's), on the Solar Cosmic Rays (SCR's) and on the Galactic Cosmic Rays (GCR's), in the new 23rd cycle of the solar activity. Further details about NINA scientific program can be found elsewhere (cfr. A. Vacchi, this conference).

THE ACTIVE DETECTOR

The active part of the telescope NINA is made by an imaging calorimeter, development of the one used in the balloon activity the WiZard collaboration carries out since 1989 to investigate the antimatter cosmic radiation (Golden, 1990, Aversa, 1995, Bocciolini, 1996, "The WiZard collaboration", this conference). Each sensitive element consists of two n-type silicon detectors, 60×60 mm^2; the 16 strips of each of the two views are orthogonal in order to measure both the energy and the coordinates of the detected particle. The thickness of each wafer is 380 μm apart from the two on the first plane which are 150 μm thick in order to lower the energetic acceptance window (cfr. again A. Vacchi, this conference).

16 of these sensitive silicon elements are arranged in the detector set-up; interplanar distance is 1.4 cm; only planes 1 and 2 are separated by 8.5 cm, resulting in a total telescope height of 29.5 cm. Each silicon plane is read by a double 16 channel preamplifier; the signal coming from every strip is shaped by a unipolar $CR - RC * RC$ filter before entering an ADC.

An aluminum cover of just 300 μm is placed on top of the detector. Finally, lateral and plane 16 strips work as a veto system for NINA, ensuring the particles stop inside.

SIMULATED PERFORMANCES

Nina response to incoming particles has been studied with MC simulations (Geant 3.21)

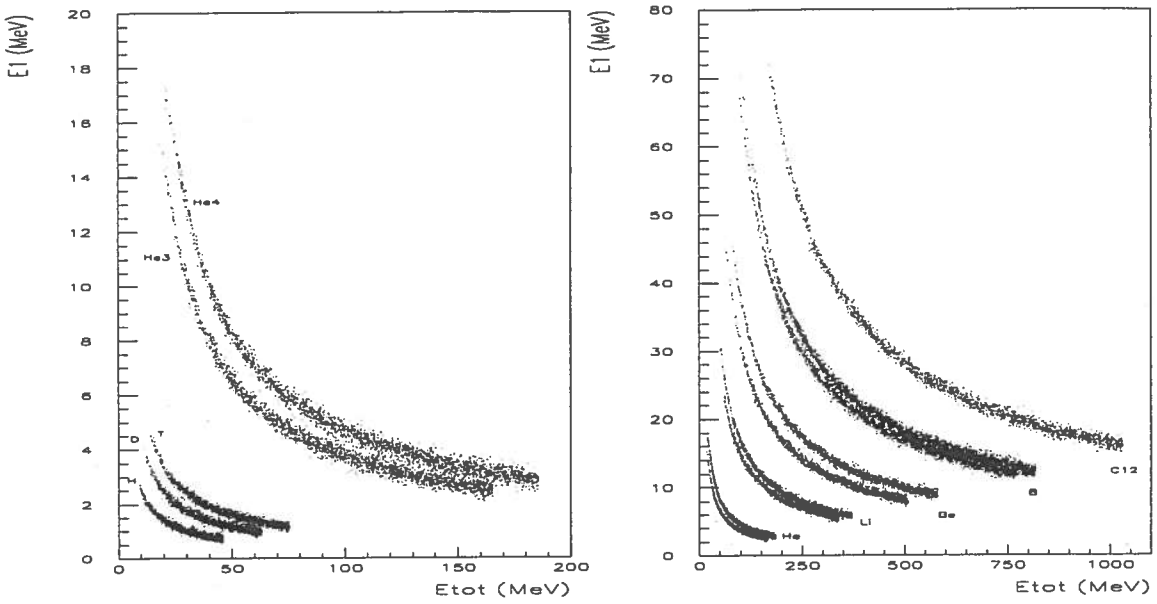

Figure 1: E_1 vs. E_{tot} for several nuclei in NINA (MC simulations); energies are in MeV. Left: H, D, T, ^{3}He, ^{4}He. Right: He, Li, Be, B, ^{12}C.

guaranteeing the full containment of the particle. For low Z ions, nuclear as well as isotope discrimination is successfully performed.

For heavy particles, instead, releasing energy deposits exceeding 280 MeV, the ADC saturation phenomenon starts to occur, making mass discrimination more difficult with this technique; therefore, other algorithms that make use of the information coming from all Si detectors (Hasebe, 1993), to improve NINA recognition, have been developed. Among them, quite suitable for NINA set-up is the χ^2 minimization analysis. This is performed between the real Bragg curve, obtained by the partial energy deposits in the 32 Si layers, and the expected ones, derived by MC or beam test data, corresponding to different isotopes. The Z and A minimising the χ^2 will identify the real particle. Results from ^{3}He/^{4}He discrimination obtained with this technique are shown in Figure 2.

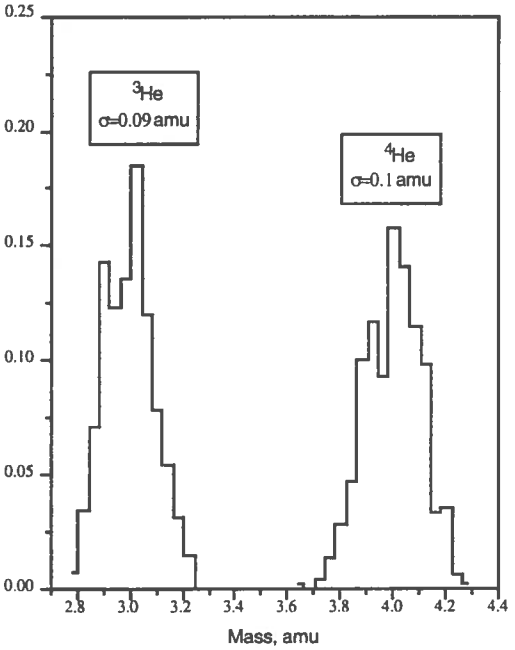

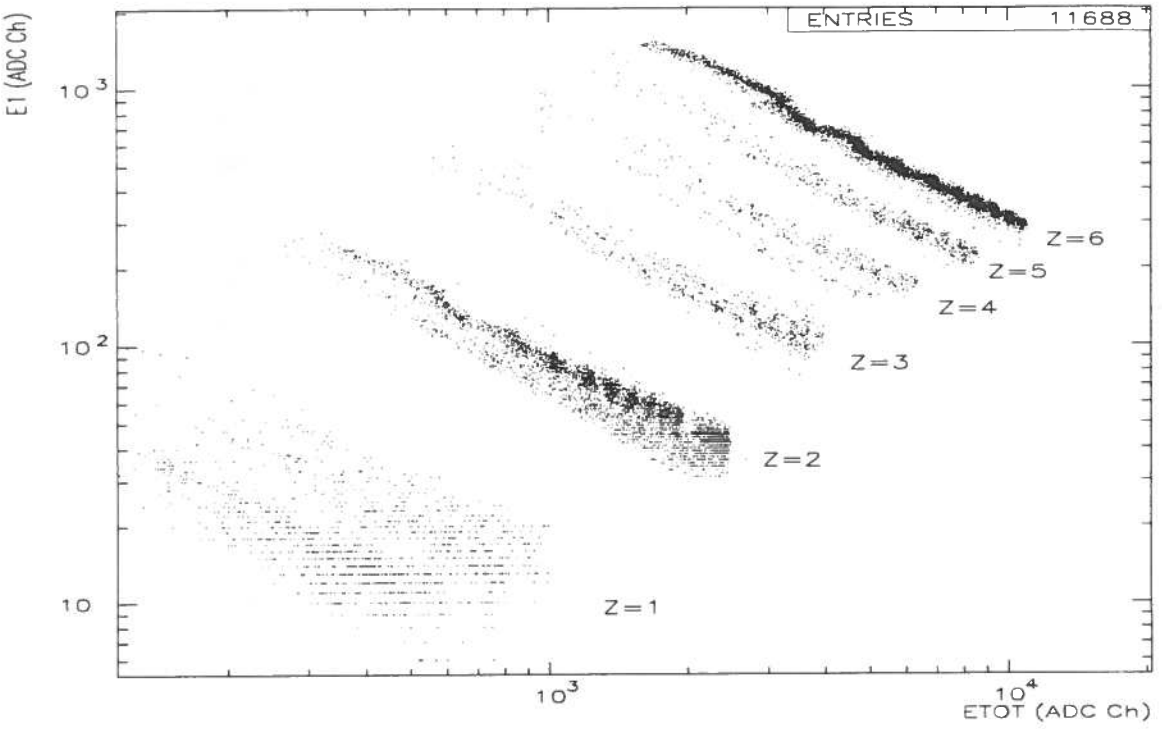

Figure 3: E_1 vs E_{tot} for real data at GSI (April-May 1997); energies are in ADC channels. Products from ^{12}C (Z=6) fragmentation are visible.

The best Mass reconstruction, anyway, can be achieved in NINA by means of the following relation (Baker, 1993), relating the mass of the particle M to its charge Z, to the total energy E it releases in the detector and to the portion ΔE deposited in the pathlength Δx:

$$M = \left(\frac{a(E^b - (E - \Delta E)^b)}{Z^2 \Delta x} \right)^{\frac{1}{b-1}} \qquad (1)$$

where a is a constant depending on the medium and b in this energy range has a value between 1.5 and 1.8. To obtain precise values for these constants, power low fits of the Range of the particle as a function of the total energy released, with simulated as well as real data, can be made.

Eq. 1 depends on the chosen pathlenght Δx, which corresponds, in NINA detector, to a certain number of crossed Si views. It has been seen that the RMS values of the reconstructed masses decrease increasing the number of views taken to compute Δx and so ΔE.

Results on simulated data by means of Eq. 1, performed in the whole particle NINA

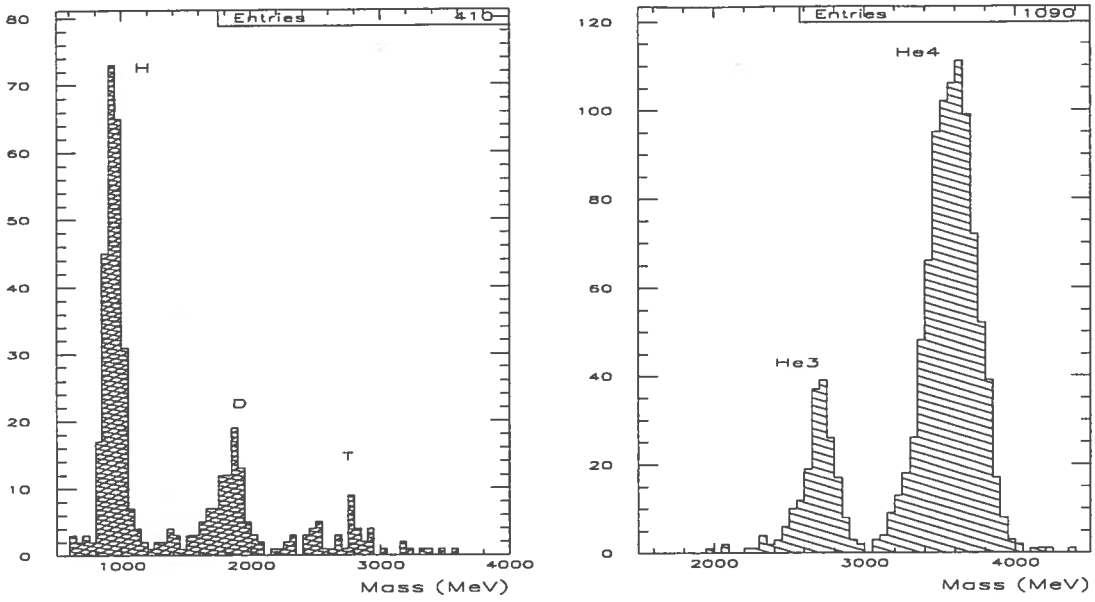

Figure 4: Mass reconstruction with Eq. 1 for real data at GSI (April-May 1997). Masses are in MeV. Left: H, D, T; Right: ^3He, ^4He.

At PSI 120 MeV alphas, 60 MeV deuterons, 50 and 71 MeV protons have been used to test the telescope performances and measure the trigger and the anticoincidence efficiencies. At GSI, instaed, a ^{12}C beam at energies of 65, 80, 100 and 300 MeV/n was available, to test NINA in its final space configuration, using therefore all the devices to be finally installed on the Resource satellite.

Data at GSI have been taken in different conditions. Direct ^{12}C runs have been used for energy calibration; others, by interposing a poliethylene target between the detector and the beam, to favour fragmentation products and so test NINA discrimination capability, have also been performed.

Some significant results obtained with GSI data are reported in Figures 3 and 4. In figure 3 it is shown that the E_1 vs E_{tot} technique is quite an effective means to determine the nuclear charge of the particles; energies are expressed in ADC channels, each channel corresponding to 74 keV. In Figure 4, instead, a good mass reconstruction (MeV) by Eq. 1 for Z=1 and Z=2 nuclei is presented. Nuclei in both graphs derive from fragmentation of a 300 MeV/n ^{12}C beam.

CONCLUSIONS

Some characteristics of the experiment NINA have been described, expecially those related to the silicon detector, its active core, and the way the information is handled.

NINA's physical observations will deepen our knowledge on the cosmic ray composition of both solar and galactic origins, thank to its good nuclear and isotope discrimination capability briefly shown in this article.

REFERENCES

SH 6.3.2

ELFO: EXPERIMENT FOR LIGHT FLASH OBSERVATION IN SPACE

The ELFO Collaboration (presented by S. Bartalucci)

ABSTRACT

We present the scientific case for a thorough investigation of the phenomenon of Light Flashes observed by astronauts since early lunar missions. A complete assessment of the phenomenon is achieved through a sophisticated, helmet-shaped silicon detector, which is able to identify high-Z energetic particles and measure their energy and trajectory.

In addition, a study of precise time correlation between cosmic ray impinging on the head of the astronaut and function of the Central Nervous System is addressed via investigation of the concurrent spontaneous bioelectrical cortical activity in the cortex and of retinal and cortical responses at luminance and contrast stimuli.

The silicon detector will also give information for a more accurate biological dosimetry by the knowledge of the relative fluences of the different particles: a contribution for a deeper understanding of the physiological modifications during long manned missions.

THE SCIENTIFIC CASE

The phenomenon of light flashes (LF) observed by astronauts since the early lunar missions (Apollo-11 and following) is certainly the most impressive example of radiation-induced effects on living objects in space and almost the only one detected on humans, to our knowledge. Although many attempts have been done in the past to fully assess the origin and nature of this phenomenon but a systematic, thorough investigation has never been performed. Still many questions remained to be answered, such as which particles in space cause the LFs and how frequent are they in Earth orbits (Horneck, 1992 and references therein).

Very recently, the WIZARD Collaboration has shown a renewed interest in this field.To make a systematic study over several space missions and with many subjects of LF phenomena, we first sent an active particle detector (Si-eye 1) to the MIR space station. Our main goal was to nail down which particle caused which kind of LF phenomena in space. The hardware was recovered from an old apparatus. Data have been taken on the MIR for some months and the very first results show the correlation of at least one LF event with a determined, rather low-energy proton (Galper, 1996). Of course, this hypothesis requires confirmation, so that we are presently testing an improved detector (Si-Eye 2) that will be sent to the MIR this year. The basic sensitive element of Si-Eye 2, which is similar to Si-Eye 1, and the more performant front-end and read-out systems are derived from the NINA telescope (Barbiellini, 1995). The new electronics widens the dynamical range allowing for studying high Z nuclei. It must be pointed out that a rather poor agreement exists among the various results, particulary when looking at the number of LFs. This is due to basic differences not only in the experimental methods but also in experimental conditions, like orbits, altitude, shielding, changes of the solar activity, human reactivity and so on. In particular, the present detectors do not allow for identifying correlation between LF and passage of a given particle with good statistical acceptance level.

In the following we present a synthesis of the scientific motivations for a new experiment, which will make use of a sophisticated, helmet-shaped particle silicon detector.

This device will be integrated with other systems, like whole head computerized Electroencephalography (EEG) and Visual Evoked Potentials (VEP), needed to investigate the effects of the particles on the brain and, in particular, on the visual system. These methods allow for a high time resolution discrimination of events in the bioelectrical functions in the cortex and often permit to localize the cortical site where such events occur.

The fundamental goals of our project are summarized as follows:

Furthermore, the increased number of manned space missions stresses the importance of estimating the biological risks encountered by astronauts. As they are exposed to space radiation it is necessary to measure the doses they receive.

The proposed silicon detector, which is able to identify charged particles and measure their energy, will provide additional information for more accurate dosimetry. This topic will be fully described in a sequal paper.

This experiment, named ELFO (Experiment for Light Flash Observation in Space), will be carried out on the Russian MIR or on the International Space Station ALPHA.

Physiological motivation

In spite of the observed correlation between particles flux at retinal level and reported perceptual phenomena, the neurophysiological relevance and mechanism(s) of generation of these events have not been investigated and it is unclear whether the observed perceptual events are the result of activation of physiological mechanisms of vision.

It appears a practicable hypothesis that the particle flux may, in peculiar conditions, trigger (directly or indirectly) physiological mechanisms of the visual system or, in alternative, alter its functional status (e.g. sensitivity) so to change the effect of external events (e.g. particles). Retina and visual cortex are both putative sites of action of triggering particles.

The project is aimed at identifying physiological functions/mechanisms of the visual system that are dedicated to simple feature detection.

The approach will be electrophysiological and the study will be carried out both on laboratories at sea level and on spacecraft in orbit. Among the non-invasive measurement strategies which share the ability to resolve activities within the millisecond range the ElectroEncephaloGraphy (EEG) - a measurement of the dynamics of the electric potential on the scalp generated by the underlying bioelectrical currents - is of easier implementation in space environment, features a good time resolution and offers useful insights about dynamics and source locations of cortical activity. Prior to the space implementation of more powerful and sophisticated techniques, EEG seems a good choice for a neurophysiological investigation of the mechanisms linked to LF perception, such as the potentials originating at retinal or cortical levels in response to visual stimuli (cortical visual evoked potentials, VEP; electroretinogram, ERG; retinal oscillatory potentials, OPs). We should mention here that EEG studies in space have been occasional. Furthermore most of them were designed primarily to evaluate sleep characteristics under weightless conditions (Niedermeyer, 1987), following complaints for insomnia and fatigue, presented by the crews of three of the earlier Skylab missions. Postflight analyses of these recorded EEG data revealed no abnormalities throughout the flight and postflight periods.

Spaceflight environment and radiation risks

Looking for a deeper understanding of the physiological modifications during a prolonged manned mission, we also propose the use of the our silicon detector for advanced fluence dosimetry. The combined influence of different space flight factors is indeed one of the key problems in space medicine; it is of particular interest to understand the mechanisms underlying the interaction of radiation and microgravity. Along the radiobiological chain of events, every step is affected by internal and external modifiers, thereby influencing the final radiation response.

The conventional risk assessment approach is based on the concept of dose equivalent , which assumes uniform distribution of energy through the tissue of interest, and doesn't distinguish among different particles having the same LET (Linear Energy Transfer). It is, however, definitely clear that the risk factors are related more to the fluence spectrum of each particle and a fluence-based risk assessment must be introduced. A series of measurements at various positions on the different orbits can be performed with the particle detector used for the LFs study. This is able to identify charged particles and measure their energy, and, therefore, will give a good evaluation of the relative fluence of the different particles at fixed LET.

THE BASIC FEATURES OF THE EXPERIMENT

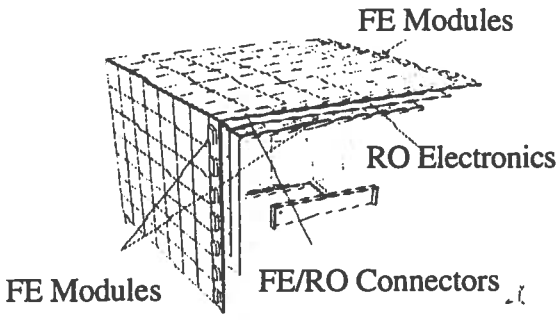

Fig. 1a A sketch of the detector

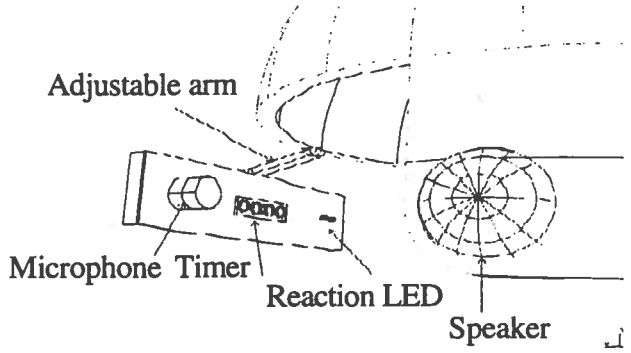

Fig. 1b The service panel

With regard to the LF responsible mechanism, there is the hypothesis that they are due to primary ionization in the retina by heavy ions. We first consider three typical abundant nuclei in the GCR component, like C-12, N-14 and O-16 and assume the sensitive part of the retina to be about 50 μm thick and the traversed human body to be equivalent to 3 g/cm^2. From relevant measurement made on accelerators we deduce that a typical LET threshold value for LF generation is between 10 and 20 KeV/μm. In our calculation, we have considered a detector consisting of 3 Silicon planes, each made of a double 380 μm thick chip as in Si-Eye. It is shown that, in order to have an energy deposition in the retina above 1 MeV for O, the energy of the particles impinging on the detector ranges from ~ 150 up to ~ 400 MeV/n, while for C and N it is quite narrower. This region corresponds to the maximum flux of Oxygen GCR, as averaged over a polar orbit.

In fig. 2 is shown the particle separation capability of three silicon plane

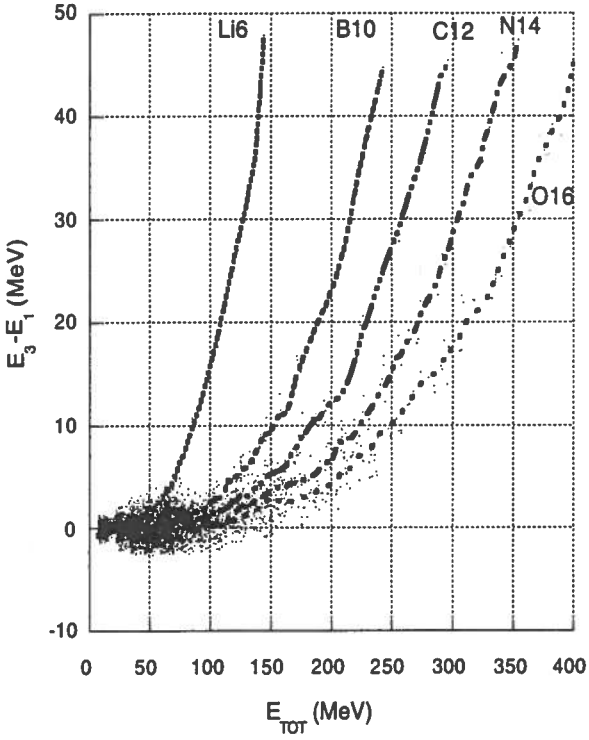

Fig. 2 Discrimination of nuclei with low incident energy

detector for five nuclei, Li6, B10, C12, N14, O16, in the energy range 0-400 MeV. Even in the region of E3-E1 ≤ 0 (corresponding to particles with high cinetic energy) it is possible to discriminate the nuclei, as shown in figure 1.4, using E_{tot} as parameter.

At present, new performant algorithms are under testing with Si-Eye 1 and accelerator data, in order to obtain a better discrimination among the different nuclei.

<u>The silicon detector</u>

The sensitive element of the particle detector is a silicon chip, 0.380 mm thick, with ion-implanted resistive strips on one side. Two such chips are glued back to back with perpendicular strips, to measure x and y coordinates of the traversing particle. The sensitive area is 60x60 mm^2 , divided in 16 strips, with 3.6 mm pitch.

The whole detector (fig.1a) consists of 3 sets of 3 stacked sensitive planes divided in

- Seven ladders of seven detectors for the planes of the external layer, six ladders of six detectors each for the intermediate layer and five ladders of five detectors for the internal layer.

-The Front End (F.E.) electronics placed at the end of the related ladder.

A dedicate space will be foreseen over one of the external planes for the Read Out electronics. A general scheme of a detector plain and read out chain is shown in figure 3.

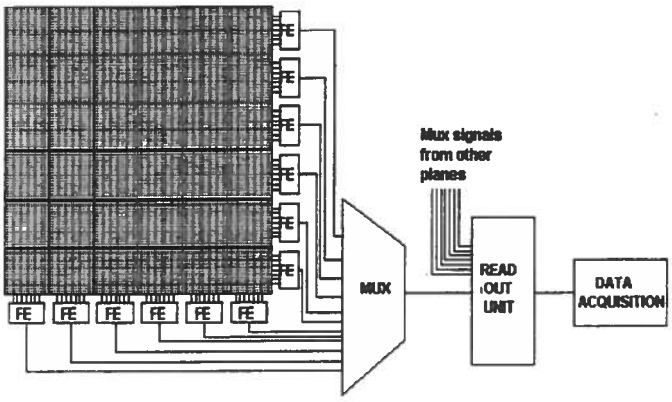

Fig. 3 General scheme of a detector plane and read out chain.

The EEG system

Non invasive measurements of the electrophysiological signals will be performed via an array of electrodes, covering the entire scalp or proper portions of the projections to scalp of the stimulated cortex, positioned in accordance with international guidelines, under the silicon whole head helmet. Additional four electrodes will be used to monitor retinal potentials.

Each electrode will be connected to a multiplexer through a filter and a low noise preamplifier. The signal will be recorded onto a storage media for off-line analysis. A computer controlled visual stimulator will deliver proper stimuli.

At sampling frequency of 1 KHz a 90 minutes experiment would require 5.4 MBytes of data for channel.

Data taking and analysis

A measurement session as a rule will last about 90 minutes, which is about one orbit. The orbit will be normally chosen such that it passed through the SAA. The astronaut wears the helmet and sits with his hands on two push-button transducers. Fifteen minutes of dark adaptation for the eyes are required, such that the subjects could confidently observe LFs.

The measurement approach will follow two parallel lines of investigation:

a. Identification of the electrophysiological concomitants of perceptual events observed while in orbit.

b. Determination by electrophysiological methods of the functional status of (retinal and cortical) visual mechanisms in baseline conditions (laboratory setting at sea level) and comparison with the functional conditions during orbital operations. The spontaneous EEG activity and the electrophysiological responses (VEP; ERG; OPs) to visual stimuli will be used for this purpose.

Data processing

The basic step in data processing consists of finding particle tracks through the detector. Then, the consecutive change of energy losses of the charged particle in the silicon plates, together with the total energy loss in all plates, allows us to characterize energy and charge of each particle. It is, therefore, feasible to reconstruct the trajectory of the particle and estimate, by using Bethe-Bloch technique, the energy left in the different points of the brain. The recorded time connects the event with the position in the orbit.

The analysis of the electrophysiological data will be treated extensively in a sequal paper.

REFERENCES

G. Barbiellini, A.G. Batischev, A.V. Bakaldin et al., *Proc.24th ICRC*, **3**, 607(1995).

OG 5.2.1

A MEASUREMENT OF THE PROTON SPECTRUM AT 1 AU NEAR SOLAR MINIMUM WITH THE CAPRICE EXPERIMENT

G. Barbiellini[12], G. Basini[4], R. Bellotti[1], M. Bocciolini[3], M. Boezio[10], U. Bravar[12], F. Cafagna[1], P. Carlson[10], M. Casolino[8], M. Castellano[1], M. Circella[1], A. Codino[7], G. De Cataldo[1], C. De Marzo[1], M.P. De Pascale[8], N. Finetti[7], T. Francke[10], N. Giglietto[1], R.L. Golden[0,6], C. Grimani[7], M. Hof[9], W. Menn[9], J.W. Mitchell[5], A. Morselli[8], J.F. Ormes[5], P. Papini[3], A. Perego[3], S. Piccardi[3], P. Picozza[8], M. Ricci[4], P. Schiavon[12], M. Simon[9], R. Sparvoli[8], P. Spillantini[3], P. Spinelli[1], S.A. Stephens[2], S.J. Stochaj[6], R.E. Streitmatter[5], M. Suffert[11], A. Vacchi[12], N. Weber[10], N. Zampa[12]

[1]*Dipartimento di Fisica dell'Università and Sezione INFN di Bari, Bari, Italy* [2]*Tata Institute of Fundamental Research, Bombay , India* [3]*Dipartimento di Fisica dell'Università and Sezione INFN di Firenze, Firenze, Italy* [4]*Laboratori Nazionali INFN, Frascati, Italy* [5]*NASA/Goddard Space Flight Center, Greenbelt, USA* [6]*New Mexico State University, Las Cruces, USA* [7]*Dipartimento di Fisica dell'Università and Sezione INFN di Perugia, Perugia, Italy* [8]*Dipartimento di Fisica dell'Università and Sezione INFN di Roma, Roma, Italy* [9]*Universität Siegen, Siegen, Germany* [10]*Royal Institute of Technology, Stockholm, Sweden* [11]*Centre des Recherches Nucléaires, Strasbourg-Cedex, France* [12]*Dipartimento di Fisica dell' Università and Sezione INFN di Trieste, Trieste, Italy*

ABSTRACT

We report on a preliminary result of the absolute proton spectrum in the energy range 0.15 to 100 GeV at the top of the atmosphere as measured by the balloon-borne experiment CAPRICE flown from Lynn Lake, Manitoba, Canada, on August 8-9, 1994. The experiment used the NMSU-WiZard/CAPRICE balloon-borne magnet spectrometer equipped with a solid radiator Ring Imaging CHerenkov (RICH) detector and a silicon-tungsten calorimeter for particle identification. More than 365 000 protons were identified in the energy range 0.15 to 100 GeV at the spectrometer. The proton spectrum is obtained with a negligible contamination below 4 GeV. Above this energy there is a small (1-2%) contamination from deuterons. The data were collected over 18 hours at a mean residual atmosphere of 3.9 g/cm^2. Observation of the proton spectrum below a few GeV without the contamination of D, e^+, μ^+ and π^+ has been made for the first time.

INTRODUCTION

Detailed measurements of the proton flux at 1 AU over a wide energy range is important to understand the production and acceleration mechanism of cosmic rays, as well as the solar modulation effect on these particles. Combining proton spectrum measurements from a number of different experiments, Gaisser and Schaefer (1992) find that the spectral index is in the range 2.65-2.75. However, they show that an uncertainty of ± 0.05 is significant and e.g. leads to a 20% spread in the predicted secondary antiproton flux between 5 and 15 GeV. There is also a large disagreement in the reported absolute proton flux values, the spread is of the order of $\pm 25\%$ at energies above 10 GeV and as much as a factor of 2 at lower energies after correcting for solar modulation effects. A detailed measurement with accurate determination of the detector efficiencies is therefore important.

DETECTOR SYSTEM

The NMSU-WiZard/CAPRICE spectrometer was flown by balloon from Lynn Lake, Manitoba, Canada (56.5° North Latitude, 101.0° West Longitude), on 8-9 August 1994 at an atmospheric pressure of 3.2

PROTON SELECTION

The analysis was based on 18 hours of data collection for a total acquisition time of 60520 seconds under an average residual atmosphere of 3.9 g/cm^2. The fractional dead time during the flight was 0.7310 ± 0.0006 resulting in a total live time of 16280 ± 36 s.

Protons are the most abundant positively charged particles in the cosmic radiation, accounting for about 98% of all single charged particles . The remaining fraction is mainly deuterons and a small fraction of positrons (Reimer et al. 1995, Barbiellini et al. 1996b). As a result, the concern in determining an absolute flux of protons is not primarily to eliminate the contamination, but to estimate reliable detector efficiencies. Strict requirements on the tracking and scintillator information resulted in a clean sample of positive unit charged particles from which the protons were selected. The requirements represent a compromise between rejection power and efficiency and are partly based on experience gained previously using the same tracking and scintillator system (Golden et al. 1991, Mitchel et al. 1996, Hof et al. 1996). The average maximum detectable rigidity of the instrument was 172 GV/c.

The separation between protons and deuterons was possible between 0.4 and 5 GV/c using the calorimeter and the RICH. The calorimeter could separate protons from deuterons between 0.4 and 2 GV/c from the dE/dx measurements in the silicon strip layers. The RICH was used to measure the Cherenkov angle of the particle and thereby its velocity, and could separate protons from deuterons between 1.2 and 5 GV/c (Weber 1997).

EFFICIENCY AND CONTAMINATION

The NMSU-WiZard/CAPRICE instrument has a unique capability to reliably determine the detector efficiencies as well as to eliminate the contamination, as it allows selection of clean particle samples using independent sets of detectors. The detector efficiencies as a function of rigidity were determined using a large proton sample from the flight data.

The instrument allows the selection of protons with a negligible contamination between 0.4 and 5 GV/c. Above 5 GV/c the instrument cannot distinguish between protons and deuterons, and the small deuteron component is included in the proton sample.

PROTON SPECTRUM AT THE TOP OF THE ATMOSPHERE

All protons interacting with the payload material above the tracking system were assumed to be rejected by the selection criteria. The data were corrected for these losses with multiplicative factors, using the expression for the interaction mean free path for the different materials in the detectors given by Stephens (1997).

For the atmospheric secondary proton production, we used the data of Papini et al. (1996). The secondary produced particles were normalized with the acceptance and live time of the experiment, and subtracted from the corrected numbers using a mean residual atmosphere of 3.9 g/cm^2. Finally, the data were corrected for losses in the atmosphere above the detector due to interactions, giving the number of protons at the top of the atmosphere. The geometrical factor at different rigidities was obtained with a Monte Carlo technique (Sullivan 1971).

The resulting preliminary proton spectrum values are is shown in Table 1 and Figure 1. The errors include both statistical and systematic uncertainties. A fit of a power law spectrum between 20 and 100 GeV results in a flux of $(1.01 \pm 0.13) \times 10^4 \times E^{-2.70 \pm 0.07}$.

CONCLUSION

The proton spectrum at solar minimum has been measured without the contamination of D, e^+, μ^+

REFERENCES

Barbiellini, G., et al., *Nucl. Instr. and Meth.*, **A371**, 169 (1996a)
Barbiellini, G., et al., *A&A*, **309**, L15 (1996b)
Bocciolini, M., et al., *Nucl. Instr. and Meth.*, **A370**, 403 (1996)
Carlson, P., et al., *Nucl. Instr. and Meth.*, **A349**, 577 (1994)
Gaisser, T. K., & Schaeffer, R. K., *ApJ*, 394, 174 (1992)
Golden, R. L., et al., *Nucl. Instr. and Meth.*, **148**, 179 (1978)
Golden, R. L., et al., *Nucl. Instr. and Meth.*, **A306**, 366 (1991)
Hof, M., et al., *Nucl. Instr. and Meth.*, **A345**, 561 (1994)
Hof, M., et al., *ApJ*, 467, L33 (1996)
Mitchell, J., et al., *Phys. Rev. Lett.*, **76**, 3057 (1996)
Papini, P., Grimani, C., & Stephens, S. A., *Il Nuovo Cimento*, **19**, 367 (1996)
Reimer, O., et al., *Proc. of XXIV ICRC, Rome*, **2**, 614 (1995)
Stephens, S. A., Astropart. Phys., 6, 229 (1997)
Sullivan, J. D., *Nucl. Instr. and Meth.*, **95**, 5 (1971)
Weber, N., "A measurement of the antiproton and proton fluxes in the cosmic rays by the CAPRICE experiment" (PhD thesis, KTH Stockholm, Sweden) (1997)

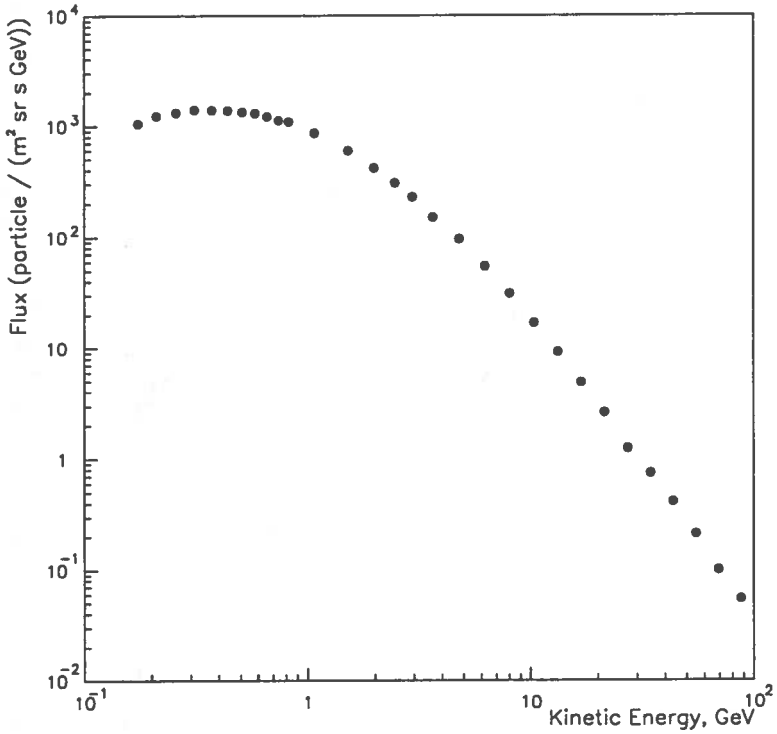

Table 1: The Proton Spectrum at the Top of the Atmosphere.

Kinetic energy (GeV)		Proton Spectrum (particles/(m^2 sr s GeV))
0.15 - 0.18	0.17	$(1.05 \pm 0.09) \cdot 10^3$
0.18 - 0.23	0.21	$(1.23 \pm 0.06) \cdot 10^3$
0.23 - 0.28	0.26	$(1.32 \pm 0.05) \cdot 10^3$
0.28 - 0.34	0.31	$(1.40 \pm 0.04) \cdot 10^3$
0.34 - 0.40	0.37	$(1.39 \pm 0.03) \cdot 10^3$
0.40 - 0.47	0.44	$(1.38 \pm 0.03) \cdot 10^3$
0.47 - 0.54	0.51	$(1.34 \pm 0.03) \cdot 10^3$
0.54 - 0.62	0.58	$(1.29 \pm 0.03) \cdot 10^3$
0.62 - 0.70	0.66	$(1.21 \pm 0.03) \cdot 10^3$
0.70 - 0.78	0.74	$(1.12 \pm 0.03) \cdot 10^3$
0.78 - 0.86	0.82	$(1.09 \pm 0.03) \cdot 10^3$
0.86 - 1.30	1.07	$(8.58 \pm 0.18) \cdot 10^2$
1.3 - 1.8	1.5	$(5.95 \pm 0.14) \cdot 10^2$
1.8 - 2.2	2.0	$(4.18 \pm 0.12) \cdot 10^2$
2.2 - 2.7	2.5	$(3.08 \pm 0.07) \cdot 10^2$
2.7 - 3.2	2.9	$(2.29 \pm 0.06) \cdot 10^2$
3.2 - 4.2	3.6	$(1.51 \pm 0.04) \cdot 10^2$
4.2 - 5.5	4.8	$(9.65 \pm 0.17) \cdot 10^1$
5.5 - 7.1	6.2	$(5.51 \pm 0.10) \cdot 10^1$
7.1 - 9.2	8.1	$(3.11 \pm 0.06) \cdot 10^1$
9.2 - 11.8	10.3	$(1.70 \pm 0.04) \cdot 10^1$
11.8 - 15.0	13.2	$(9.29 \pm 0.21) \cdot 10^0$
15.0 - 19.1	16.8	$(4.92 \pm 0.12) \cdot 10^0$
19.1 - 24.2	21.4	$(2.65 \pm 0.07) \cdot 10^0$
24.2 - 30.7	27.1	$(1.25 \pm 0.04) \cdot 10^0$
30.7 - 38.9	34.4	$(7.52 \pm 0.27) \cdot 10^{-1}$
38.9 - 49.1	43.5	$(4.18 \pm 0.17) \cdot 10^{-1}$
49.1 - 62.0	54.9	$(2.12 \pm 0.11) \cdot 10^{-1}$
62.0 - 78.2	69.3	$(1.00 \pm 0.06) \cdot 10^{-1}$
78.2 - 99.1	87.5	$(5.46 \pm 0.41) \cdot 10^{-2}$

Durban 1997 XXV ICRC OG 5.2.4, Vol.3

THE $^3He/^4He$ RATIO WITH THE CAPRICE APPARATUS

G. Barbiellini[12], G. Basini[4], R. Bellotti[1], M. Bocciolini[3], M. Boezio[10], U. Bravar[12], F. Cafagna[1], P. Carlson[10], M. Casolino[8], M. Castellano[1], M. Circella[1], A. Codino[7], G. De Cataldo[1], C. De Marzo[1], M.P. De Pascale[8], N. Finetti[7], T. Franke[10], N. Giglietto[1], R.L. Golden[0,6], C. Grimani[7], M. Hof[9], W. Menn[9], J.W. Mitchell[5], A. Morselli[8], J.F. Ormes[5], P. Papini[3], A. Perego[3], S. Piccardi[3], P. Picozza[8], M. Ricci[4], P. Schiavon[12], M. Simon[9], R. Sparvoli[8], P. Spillantini[3], P. Spinelli[1], S.A. Stephens[2], S.J. Stochaj[6], R.E. Streitmatter[5], M. Suffert[11], A. Vacchi[12], N. Weber[10], N. Zampa[12]

[0] *Deceased*

[1] *Dipartimento di Fisica dell'Università and Sezione INFN di Bari, Bari, Italy,* [2] *Tata Institute of Fundamental Research, Bombay, India,* [3] *Dipartimento di Fisica dell'Università and Sezione INFN di Firenze, Firenze, Italy,* [4] *Laboratori Nazionali INFN, Frascati, Italy,* [5] *NASA/Goddard Space Flight Center, Greenbelt, Maryland, USA,* [6] *New Mexico State University, Las Cruces, New Mexico, USA,* [7] *Dipartimento di Fisica dell'Università and Sezione INFN di Perugia, Perugia, Italy,* [8] *Dipartimento di Fisica dell'Università and Sezione INFN di Roma Tor Vergata, Roma, Italy,* [9] *Universitat Siegen, Siegen, Germany,* [10] *Royal Institute of Technology, Stockholm, Sweden,* [11] *Centre de Recherches Nucleaires, Strasbourg, France,* [12] *Dipartimento di Fisica dell'Università and Sezione INFN di Trieste, Trieste, Italy*

ABSTRACT

We report on the performance of the CAPRICE apparatus in the determination of both ^3He and ^4He fluxes. The combination of different detectors of CAPRICE makes it possible to have different independent selections for the helium isotopes. This allows a very clean separation of ^3He and a precise determination of the selection efficiencies. The method of analysis is described here and some preliminary results will be presented at the ICRC.

THE CAPRICE APPARATUS

The flight took place on 8-9 August 1994 from Lynn Lake, Canada (Lat. 56.5° N, Long. 101.0° W) with a low geomagnetic cutoff of about 0.4 GV/c. The data were collected during the float over 23 h at a mean altitude corresponding to 3.9 g/cm^2 of residual atmosphere.

The CAPRICE apparatus consists of a solid radiator Ring Imaging Cherenkov (RICH) (Carlson et al. 1994, Barbiellini et al. 1996), a time-of-flight (TOF) scintillator system, a silicon-tungsten electromagnetic calorimeter (Bocciolini et al. 1996), and a superconducting magnet spectrometer (Golden et al. 1991, Hof et al. 1994) with 8 multiwire proportional chambers (MWPC) and two sets of drift chambers (DC).

Four 1×25×50 cm Bicron scintillator paddles are arranged in two planes located above and below the chamber stack of the magnet spectrometer (respectively top and bottom scintillators), each paddle being observed by two photomultipliers; a coincidence between the two planes triggers the data acquisition. The TOF system allows 4 (2 independent) dE/dx measurements for absolute charge determination and a time-of-flight measurement with a resolution of about 280 ps over a distance of about 1.1 m.

The solid radiator RICH is composed of a 10 mm thick NaF crystal, a drift volume for the Cherenkov light and a photosensitive chamber (a MWPC with a pad plane having 4096 pads, each of size of 8 × 8 mm^2). This chamber, filled with a mixture of ethane and TMAE, allows

The calorimeter consists of 8 layers of double sided silicon strip detectors, interleaved by 7 tungsten layers for a total of 7 radiation length and about 0.3 nuclear interaction length. Each strip is 0.36 cm wide, and each silicon plane gives 128 readouts per side for the energy loss in the strips. This calorimeter allows the reconstruction of the particle interaction topology and a measurement of the energy losses.

The spectrometer consists of a single coil of superconducting magnet that operates with 120A current, which produce a field of about 0.1-2 T in the region of the chambers. The MWPC and DC chambers provide 19 measurements in the direction of maximum bending and 12 in the perpendicular one. The average maximum detectable rigidity of the spectrometer is around 170 GV/c.

SELECTION METHODS

The dE/dx measurement of the TOF system allows a clean separation of particles of charge $Z = 1$ and $Z = 2$ over the whole rigidity range. The efficiency of this selection as a function of the rigidity can easily be computed from an independent selection using the calorimeter silicon strip dE/dx measurement.

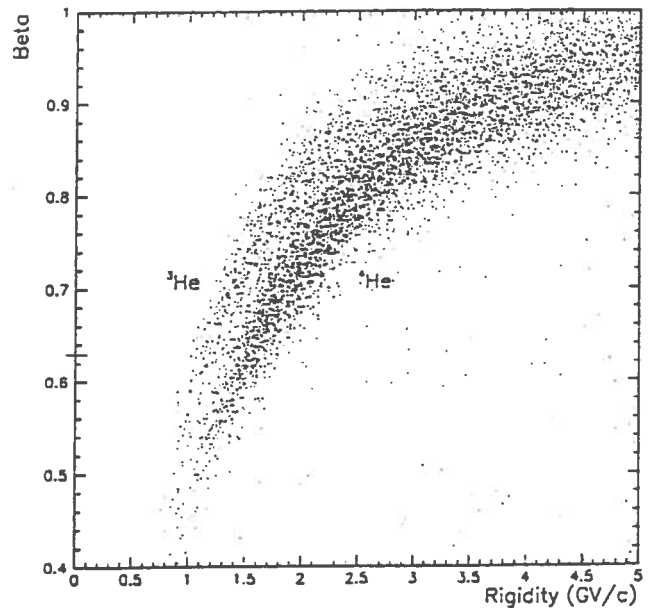

Fig. 1: Distribution of β measured by TOF for $Z = 2$ particles.

The spectrometer is used to measure the rigidity of the particles. Using standard cuts this spectrometer provides a reliable measurement of the rigidity as well as rejection of particles interacting inside the apparatus. Since the CAPRICE spectrometer can be split into two parts of absolutely independent detectors (MWPC and DC) each one of them can be used for particle selection and to determine the efficiency of the other.

In the rigidity range between 1 and 2 GV/c the β measured by the TOF can be used to

between 1 and 2 GV/c (see fig 2). Because of the low efficiency and of the difficulty in correcting for the interaction in the calorimeter this method is not used in this analysis. However this sample of particles can be used to determine the efficiency for the other selection criteria.

The Cherenkov angle measured by the RICH allows the best separation between the helium isotopes (see fig. 3). Using the Cherenkov angle the ^{3}He can be selected from 1.5 GV/c to 4 GV/c and the ^{4}He can selected from 2.0 GV/c up to at least 4 GV/c.

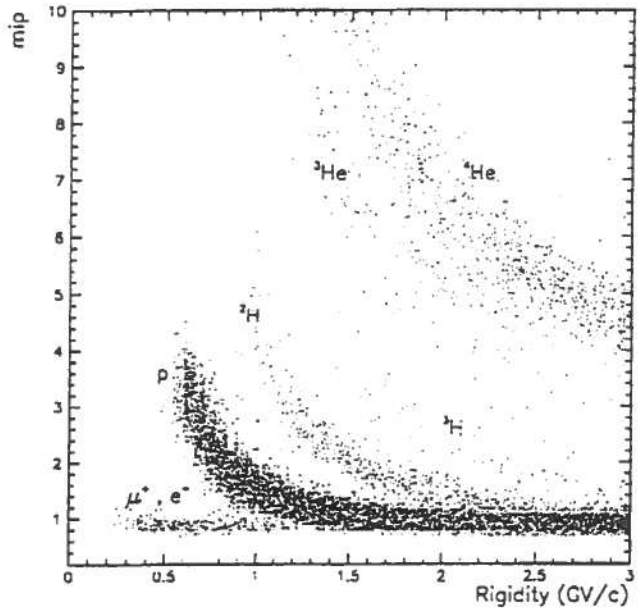

Fig. 2: Distribution of dE/dx measured by the calorimeter for crossing particles.

The efficiency of the RICH is mainly dependent on the β of the particle so we can compute this efficiency with a sample of protons selected by the calorimeter and obtain the efficiency for both He^3 and He^4 by rescaling to the same beta. Due to multiple scattering, the RICH efficiency depends also on the particle momentum at the low rigidities, below about 2 GV/c. In this region the efficiency of the RICH can be determined from the samples selected by the calorimeter and TOF.

The combination of all the above detector information allows a clean selection of both ^{3}He and ^{4}He starting from 1 GV/c up to 4 GV/c. The CAPRICE unique capability to use different sets of detectors to select particle samples, allows a very reliable determination of the detector efficiencies using the data itself.

PAYLOAD AND ATMOSPHERIC CORRECTIONS

A clear selection of ^{3}He with well determined efficiencies is not enough to obtain the primary flux, and two further steps are required. The measured flux at the spectrometer needs to be corrected for the loss due to interaction and for the gain from ^{4}He stripping in the material above the spectrometer, and extrapolated to the top of the payload taking in to account the ionization

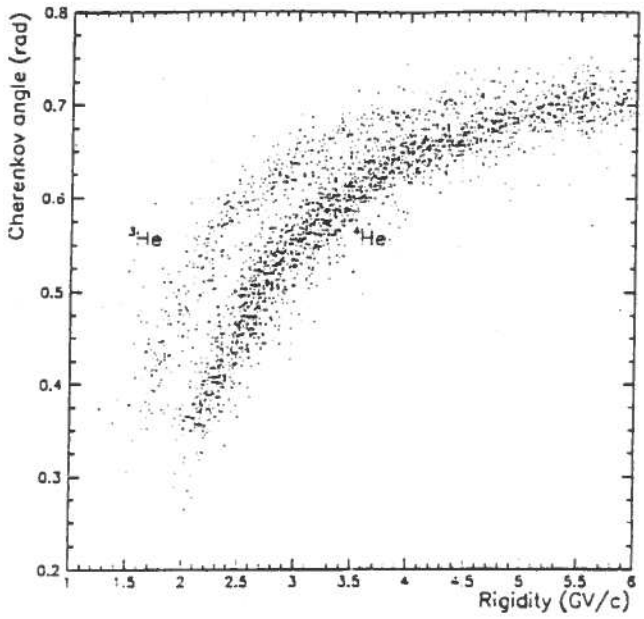

Fig. 3: Distribution of Cherenkov angle measured by the RICH for $Z = 2$ particles.

Estimating these corrections is not easy as one requires the fraction of ^{4}He in the primary radiation to determine the stripping reaction by which ^{4}He go to ^{3}He. It has been shown by Papini et al. (1993) that the measurement of the flux of ^{3}H by the same experiment provides a reliable method to make correction for the secondary production of ^{3}He in the atmosphere. Therefore, we plan to extimate the spectrum of ^{3}H also from this experiment and make the necessary correction. The final results will be presented at the conference.

ACKNOWLEDGMENTS

This work has been supported by NASA Grant NAGW-110, the Istituto Nazionale di Fisica Nucleare (INFN), Italy, the Agenzia Spaziale Italiana, the DARA and DGF, Germany, EU SCIENCE, the Swedish Council for Planning and Coordination of Research. We thank the National Scientific Balloon Facility and the tecnicians from NSMU and INFN that supported the flight campaign and launch.

REFERENCES

Carlson P. et al., *Nucl. Instr. Meth.* **A349**, 577 (1994).

Barbiellini G. et al., *Nucl. Instr. Meth.* **A371**, 169 (1996).

Bocciolini M. et al., *Nucl. Instr. Meth.* **A370**, 403 (1996).

Golden at al., *Nucl. Instr. Meth.* **A306**, 366 (1991).

Hof M. et al., *Nucl. Instr. Meth.* **A345**, 561 (1994).

Papini P. et al., 23rd ICRC Calgary, **1**, 499, (1993).

Weber N., *A measurement of the $\bar{p}$ and p fluxes in the cosmic rays by the CAPRICE experiment*, PhD Thesis, KTH Stockholm, Sweden, (1997).

OG 6.1.33

A SILICON-TUNGSTEN IMAGING CALORIMETER FOR HIGH ENERGY COSMIC RAY MEASUREMENTS

U. Bravar[1,2], S. J. Stochaj[1], and the WiZard collaboration

[1] New Mexico State University, Las Cruces, New Mexico, USA, [2] on Italian National Institute of Nuclear Physics (INFN) fellowship

ABSTRACT

A Silicon-Tungsten (Si-W) Imaging Calorimeter has been successfully flown in past balloon-borne cosmic ray payloads. In this paper we examine how this instrument can be used to measure the spectra of cosmic ray components in the energy range from 100 GeV to 10 TeV.

INTRODUCTION

The investigation of cosmic rays over their broad energy spectrum, aimed to provide a better understanding of the astrophysical processes that are at the basis of their production and acceleration, presents several open tematics. Two experimental priorities in the energy region below the knee ($<10^{14}$ eV), as emphasized in a recent National Academy of Science report (Gaisser et al. 1995), are the study of the charge composition and energy spectra of the nuclear component of the cosmic radiation above 10^{12} eV (particularly for heavier nuclei) and the measurement of the electron spectrum, together with the arrival direction, above a few hundred GeV.

A Si-W Imaging Calorimeter, in slightly different configurations, was flown in past cosmic ray payloads (Aversa et al. 1995, Golden et al. 1996, Barbiellini et al. 1996) that were based on the NMSU/WiZard Balloon Borne Magnet Spectrometer. The primary objective of these experiments was the measurement of the fluxes of the various components of the cosmic radiation, with special emphasis on positrons and antiprotons, in the energy range 1-50 GeV/amu. This imaging calorimeter, in a new configuration involving minor modifications, is capable of being used to measure the energy spectra of cosmic ray protons, light and heavy nuclei - from He to Fe - and electrons at energies ranging from 100 GeV/amu to and above 10 TeV/amu. The exposure time necessary to collect a data sample with sufficient statistics can be achieved by a long duration flight, such as the 100 day balloon program recently announced by NASA (GSFC 1996).

THE WIZARD CALORIMETER

The WiZard Imaging Calorimeter in its current configuration is composed of 8 sensitive Si planes, with an active area of 48x48 cm^2, interleaved with 7 W absorbing layers, each W layer 3.5 mm thick (which corresponds to 1 radiation length X_0 and 0.036 interaction lengths λ_I). The Si plane is made of two position sensitive Si layers. Each Si layer is 380 μm thick and is divided into 128 Si strips 3.6 mm wide. The two Si layers are mounted back to back with perpendicular strips to

Chambers (Hof et al. 1994), a Time of Flight scintillator system and either a Transition Radiation Detector (TRD - Barbarito et al. 1995) or a Ring Imaging Cherenkov (RICH) detector (Carlson et al. 1994). The granularity and energy resolution of the calorimeter enable it to measure the transverse and longitudinal shower profiles and to track the particles with high accuracy. In this configuration, the task of the calorimeter is the identification of different particles and nuclei by distinguishing between hadronic and electromagnetic showers and from the energy release in each sampling layer, while the total energy of the primary particle is obtained from its rigidity, measured by the spectrometer.

CALORIMETER RECONFIGURATION

Using the present spectrometer, rigidity measurements are not accurate above a few hundred GeV, while the energy resolution of a calorimeter becomes better as the energy increases. Therefore, we analyzed the possibility of optimizing the WiZard calorimeter to measure the particle's energy, while still performing the identification of particles.

We studied different possible new configurations where the basic structure of the Si plane remained unaltered, the number of Si planes was increased to 10 and the total thickness of the absorbing layers ranged from 0.5 to 5 λ_I. The possible advantages of using different thicknesses for different layers were also studied, as well as the possible advantages of thicker configurations, up to 10 λ_I. Tungsten was chosen again as the absorbing material primarily because of its short interaction length that allows the combination of the large thickness necessary for energy measurements with a compact vertical structure of the calorimeter, ideal from the engineering point of view. Compared to a same thickness (in interaction lengths) obtained with a lighter material, tungsten provides a larger geometric factor for the calorimeter, but also a larger weight.

Monte Carlo simulations with a program based on the GEANT code (Brun et al. 1992) were performed to study the performances of these different configurations in energy measurements. We simulated several samples of protons and electrons at different energies in the range 100 GeV - 10 TeV. The energy resolution was determined as the ratio $\delta E/E$. For protons, we obtained two values of energy resolution, by computing the $\delta E/E$ separately on the whole sample of simulated events and by considering only those particles that interact in the 1st absorbing layer. The latter procedure gives a much better resolution, especially in thinner configurations. However this method also reduces the percentage of events where the energy is measured. This procedure was not followed for the electrons, since even in the thinner configuration that we analyzed the great majority of the electrons interacts in the first absorbers (1 λ_I of W corresponds to 27.4 X_0). It should be noted that in a thin configuration a proton has a smaller probability to interact in the 1st layer. However, this configuration has also a larger geometric factor, therefore allowing the collection of a larger number of events.

The energy resolutions for 1000 GeV protons and electrons obtained with the above method for different thicknesses of the calorimeter are represented in figure 1. Figure 2 gives the geometric efficiency for protons. We define the geometric efficiency as the product of the probability for a proton to interact in the 1st W layer and the geometric factor of that configuration (the geometric factor of the calorimeter is of the order of 10^3 $cm^2 \cdot sr$). This parameter was used to select the optimal

both the geometric efficiency and the energy resolution for hadrons are lower. The use of different thicknesses for different absorbing layers (for a constant total thickness) does not affect the resolution considerably.

The proposed configuration would provide an average energy resolution of about 20% for hadrons, as shown in figure 3, and about 10% or less for electrons. It might be possible to further improve these values by adding the information on the topology of the particle's interaction provided by the granularity of the calorimeter.

CONCLUSION

From the analysis presented above we conclude that the proposed measurement can be accomplished by using a modified version of the WiZard calorimeter. The accuracy of the charge measurement performed by the calorimeter (Aversa et al. 1995) allows a direct separation of particles with different charges (protons and nuclei). An additional detector, such as a TRD, will be needed to separate the electron component (the ratio e^-/p is of the order of 10^{-3}, while the contamination of protons in electron selections is of the order of 10^{-2}).

The expected statistics for this experiment, computed by assuming a total exposure time of 100 days and a geometric factor of 10^3 $cm^2 \cdot sr$, are reported in table 1. The amount of collected data should enable an accurate measurement of the spectra of the considered particles and nuclei up to 10 TeV.

Table 1. Expected Statistics for the Proposed Flight

particle	100 - 1000 GeV	above 1000 GeV
p	$2 \cdot 10^6$	$4 \cdot 10^4$
α	$2 \cdot 10^5$	$4 \cdot 10^3$
e^-	$5 \cdot 10^3$	$3 \cdot 10^1$
C	10^4	$2 \cdot 10^2$
O	10^4	$2 \cdot 10^2$
Ne-S	$7 \cdot 10^3$	10^2
Fe	10^3	$2 \cdot 10^1$

REFERENCES

Aversa, F., et al., *Nucl. Instr. Meth.* **A360**, 17 (1995)
Barbarito, E., et al., *Nucl. Instr. Meth.* **A357**, 588 (1995)
Barbiellini, G., et al., *A&A* **309**, L15 (1996)
Bocciolini, M., et al., *Nucl. Instr. Meth.* **A370**, 403 (1996)
Brun, R., et al., *CERN GEANT 3 User's Guide*, CERN, Geneve, DD/EE/84-1 (1992)
Carlson, P., et al., *Nucl. Instr. Meth.* **A349**, 577 (1994)
Gaisser, T.K., et al., *Opportunities in Cosmic-Ray Physics and Astrophysics*, National Academy

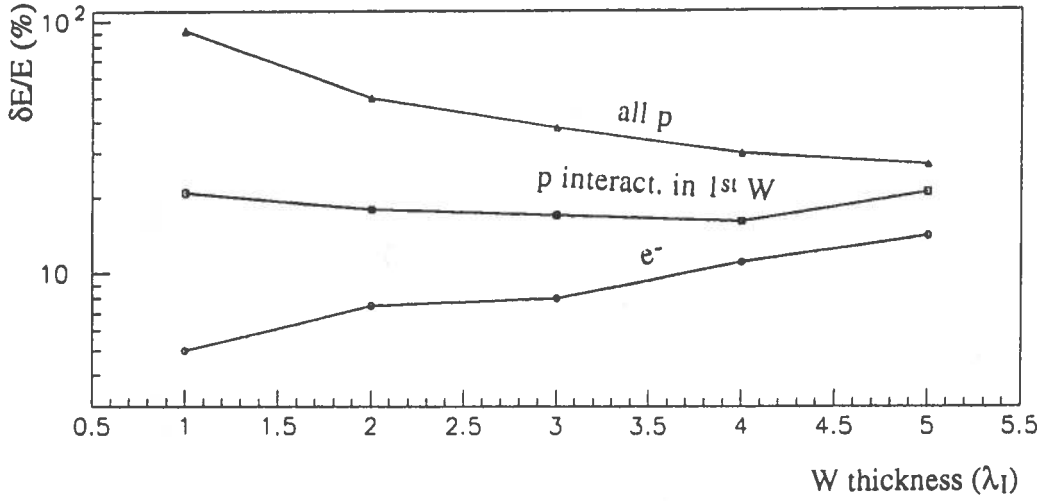

Fig. 1. Energy resolution for 1000 GeV protons and electrons for calorimeter thicknesses varying from 1 to 5 λ_I.

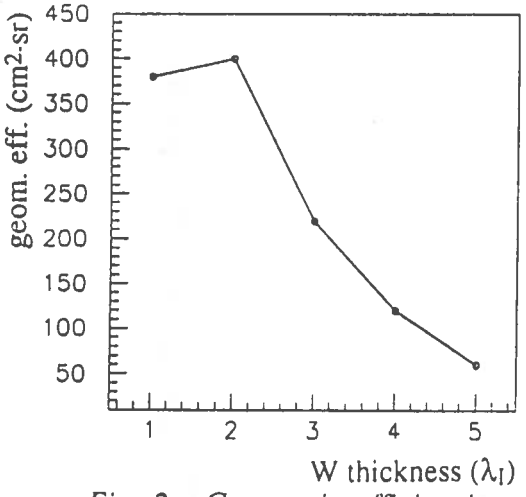

Fig. 2. Geometric efficiencies of the calorimeter configurations represented in figure 1.

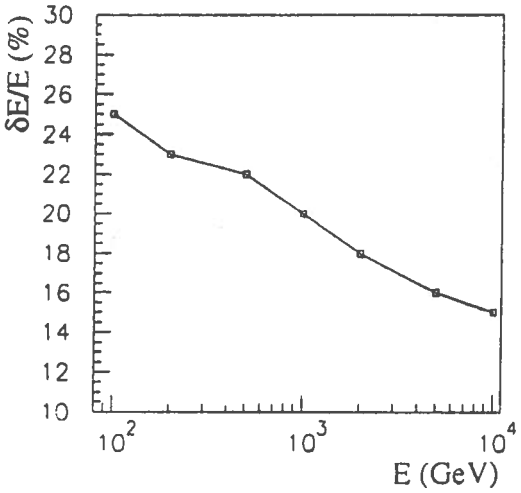

Fig. 3 Energy resolution for protons in the range 10^2 - 10^4 GeV in a 2 λ_I calorimeter.

OG 7.1.4

THE ANTIPROTON FLUX NEAR SOLAR MINIMUM MEASURED WITH THE CAPRICE EXPERIMENT

G. Barbiellini[12], G. Basini[4], R. Bellotti[1], M. Bocciolini[3], M. Boezio[10], U. Bravar[12], F. Cafagna[1], P. Carlson[10], M. Casolino[8], M. Castellano[1], M. Circella[1], A. Codino[7], G. De Cataldo[1], C. De Marzo[1], M.P. De Pascale[8], N. Finetti[7], T. Francke[10], N. Giglietto[1], R.L. Golden[0,6], C. Grimani[7], M. Hof[9], W. Menn[9], J.W. Mitchell[5], A. Morselli[8], J.F. Ormes[5], P. Papini[3], A. Perego[3], S. Piccardi[3], P. Picozza[8], M. Ricci[4], P. Schiavon[12], M. Simon[9], R. Sparvoli[8], P. Spillantini[3], P. Spinelli[1], S.A. Stephens[2], S.J. Stochaj[6], R.E. Streitmatter[5], M. Suffert[11], A. Vacchi[12], N. Weber[10], N. Zampa[12]

[1]*Dipartimento di Fisica dell'Università and Sezione INFN di Bari, Bari, Italy* [2]*Tata Institute of Fundamental Research, Bombay , India* [3]*Dipartimento di Fisica dell'Università and Sezione INFN di Firenze, Firenze, Italy* [4]*Laboratori Nazionali INFN, Frascati, Italy* [5]*NASA/Goddard Space Flight Center, Greenbelt, USA* [6]*New Mexico State University, Las Cruces, USA* [7]*Dipartimento di Fisica dell'Università and Sezione INFN di Perugia, Perugia, Italy* [8]*Dipartimento di Fisica dell'Università and Sezione INFN di Roma, Roma, Italy* [9]*Universität Siegen, Siegen, Germany* [10]*Royal Institute of Technology, Stockholm, Sweden* [11]*Centre des Recherches Nucléaires, Strasbourg-Cedex, France* [12]*Dipartimento di Fisica dell' Università and Sezione INFN di Trieste, Trieste, Italy*

ABSTRACT

We report on the absolute antiproton flux and the antiproton to proton ratio in the energy range 0.62 to 3.19 GeV at the top of the atmosphere, measured by the balloon-borne experiment CAPRICE flown from Lynn Lake, Manitoba, Canada, on August 8-9, 1994. The experiment used the NMSU-WiZard/-CAPRICE balloon-borne magnet spectrometer equipped with a solid radiator Ring Imaging CHerenkov (RICH) detector and a silicon-tungsten calorimeter for particle identification. The data were collected over 18 hours at a mean residual atmosphere of 3.9 g/cm^2. Nine antiprotons were identified. The absolute antiproton flux is consistent with the secondary production of antiprotons during the propagation of cosmic rays in the Galaxy.

DETECTOR SYSTEM

The NMSU-WiZard/CAPRICE spectrometer was flown by balloon from Lynn Lake, Manitoba, Canada (56.5° North Latitude, 101.0° West Longitude), on 8-9 August 1994 at an atmospheric pressure of 3.2 to 4.5 mbar (altitude of 36.0 - 38.1 km) for 23 hours. It included from top to bottom: a Ring Imaging Cherenkov (RICH) detector, (Carlson et al. 1994, Barbiellini et al. 1996), a time-of-flight (ToF) system, a magnet spectrometer equipped with multiwire proportional chambers (MWPC) and drift chambers (DC) (Golden et al. 1978, Golden et al. 1991, Hof et al. 1994) and a silicon-tungsten imaging calorimeter (Bocciolini et al. 1996) .

ANTIPROTON AND PROTON SELECTION

The analysis was based on 18 hours of data collection for a total acquisition time of 60520 seconds under an average residual atmosphere of 3.9 g/cm^2. The fractional dead time during the flight was 0.7310 ± 0.0006 resulting in a total live time of 16280 ± 36 s.

Albedo particles were rejected using the time-of-flight system and verified with the RICH where no Cherenkov light is detected for albedo particles. Strict requirements on the tracking and scintillator information resulted against clean sample of negative unit charged particles from which the antiprotons

ity. It was used to identify the rare antiprotons in a significant background of mainly muons and pions (Boezio et al. 1997, Weber 1997). Nine antiprotons and 149918 protons were identified in the rigidity range 1.2 to 4.0 GV.

EFFICIENCY AND CONTAMINATION

The NMSU-WiZard/CAPRICE instrument has a unique capability to reliably determine the detector efficiencies as well as contamination, as it allows selection of clean particle samples using independent sets of detectors.

Whereas protons and antiprotons have very similar efficiencies in the RICH, scintillators, and the tracking system, this is not the case for the calorimeter due to the large difference in interaction properties. The RICH, scintillator and tracking efficiencies as a function of rigidity were determined using a large proton sample from the flight data. GEANT simulations were used to determine the calorimeter efficiency for antiprotons.

The contamination due to e^-, μ^- and π^- in the antiproton sample was carefully studied using the two independent detectors: the RICH and the calorimeter. Simulations and experimental data taken during the flight and on the ground before the flight were used. The combination of the calorimeter and the RICH resulted in a very small background from electrons (and interacting pions) in the antiproton sample, less than 0.15 electrons (and interacting pions) in the whole sample. Tests in particle beams showed that muons and electrons have the same detection efficiency in the RICH. Therefore, it was assumed that the surviving fraction of muons was equal to the surviving fraction of electrons, and it was determined using ground data. The number of negative muons (and non-interacting pions), selected from flight data as events with a minimum ionizing behaviour in the calorimeter, was multiplyed with the surviving fraction numbers. The muon/pion contamination was found to be 0.9 ± 0.2 muons/pions between 1.2 and 2.8 GV/c, and 0.7 ± 0.1 between 2.8 and 4.0 GV/c. This contamination, and the small electron and non-interacting pion contamination, was later subtracted from the antiproton signal.

ANTIPROTON FLUX AND ANTIPROTON TO PROTON RATIO

All antiprotons and protons interacting with the payload material above the tracking system were assumed to be rejected by the selection criteria. The data were corrected for these losses with multiplicative factors, using the expression for the interaction mean free path for the different materials in the detectors given by Stephens (1997).

For the atmospheric secondary antiproton production, we used the calculation by Stephens (1997) and for that of protons the data of Papini et al. (1996). The secondary produced particles were normalized with the acceptance and live time of the experiment, and subtracted from the corrected numbers using a mean residual atmosphere of 3.9 g/cm^2. Finally, the data were corrected for losses in the atmosphere above the detector due to interactions, giving the number of antiprotons and protons at the top of the atmosphere. The geometrical factor at different rigidities was obtained with a Monte Carlo technique (Sullivan 1971).

The antiproton flux at the top of the atmosphere was found to be 1.9 (+2.4, -1.4) $\times 10^{-2}$ and 5.3 (+4.5, -2.9) $\times 10^{-2}$ (m^2 sr s GeV)$^{-1}$ in the kinetic energy region 0.6-2.0 and 2.0-3.2, respectively. The errors include both statistic and systematic uncertainties. The antiproton flux is shown in Figure 1 together with other recent experiments and theoretical predictions. The theoretical antiproton limits were set by Gaisser and Schaefer (1992), assuming that the source of interstellar antiprotons is interaction of cosmic rays with the interstellar medium. The theoretical fluxes, but not the experimental

CONCLUSION

For the first time, the combination of an electromagnetic calorimeter and a ring imaging Cherenkov detector has been used to measure the cosmic ray flux of antiprotons. This combination has made it possible to accurately identify antiprotons in the presence of a large background of lighter, negatively charge particles. It also allows an accurate determination of the detector efficiencies as well as the contamination within the antiproton sample.

The flux of antiprotons and the ratio of antiprotons to protons increase over the kinetic energy interval 0.6 to 3.2 GeV. In agreement with other recent data (e.g. Mitchell et al. 1996), it supports the conjecture that the antiprotons in this energy range are produced in the interstellar medium by primary cosmic rays colliding with interstellar gas.

REFERENCES

Barbiellini, G., et al., *Nucl. Instr. and Meth.*, **A371**, 169 (1996)

Bocciolini, M., et al., *Nucl. Instr. and Meth.*, **A370**, 403 (1996)

Bogomolov, E. A. et al., *Proc. 20th ICRC*, **2**, 72 (1987)

Bogomolov, E. A. et al., *Proc. 21th ICRC*, **3**, 288 (1990)

Boezio, M. et al., "The Cosmic Ray Antiproton Flux between 0.62 and 3.19 GeV Measured near Solar Minimum Activity", To appear in **ApJ** (1997)

Carlson, P., et al., *Nucl. Instr. and Meth.*, **A349**, 577 (1994)

Gaisser, T. K., & Schaeffer, R. K., *ApJ*, **394**, 174 (1996)

Golden, R. L., et al., *Nucl. Instr. and Meth.*, **148**, 179 (1978)

Golden, R. L., et al., *Astrophys. Lett.*, **24**, 75 (1984)

Golden, R. L., et al., *Nucl. Instr. and Meth.*, **A306**, 366 (1991)

Hof, M., et al., *Nucl. Instr. and Meth.*, **A345**, 561 (1994)

Hof, M., et al., *ApJ*, **467**, L33 (1996)

Mitchell, J., et al., *Phys. Rev. Lett.*, **76**, 3057 (1996)

Moiseev, A., et al., *ApJ*, **474**, 479 (1997)

Papini, P., Grimani, C., & Stephens, S. A., *Il Nuovo Cimento*, **19**, 367 (1996)

Stephens, S. A., *Astropart. Phys.*, **6**, 229 (1997)

Sullivan, J. D., *Nucl. Instr. and Meth.*, **95**, 5 (1971)

Weber, N. 1997, "A Measurement of the Antiproton and Proton Fluxes in the Cosmic Rays by the CAPRICE Experiment", (PhD thesis, KTH Stockholm, Sweden)

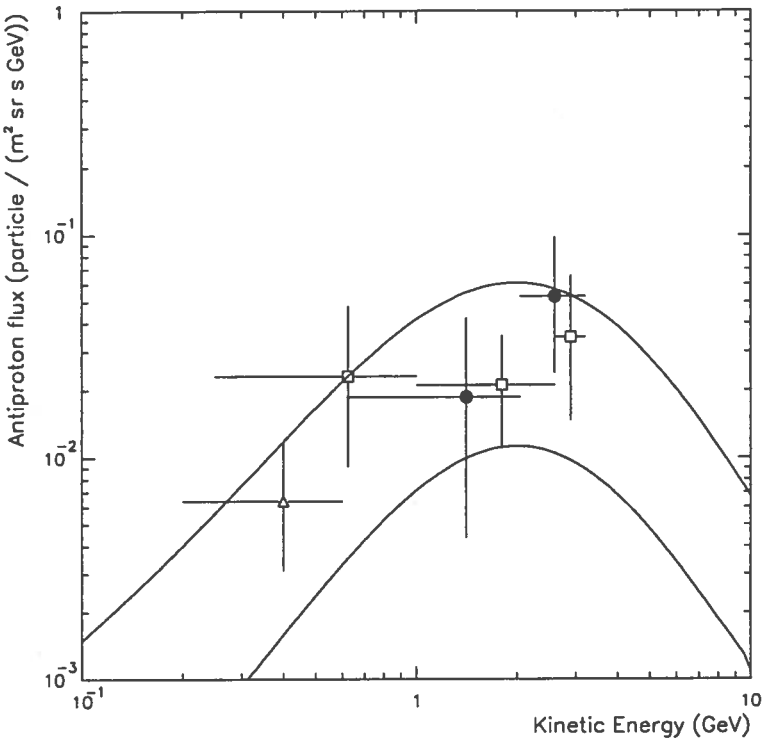

Fig. 1: The antiproton flux at thet top of the atmosphere obtained in this work (filled circle) and compared to other recent experiments, Mitchell et al. 1996 (open box) and Moiseev et al. 1997 (open triangle).

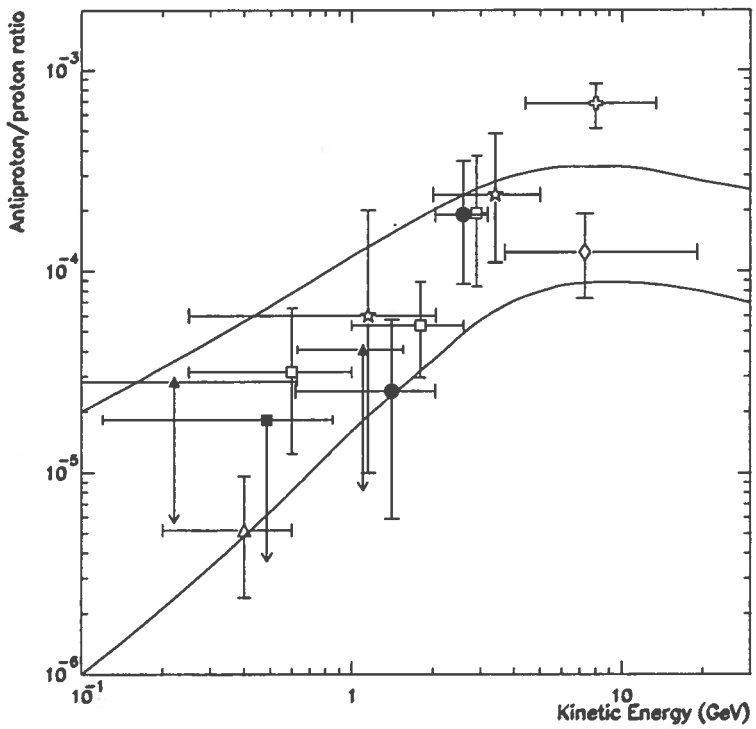

OG 7.1.5

MEASUREMENT OF THE POSITRON AND ELECTRON SPECTRA WITH THE CAPRICE EXPERIMENT

G. Barbiellini[12], G. Basini[4], R. Bellotti[1], M. Bocciolini[3], M. Boezio[10], U. Bravar[12], F. Cafagna[1], P. Carlson[10], M. Casolino[8], M. Castellano[1], M. Circella[1], A. Codino[7], G. De Cataldo[1], C. De Marzo[1], M.P. De Pascale[8], N. Finetti[7], T. Francke[10], N. Giglietto[1], R.L. Golden[0,6], C. Grimani[7], M. Hof[9], W. Menn[9], J.W. Mitchell[5], A. Morselli[8], J.F. Ormes[5], P. Papini[3], A. Perego[3], S. Piccardi[3], P. Picozza[8], M. Ricci[4], P. Schiavon[12], M. Simon[9], R. Sparvoli[8], P. Spillantini[3], P. Spinelli[1], S.A. Stephens[2], S.J. Stochaj[6], R.E. Streitmatter[5], M. Suffert[11], A. Vacchi[12], N. Weber[10], N. Zampa[12]

[0] *Deceased*

[1] *Dipartimento di Fisica dell'Università and Sezione INFN di Bari, Bari, Italy,* [2] *Tata Institute of Fundamental Research, Bombay, India,* [3] *Dipartimento di Fisica dell'Università and Sezione INFN di Firenze, Firenze, Italy,* [4] *Laboratori Nazionali INFN, Frascati, Italy,* [5] *NASA/Goddard Space Flight Center, Greenbelt, Maryland, USA,* [6] *New Mexico State University, Las Cruces, New Mexico, USA,* [7] *Dipartimento di Fisica dell'Università and Sezione INFN di Perugia, Perugia, Italy,* [8] *Dip. di Fisica dell'Università and Sezione INFN di Roma, Tor Vergata, Roma, Italy,* [9] *Universität Siegen, Siegen, Germany,* [10] *Royal Institute of Technology, Stockholm, Sweden,* [11] *Centre des Recherches Nucléaires, Strasbourg, France,* [12] *Dipartimento di Fisica dell'Università and Sezione INFN di Trieste, Trieste, Italy*

ABSTRACT

We report on the absolute energy spectra of positrons and electrons and the positron fraction in the energy range from 0.38 to 14.2 GeV at the top of the atmosphere. The data were collected by the balloon-borne experiment CAPRICE flown from Lynn Lake, Canada, on August 8-9, 1994, at an altitude corresponding to 3.9 g/cm^2 of average residual atmosphere. The experiment used the NMSU-WIZARD/CAPRICE balloon-borne magnet spectrometer equipped with a solid radiator Ring Imaging Cherenkov (RICH) detector and a silicon-tungsten calorimeter for particle identification. A total of 3243 e^- and 803 e^+ were identified with very small background of other particles. The resulting positron fraction is consistent with the simple leaky box model.

INTRODUCTION

Detailed measurements of the electron component of the cosmic rays are important to understand the propagation of cosmic rays in the Galaxy. This is because electrons undergo severe energy loss through synchrotron radiation in the magnetic field and inverse Compton scattering with the ambient photons, while these processes do not significantly affect the nucleonic cosmic-ray component. Cosmic ray positrons are believed to be produced in collisions of cosmic ray nucleons with interstellar matter and measurement of the positron spectrum permits to examine propagation models, production mechanism and other possible new sources of its origin. Besides, comparison between the two spectra gives useful information about solar wind effects on the cosmic rays.

Most of the recent measurements on the electron-positron component have been carried out above 5 GeV (e.g. Barwick et al., 1995, Golden et al., 1996). Below 5 GeV just a few results have been published (Clem et al., 1996, Barbiellini et al., 1996b) since early seventies (Fanselow et al., 1969, Daugherty et al., 1975). The unambiguous detection of positrons is difficult because of the vast background of protons. Another problem associated with the balloon borne positron and electron mea-

38.1 km and at a low geomagnetic cut off, which varied from about 0.4 to 0.6 GV/c during the flight, for 23 hours. From top to bottom the instrument includes a Ring Imaging Cherenkov (RICH) detector (Carlson et al., 1994, Barbiellini et al., 1996a), a time-of-flight (ToF) system, a magnet spectrometer of multiwire proportional chambers (MWPC) and drift chambers (DC) (Golden et al., 1991, Hof et al., 1994) and a silicon-tungsten imaging calorimeter (Bocciolini et al., 1996) .

DATA ANALYSIS

The analysis was based on 18 hours of data collection for a total acquisition time of 60520 seconds under an average residual atmosphere of 3.9 g/cm^2. The fractional dead time during the flight was 0.7310 ± 0.0006 resulting in a total live time of 16280 ± 36 s. Previous results on the positron to electron ratio in the range from 0.6 to 10 GV/c from the CAPRICE experiment have already been published (Barbiellini et al., 1996b). In this conference we present results over an energy range extended to lower energies and on the absolute spectra.

We selected electrons and positrons in the rigidity range from 0.25 to 10 GV/c. We required a well defined single track in the spectrometer with a good momentum resolution, characterized by acceptable chi-squares and small uncertainty in deflection. We selected singly charged particles with a signal of less than 1.8 mips (minimum ionizing particles) in the top ToF scintillator. Albedo events were rejected using both the ToF and the RICH. Electrons and positrons were selected as particles with negative and positive deflection respectively, $\beta = 1$ as detected by the RICH and an electromagnetic shower in the calorimeter.

The cuts imposed on the calorimeter to identify electromagnetic showers had a logarithmic dependence on rigidity and were based on (a) results from test beams at CERN (Bocciolini et al., 1993), (b) simulations and (c) experience gained from a previous flight with a similar instrument (Golden et al., 1996). An electromagnetic shower was characterized by a narrow shower with most of the energy deposited inside 4 Molière radii around the track. We imposed additional cuts based on the total detected energy, which should match the measured momentum, and on the longitudinal and lateral profiles of the shower. A small number of particles emit a bremsstrahlung photon before entering the calorimeter (e.g. in the RICH or the aluminum cover of the gondola) that was detected in the calorimeter as a parallel shower. These double shower events with a single track in the tracking system are clearly electron/positron events and looser cuts were used. The detection efficiency of the calorimeter using the above cuts is rigidity dependent increasing from 40% at 0.25 GV/c to 85% above 1.0 GV/c.

The RICH was used to measure the velocity (β) of the particles. Due to the high rejection factor of the calorimeter, rather loose cuts were applied on the RICH data in order to maximize the efficiency of selection. Electrons and positrons were selected by the RICH as $\beta = 1$ particles with a well defined Cherenkov light image and a good agreement between the position determined by the RICH and that from the tracking measurement. With these cuts applied, the RICH has a detection efficiency increasing from 58% at 0.25 GV/c to 72% between 0.8 and 5 GV/c. Above 5 GV/c the RICH is not capable of separating protons from positrons and was not used.

RESULTS

Table 1 gives the number of electrons and positrons that passed the cuts applied on the RICH, the ToF and the calorimeter. We estimated the protons passing the calorimeter criteria by selecting proton sample using the RICH, scintillator dE/dx and ToF. Similarly the proton contamination in the RICH selection was estimated using a proton sample selected by the ToF below 1 GV/c and by the calorime-

calorimeter and the RICH is high enough to eliminate all proton, pion and muon contamination from the positron sample between 0.25 and 3 GV/c. The proton contamination was found to be 12%, 29% and 37% of the positron sample in the rigidity bins 3 to 4 GV/c, 4 to 5 GV/c and 5 to 10 GV/c respectively. This proton contamination is shown in the parenthesis in Table 1 and was subtracted from the positron sample.

The observed electron and positron spectra were corrected for the efficiencies and were extrapolated to the top of the payload using bremsstrahlung corrections. From these spectra we subtracted the atmospheric secondary e^- and e^+ fluxes, using the theoretical estimates of Stephens (1981).

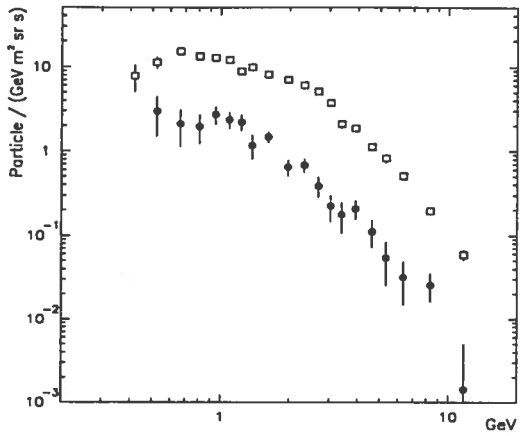

Fig. 1: Extrapolated positron and electron absolute spectra at top of the atmosphere: □ electrons; • positrons. The positron value in the lowest energy bin is zero.

The corrected electron and positron spectra were propagated backward to the top of the atmosphere (ToA) by simultaneously solving the cascade equations, which describe the propagation of all the electromagnetic components, namely, primary e^- , e^+ and secondary gamma rays that result from bremsstrahlung of the electron component. From this, we obtained the positron and electron spectra,

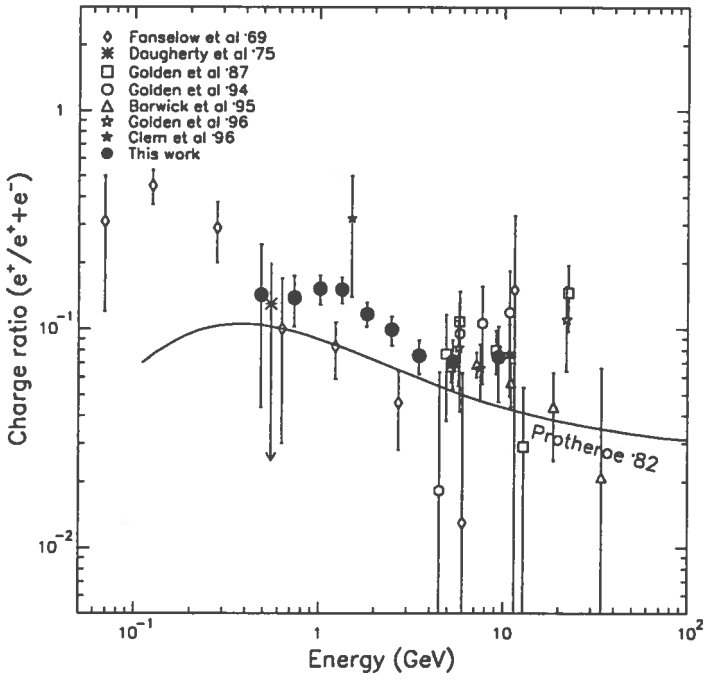

Table 1: Summary of electron - positron results.

Energy bin at spectrometer GeV	Observed number of events[b] e^-	e^+	Median energy at TOA GeV	Flux at TOA[a] (GeV m^2 sr s)$^{-1}$ e^-	e^+	$\frac{e^+}{e^+ + e^-}$
0.25-0.4	199	148	0.485	10.1 ± 1.6	1.7 ± 1.3	0.143 ± 0.099
0.4-0.6	419	164	0.73	13.7 ± 1.1	2.2 ± 0.6	0.138 ± 0.036
0.6-0.8	413	128	1.01	13.3 ± 0.85	2.4 ± 0.4	0.152 ± 0.023
0.8-1.05	388	101	1.33	9.72 ± 0.57	1.7 ± 0.26	0.151 ± 0.021
1.05-1.5	539	99	1.82	7.33 ± 0.36	0.97 ± 0.13	0.117 ± 0.015
1.5-2.0	427	60	2.475	5.06 ± 0.28	0.56 ± 0.09	0.099 ± 0.015
2.0-3.0	420	44	3.49	2.21 ± 0.12	0.18 ± 0.03	0.076 ± 0.013
3.0-5.0	279	31(5.6)	5.33	0.79 ± 0.05	0.06 ± 0.02	0.071 ± 0.018
5.0-10.0	159	28(10.4)	9.43	0.114 ± 0.009	0.009 ± 0.004	0.074 ± 0.028

[a]Top of atmosphere.

[b]The numbers shown in the brackets are the estimated proton background.

clearly notice from this figure the effect of the geomagnetic cut-off below 0.7 GeV.

After suitably combining nearby energy bins in order to decrease the statistical errors, we obtained the fraction of positrons that is tabulated in Table 1 and plotted in Figure 2 together with previous measurements . Our results are in agreement with the recent measurements (Barwick et al., 1995, Golden et al., 1996) at the upper energy bins. The observed energy dependence of our results is consistent with that expected from the simple leaky box model (Protheroe, 1982).

REFERENCES

Barbiellini, G. et al., *Nucl. Instr. Meth*, **A371**, 169 (1996a)
Barbiellini, G. et al., *Astr. Astrophys.*, **309**, L15 (1996b)
Bocciolini, M. et al., *Nucl.Instr. and Meth.*, **A370**, 403 (1996)
Bocciolini, M. et al, *Nucl. Instr. and Meth.*, **A333**, 77 (1993)
Barwick, S.W. et al., *Phys. Rev Lett.*, **75**, 390 (1995)
Carlson, P. et al, *Nucl. Instr. Meth.*, **A349**, 577(1994)
Clem, J. et al., *ApJ*, **464**, 507 (1996)
Daugherty, J. K. et al., *ApJ*, **198**, 493 (1975)
Fanselow, J. L. et al., *ApJ*, **158**, 771 (1969)
Golden, R. L. et al., *A&A*, **188**, 145 (1987)
Golden, R. L. et al., *Nucl. Instr. and Meth.*, **A306**, 366 (1991)
Golden, R. L. et al., *ApJ*, **436**, 769 (1994)
Golden, R. L. et al., *ApJ*, **457**, L103 (1996)
Hof, M. et al., *Nucl. Instr. and Meth.*, **A345**, 561 (1994)

OG 10.1.1

A GAS-RICH DETECTOR FOR COSMIC RAY STUDIES

G. Barbiellini[11], S. Bartalucci[4], G. Basini[4], R. Bellotti[1], D. Bergström[9], M. Bocciolini[3], M. Boezio[9], U. Bravar[11], F. Cafagna[1], P. Carlson[9], M. Casolino[1], M. Castellano[1], M. Circella[1], G. De Cataldo[1], C. De Marzo[1], M.P. De Pascale[7], T. Francke[9], N. Giglietto[1], M. Hof[8], J. Kremer[8] W. Menn[8], J.W. Mitchell[5], A. Morselli[7], J.F. Ormes[5], P. Papini[3], A. Perego[3], S. Piccardi[3], P. Picozza[7], M. Ricci[4], P. Schiavon[11], M. Simon[8], R. Sparvoli[7], P. Spillantini[3], P. Spinelli[1], S.A. Stephens[2], S.J. Stochaj[6], R.E. Streitmatter[5], M. Suffert[10], A. Vacchi[11], N. Weber[9], N. Zampa[11]

[1]*Dipartimento di Fisica dell'Università and Sezione INFN di Bari, Bari, Italy* [2]*Tata Institute of Fundamental Research, Bombay , India* [3]*Dipartimento di Fisica dell'Università and Sezione INFN di Firenze, Firenze, Italy* [4]*Laboratori Nazionali INFN, Frascati, Italy* [5]*NASA/Goddard Space Flight Center, Greenbelt, USA* [6]*New Mexico State University, Las Cruces, USA* [7]*Dipartimento di Fisica dell'Università and Sezione INFN di Roma, Roma, Italy* [8]*Universität Siegen, Siegen, Germany* [9]*Royal Institute of Technology, Stockholm, Sweden* [10]*Centre des Recherches Nucléaires, Strasbourg-Cedex, France* [11]*Dipartimento di Fisica dell'Università and Sezione INFN di Trieste, Trieste, Italy*

ABSTRACT

A Ring Imaging CHerenkov (RICH) detector using a gaseous radiator of C_4F_{10} has been developed for cosmic ray studies. The Cherenkov photons are detected in a photosensitive multiwire proportional chamber with pad readout. It has been used in the NMSU -WIZARD/CAPRICE97 balloon-borne magnet spectrometer together with a silicon -tungsten calorimeter for particle identification. The performance of the RICH during ground tests before the 1997 flight is presented.

INTRODUCTION

A new gas-RICH detector have been developed and tested in particle beams at CERN, as well as with cosmic rays in pre-flight operation in the NMSU-WiZard/CAPRICE97 balloon borne spectrometer. The gas-RICH detector was developed to identify particles with momentum between 2 and 50 GeV/c. The primary goals is to investigate the flux of antiprotons and positrons, and to continue the search for antimatter. Besides the gas-RICH, the NMSU-WiZard/CAPRICE97 instrument includes a time-of-flight system, an imaging silicon-tungsten calorimeter (Bocciolini et al. 1996) and a tracking system with a superconducting magnet and 3 drift chamber (Golden et al. 1978, Golden et al. 1991, Hof et al. 1994). The 1997 flight is the latest in a series of successful flights (MASS 1989, MASS2 1991, TS93 1993 and CAPRICE 1994) performed by the WiZard collaboration.

THE GAS-RICH DETECTOR

The newly developed gas-RICH shown in Figure 1. is, as the solid radiator RICH used in CAPRICE 1994 (Carlson et al. 1993, Carlson et al. 1994, Barbiellini et al. 1996), a Cherenkov detector of imaging type. It was developed to identify antiprotons and positrons in the large background of primarily protons, electrons, π-mesons and muons in the cosmic radiation.

Cherenkov photons emitted in the C_4F_{10} radiator are reflected and focused by a spherical mirror onto a photosensitive MWPC. The photons enter into the MWPC through a quartz window, and are converted into photoelectrons via photoeffect with the photosensitive vapor tetrakis (dimeylamino)-

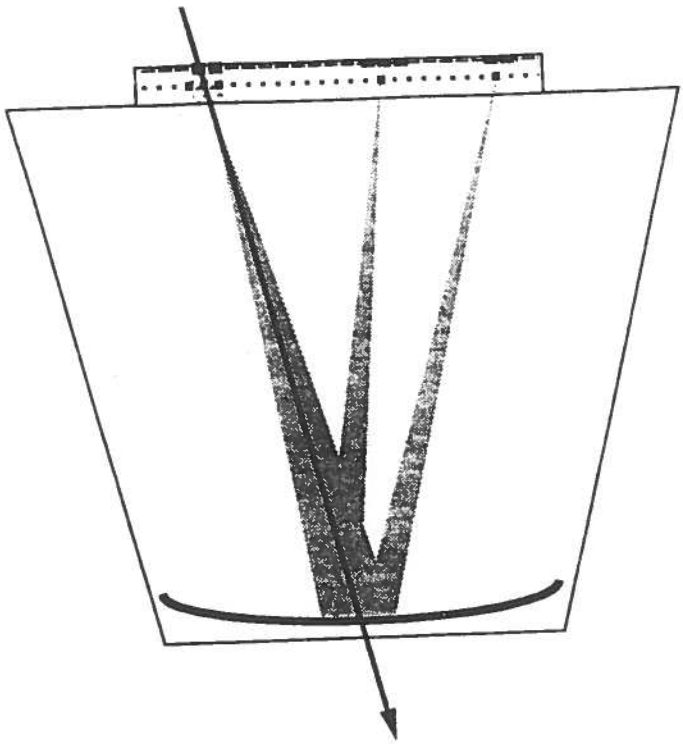

Fig. 1: Schematic principle of the CAPRICE97 gas-RICH. A charged particle passes through the chamber, where it ionizes the gas and gives a large and distinctive signal. Cherenkov photons emitted in the radiator are reflected and focused by the mirror into a sharp ring on the MWPC, where the pad plane gives a two-dimentional image of the light.

Multiwire Proportional Chamber

The photosensitive MWPC consists of an anode wire plane inbetween two cathode planes. The upper cathode is a gold plated pad plane of 64 by 64 8*8 mm^2 pads. The lower cathode consists of strips evaporated onto the quartz window that separates the MWPC from the radiator. The MWPC has an area of 51.2*51.2 cm^2. The cathodes are placed asymmetric around the anode wire plane with the pad plane and the strip plane 2 and 10 mm away from the anode wires, respectively. The chamber is operated with an anode voltage of +1800 V, keeping the pads at ground and the strips at -1700 V. This gives a parallell plate amplification in the strip-anode volume making it possible to reduce the anode voltage compared to a symmetric 2+2 mm chamber with ground potential on both cathode planes, thus giving a more stable operation. The chamber is constantly flushed with ethane saturated with TMAE vapor.

Radiator

The radiator is 1 m tall and has a volume of more than 800 liters. It is flushed with high- purity perfluorobutane gas, C_4F_{10}. The spherical mirror with a radius of 99.5 mm is positioned below the quartz window at the bottom of the radiator focusing the light from particles above the Cherenkov threshold, onto the active surface of the MWPC.

Readout Electronics

DETECTOR PERFORMANCE

In pre-flight operation on the ground, more than 5 million cosmic ray particles were recorded. The main bulk of these particles are atmospheric muons.

Figure 2 shows a 0.86 GeV/c positron in the RICH during the ground runs. The pads and wires with a signal above threshold are represented by the squares and the vertical lines at the top of the figure, respectively. The cluster of pads to the upper left in the figure are due to the ionization of the chamber gas by the charged particle. The ring of clusters of pads to the right in the figure is from the Cherenkov light. The single cluster to the lower left of the ionization cluster is due to a single photon reflected in the quartz window back down on the mirror and up again onto the MWPC.

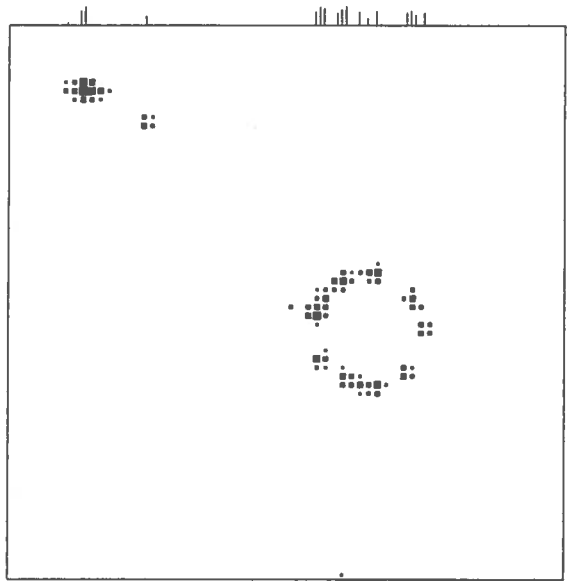

Fig. 2: The image of a single 0.86 GV/c positron passing through the Gas-RICH. Each square corresponds to a pad with signal above threshold. The size of a square is proportional to the amplitude of the signal. The vertical lines on top of the figure indicate anode wires that are hit.

Note that the signal from each photoelectron is spread out over several pads. This implies an increased rejection of noise pads since isolated pads are considered to be due to noise. A gaussian potential method (Ullrich et al. 1996), where pads with Cherenkov angle far from the mean value are suppressed, is used to determine the Cherenkov angle of each event. Figure 3. shows the reconstructed Cherenkov angle as a function of rigidity for cosmic ray particles with a rigidity greater than 2 GV/c detected on the ground. Negative particles are assigned a negative rigidity for clarity. The Cherenkov angle resolution decreases rapidly below 2 mrad as the Cherenkov angle approaches 50 mrad giving excellent particle identification capabilities. On average 10 photoelectrons are detected per event for β=1 particles.

CONCLUSIONS

A gas RICH detector for cosmic ray studies have been developed. 10 photoelectrons per event are

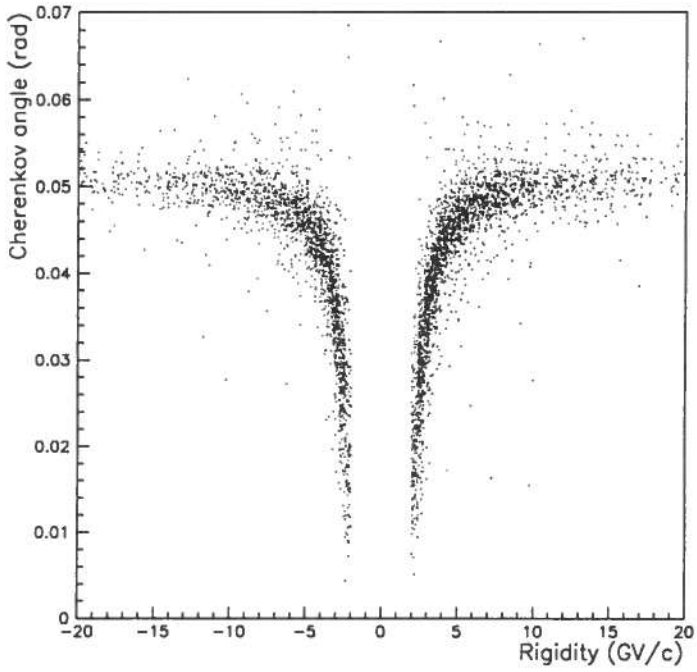

Fig. 3: The Cherenkov angle as function of rigidity for cosmic ray particles detected on the ground. For clarity, negative particles have been assigned a negative rigidity.

REFERENCES

Barbiellini, G., et al., *Nucl. Instr. and Meth.*, **A371**, 169 (1996)
Bocciolini, M., et al., *Nucl. Instr. and Meth.*, **A370**, 403 (1996)
Boezio, M. et al., "The Cosmic Ray Antiproton Flux between 0.62 and 3.19 GeV Measured near Solar Minimum Activity", To appear in *ApJ* (1997)
Carlson, P., et al., *Proc. 23th ICRC*, **2**, 504 (1993)
Carlson, P., et al., *Nucl. Instr. and Meth.*, **A349**, 577 (1994)
de Beuville, E., et al., *Nucl. Instr. and Meth.*, **A288**, 157 (1990)
Golden, R. L., et al., *Nucl. Instr. and Meth.*, **148**, 179 (1978)
Golden, R. L., et al., *Nucl. Instr. and Meth.*, **A306**, 366 (1991)
Hof, M., et al., *Nucl. Instr. and Meth.*, **A345**, 561 (1994)

OG 10.2.8

COSMIC RAY STUDIES ON THE MIR SPACE STATION: THE EXPERIMENT SILEYE

A.Morselli [1] on behalf of the Sileye collaboration
[1] *Dept. of Physics, II Univ. of Rome "Tor Vergata" and INFN, Italy*

ABSTRACT

The Sileye detector can simultaneously measure particle energy losses from 2.5 Minimum Ionizing Particles (MIPs) to 2500 MIPs and determine the coordinates of passing particles with an accuracy of 1.8 mm. This instrument can be used for cosmic rays studies as well as for medical-biological and technological space researches. We will present the results obtained with the first prototype of the apparatus, on board MIR since October 1995, and the performances of the second apparatus, Sileye2, that will be launched in the fall of 1997.

INTRODUCTION

Since the Apollo missions it was known that the crews, after some minutes of dark adaptation, observed brief white light flashes or pencil-thin streaks of light . The first observation was reported by E. Aldrin during the Apollo 11 mission (W.Z.Osborne et al., 1975). Other observations were later reported by Apollo-Soyuz (T.F.Budinger et al., 1977). The frequency of light flashes (LF) depends on orbit parameters, especially on the latitude, and grows in polar areas and in the area of the South Atlantic Anomaly. LF are practically absent on the equator, where the charged particles' flux is minimum. There are different hypothesis on the generation mechanisms of visual effects, like direct interaction of charged particles with the retina of the eye by ionization (Hoffman et al.1977) or Cherenkov effect in the ocular bulb (G.G.Fazio et al.,1970) or indirect effect from proton knocked out by protons (J.Fremlin, 1970). It was also suggested that scintillation in the eye lens could cause the observed LF's (I.MacAulay, 1971). For a review see G.Horneck 1992.

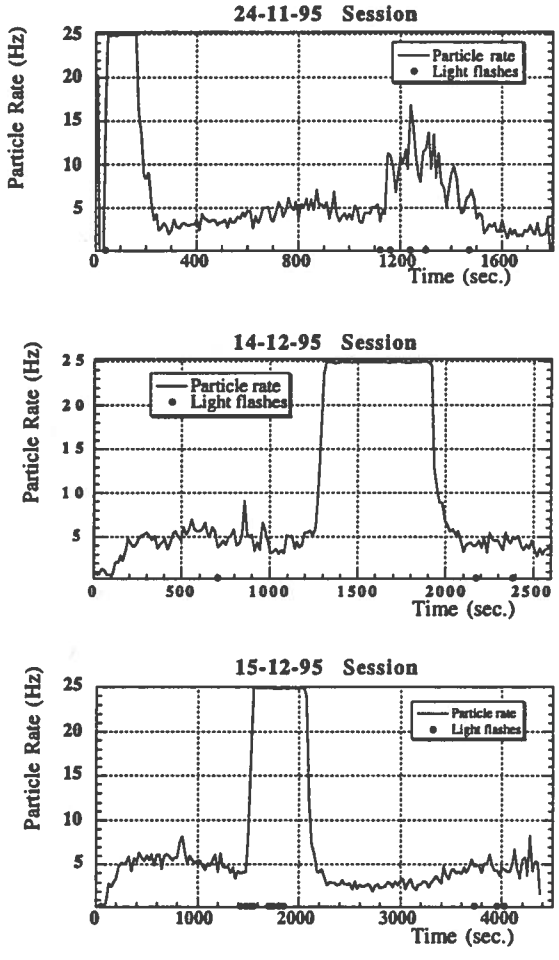

Fig. 1: Trigger rate vs. the different position in the

DESCRIPTION OF THE SILEYE APPARATA

The main body of our detectors consists of silicon views. A view is made of a square (6x6 cm^2) wafer of silicon, divided in 16 strips, each 3.6 mm wide. Two views, orthogonally attached to each other, constitute a plane. We have three planes for a total number of 96 strips. The distance between the silicon planes is 5 cm for the Sileye apparatus and 14 mm for the Sileye2. Each silicon strip is 380±15 μm thick. A more complete description of the Sileye2 apparatus can be found in V.Bidoli et al. 1997. Both the apparata can detect in real time the passage of particles which traverse the eyes and register on the on-board computer the six coordinates and energy depositions from which the direction and proprieties of the particles can be determined. Time of LF occurrence are also stored in a separate file for off-line correlation.

SILEYE RESULTS

In Fig.1 the time dependence of the detector trigger rate together with the LF registration time is shown for three different one hour sessions. For the 24/11/95 session the beginning of the acquisition coincided with a passage in the SAA area. Here the trigger rate is saturated at about 25 Hz, due to the deadtime of the detector. The second rise of the trigger's rate, at around 1200 s, is connected with the passage at high latitude. Note that all but one of the observed light flashes in this session were seen in this region, although the trigger rate is much lower then in the SAA. This is a general feature in most sessions but not in all. For example in the 15/12/96 session 5 light flashes were reported in the SAA region. The first stage of the Sileye experiment can be considered as methodical in many respects. In our experiment a rather small growth of registration of LF rate in the SAA (about 2 σ) is observed while it is known that the proton flux in the SAA increases several order of magnitudes in comparison with the equator. The likely conclusion is then that protons are not the main LF source in orbit, and it seems more probable that heavy ions are the initiators. Some differences between the results from Skylab, Apollo-Soyuz and MIR could perhaps be explained with a combination of differences in altitudes, shielding and changes of the solar activity. The latter could possibly also explain why the same subjects see less LS's during the 1995 on MIR than a couple of years ago. but if the tentative conclusion above is correct, it should imply that there was a smaller flux of heavy ions on MIR on 1995 than around 1192-1993.

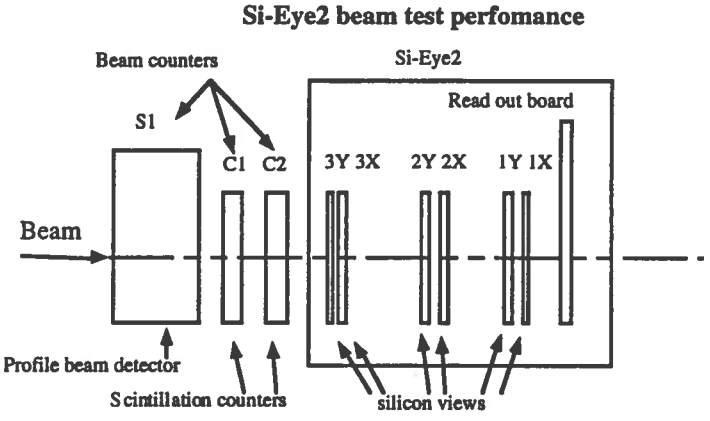

Fig. 2: Beam test set-up.

The experience gained working with Sileye has been used to develop several improvements in the new version of the apparatus (Sileye2). The new device has been developed as a complete software controlled particle detector, using the same geometry as is in the first Sieye but improving mechanics and computer interface. This new system monitors dark adaptation and reaction time and performs some reliability controls on device performances (like gain linearity, detector's noise). The astronaut uses a joystick to register light flashes in order to

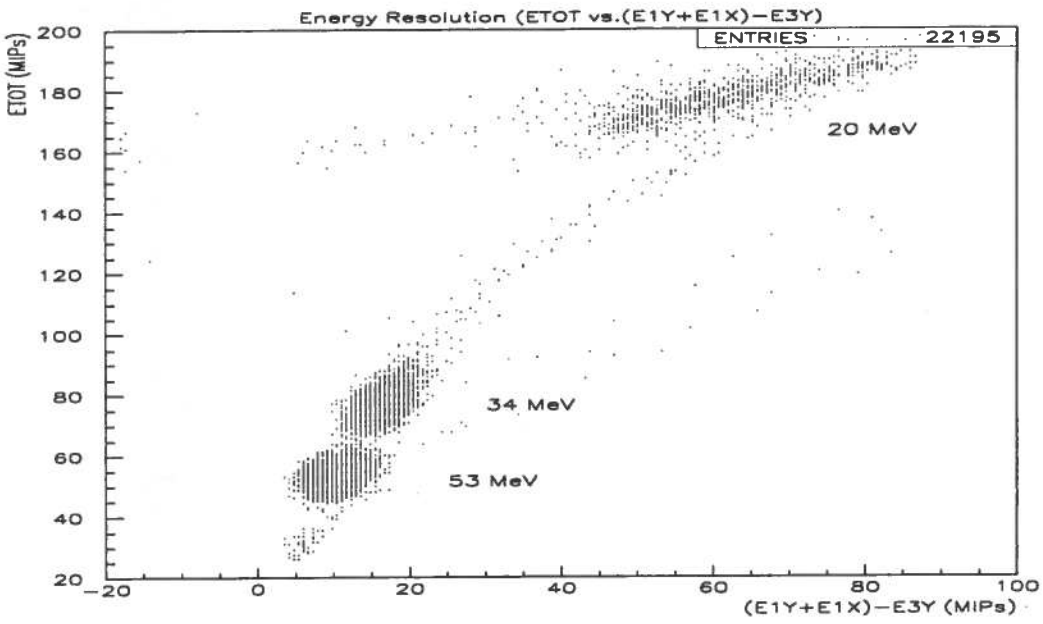

Fig. 3: Distribution of the total detected energy versus the difference between the energy loss in the last plane and in the first view.

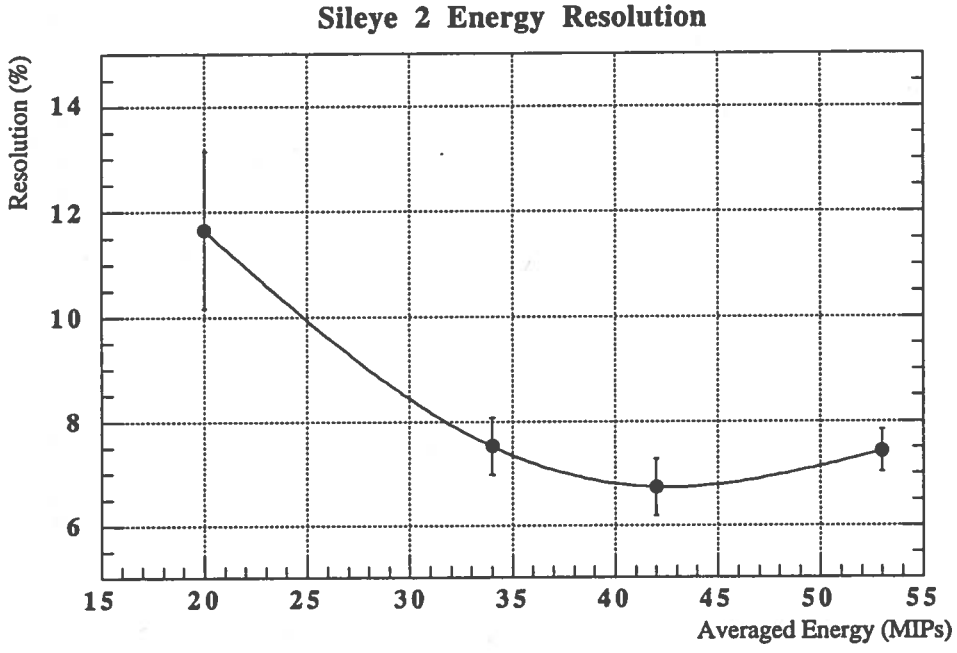

SILEYE2 BEAM TEST RESULTS

The calibration of the device SilEye2 was carried out on a proton beam from the CELSIUS storage ring at TSL, Uppsala. The device is intended for cosmic rays research, therefore there are special requirements for the beam. The basic requirements are a low intensity of the beam, which means not more than 20 particles per second ($\leq$ 20 Hz) and a low background radioactivity level in the beam room. The measurements were done at two different proton energies: 48 MeV and 70 MeV. The detector beam set up is shown in Fig. 2. Different runs have been performed, some with aluminium absorbers, in order to have more different energies. In the 48 MeV runs, protons stop in 5th or 6th silicon detector with big energy losses up to 50 MIP. This feature is very useful for us, because the device is intended for investigations of low energy protons and nuclei in cosmic rays. Most of the calibration runs was performed with vertically incident particles.

In Fig. 3 the distribution of the total detected energy versus the difference between the energy lost in the last plane and in the first view is plotted. It can be seen that the protons' energies are very well separated.

In Fig. 4 the Energy resolution (R.M.S./E) of Sileye2 as a function of reconstructed proton energy is plotted. Only events with straight tracks in both views has been taken into account. This means events which have the hitted strips on the second plane in both views no more than one strip from the fitted line. Events with two or more hitted strips in one layer were excluded.

REFERENCES

W.Z.Osborne, L.S.Pinsky, J,V.Baily, "Apollo light flash investigations", Biomedical results of Apollo. NASA SP-368, p.355 (1975).

T.F.Budinger et al, " Light flash observations. Experiment MA-106", Apollo-Soyuz test project summary science report, NASA SP-412, p. 193 (1977).

R.A.Hoffman, L.S.Pinsky,W.Z.Osborne, J.V.Baily "Visual light flash observation on Skylab 4" Biomedical results from Skylab, NASA SP-377, p. 127-130, (1977).

G.G.Fazio, J.V.Jelley, W.N.Charman " Generation of Cherenkov light flashes by cosmic radiation within the eyes of the Apollo astronauts" Nature, 228, 260-264, (1970).

J.Fremlin, New Scientist 47, 42, (1970).

I.MacAulay, Nature 232, 421, (1971).

G.Horneck "Radiobiological experiments in space: a review" Nucl. Tracks Radiat. Meas., Vol. 20, 1, 188, (1992).

A. Galper et al., SilEye on MIR - first active detector for the study of Light Flashes in space., *Proceeding of the Sixth European Symposium on Life Sciences Research in Space, 17-21 June, Trondheim, Norway (1996).*

V.Bidoli et al., Experimental beam test of the SilEye2 apparatus, INFN/AE-97/09, 18 February (1997).

G. Barbiellini et al., A satellite born charged particle telescope for the study of cosmic ray nuclei, *XXIV International Cosmic Ray Conference, OG 10.3.11, v.3, p.607, Roma (1995).*

OG 10.2.9

STATUS OF THE PAMELA EXPERIMENT FOR THE STUDY OF COSMIC ANTIMATTER IN SPACE

O. Adriani[1], M. Ambriola[2], G. Barbiellini[3], L.M. Barbier[4], S. Bartalucci[5], G. Basini[5], R. Bellotti[2], D. Bergstrom[6], M. Boezio[3], V. Bonvicini[3], F.M. Brancaccio[1], U. Bravar[3], F. Cafagna[2], R. Cardarelli[7], P. Carlson[6], M. Casolino[7], M. Castellano[2], G. Castellini[1], E.R. Christian[4], F. Ciacio[2], M. Circella[2], R. D'Alessandro[1], A.J. Davis[8], G. De Cataldo[2], C.N. De Marzo[2], M.P. De Pascale[7], T. Francke[6], C. Fuglesang[6], A.M. Galper[9], F. Giannini[7], N. Giglietto[2], M. Hof[10], S.V. Koldashov[9], M.G. Korotkov[9], J.F. Krizmanic[4], B. Marangelli[2], W. Menn[10], R.A. Mewaldt[8], V.V. Mikhailov[9], N. Mirizzi[2], J.W. Mitchell[4], A.A. Moiseev[9], A. Morselli[7], J.F. Ormes[4], J.V. Ozerov[9], P. Papini[1], A. Perego[1], S. Piccardi[1], P. Picozza[7], M. Ricci[5], P. Schiavon[3], S.M. Schindler[8], M. Simon[10], R. Sparvoli[7], P. Spillantini[1], P. Spinelli[2], S.A. Stephens[11], D.E. Stilwell[4], S.J. Stochaj[12], R.E. Streitmatter[4], F. Taccetti[1], A. Vacchi[3], V. Vignoli[1], S.A. Voronov[9], N. Weber[6], N. Zampa[3]

[1] *University and INFN, Firenze (Italy).*
[2] *University and INFN, Bari (Italy).*
[3] *University and INFN, Trieste (Italy).*
[4] *NASA Goddard Space Flight Center, Greenbelt (USA).*
[5] *Laboratori Nazionali INFN, Frascati (Italy).*
[6] *Royal Institute of Technology, Stockholm (Sweden).*
[7] *II University and INFN, Roma–Tor Vergata (Italy).*
[8] *Space Radiation Laboratory, California Institute of Technology, Pasadena (USA).*
[9] *Moscow Engineering and Physics Institute, Moscow (Russia).*
[10] *Siegen University, Physics Department, Siegen (Germany).*
[11] *Tata Institute of Fundamental Research, Bombay (India).*
[12] *Particle Astrophysics Laboratory, New Mexico State University, Las Cruces (USA).*

ABSTRACT

The PAMELA experiment is mainly devoted to the antiproton and positron flux measurements in cosmic rays, with large statistics in an energy range between 100 MeV and 100 GeV, and to the search for antinuclei, up to 30 GeV/n, with a sensitivity better than 10^{-7} in the $\overline{\text{He}}$/He ratio. The PAMELA telescope will be installed on–board of the russian Resurs–Arktika satellite to be launched in the 2000 for a mission at least 3 years long. The satellite orbit is polar, sun–synchronous and 700 km high: the peculiarity of this orbit will allow also to study several items in Astrophysics, Solar–Physics and Earth–Physics. In this paper the status report of the PAMELA project is presented.

INTRODUCTION

The PAMELA experiment (Adriani, 1995) is a part of the Russian Italian Mission (RIM) which consists of several space missions for different researches. The first step (RIM–0/1 and RIM–0/2) is the Si–eye–1/2 experiment, on board of the russian MIR Station, consisting of silicon sensors to study the particles producing light flash seen by astronauts. The RIM–1 studies low energy cosmic rays, by means of a telescope (called NINA, Barbiellini, 1995) made by 32 silicon detector planes, and it will fly in 1997 as "piggy–back" of the Resurs–4 russian polar orbit satellite. The RIM–2 mission is the PAMELA experiment and the RIM–3 project, called GILDA (Morselli, 1995), is also foreseen to

The main objectives of the PAMELA experiment are the accurate measurements of the antiproton and positron fluxes from 100 MeV to energies above 100 GeV and the search of antihelium with a sensitivity better than 10^{-7} in the $\overline{\text{He}}$/He ratio. In Table 1 are reported the expected rates in about 3 years. Profitting from the particular timing of the mission which covers the duration of the maximum activity of the 23rd solar cycle, additional research objectives can be addressed: solar modulation of cosmic rays in the heliosphere; solar flare particle spectra; distribution and acceleration of solar cosmic rays; stationary and disturbed fluxes in the Earth's magnetosphere; anomalous component of cosmic rays.

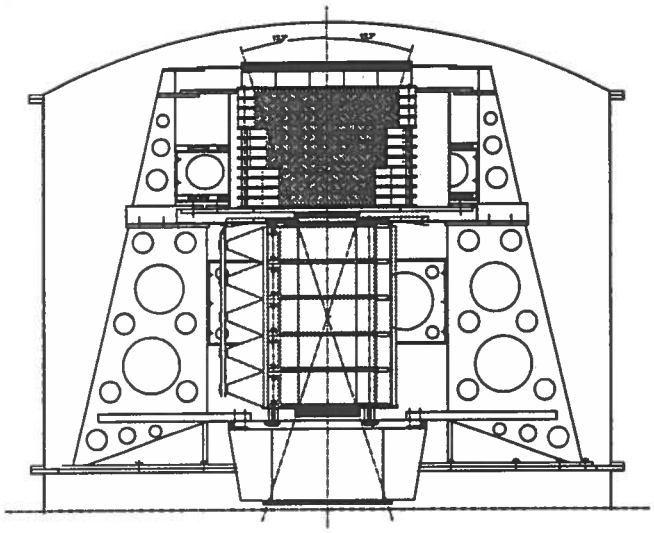

Fig. 1: The PAMELA telescope.

protons	3×10^8	antiprotons	$\geq3\times10^4$	electrons	6×10^6
positrons	$\geq3\times10^5$	He nuclei	4×10^7	Be nuclei	4×10^4
C nuclei	4×10^5	antinuclei limit	7×10^{-8}		

Table 1: Expected rates in PAMELA in 10^8s

THE PAMELA TELESCOPE

The PAMELA telescope (see Figure 1) is about 1 m high and consists of:

- a permanent magnet equipped with a tracker based on microstrip silicon detectors to measure the particle momentum;
- an imaging calorimeter consisting of silicon detectors and tungsten absorbers to measure the energy released by the particles and to identify their nature by their interactions inside the calorimeter volume;
- a Transition Radiation Detector (TRD) to identify electrons and positrons;
- a plastic scintillator system to give the first level trigger and the time of flight of the particles through the telescope;
- several scintillation anticoincidence counters surrounding the magnet for a better magnet entrance definition and for shielding the tracker from particle showering in the magnet itself.

The Maximum Detectable Rigidity (MDR) is 400 GV/c, the geometric factor of the experiment is about 21 cm^2 sr, the weight is less than 400 kg and the electrical consumption less than 300 W.

PRESENT STATUS OF THE PAMELA PROJECT

The realization of prototypes is foreseen for each sub–detector and for the mechanical structure of PAMELA, to verify performances and space qualification requirements (vibrational, thermal and EMI/EM

about 21 cm^2 sr. The magnetic material used is the sintered Nd–Fe–B with large residual magnetic induction ($\sim$ 1.3 T). The field inside the spectrometer is 0.4 T in the center. Outside the spectrometer the field is screened by a ferromagnetic shield. At present one magnetic module has been built as prototype and tested. Both mechanical and magnetic performances gave results in agreement with expectations and in the next future the whole magnetic system will be manufactured. A view of the magnetic spectrometer is shown in Figure 2.

Inside the spectrometer are inserted six detector planes composed by 3 ladders, each made by 2 silicon sensors, 70×53.33 mm^2 and thickness of 300 μm, and by an aluminium oxide hybrid 5 cm long, containing the front end electronics. Each ladder is stiffened by means of 2 carbon fiber bars, precisely glued on the lateral sides of the ladder. This mechanical configuration minimizes the thickness of material crossed by the particles, reducing the effect of the multiple scattering in the momentum measurement, due only to the silicon sensor thickness. The mechanical simulation of vibration and shock on this structure during the launch phase shows a good behaviour and laboratory tests are in progress to confirm these calculations.

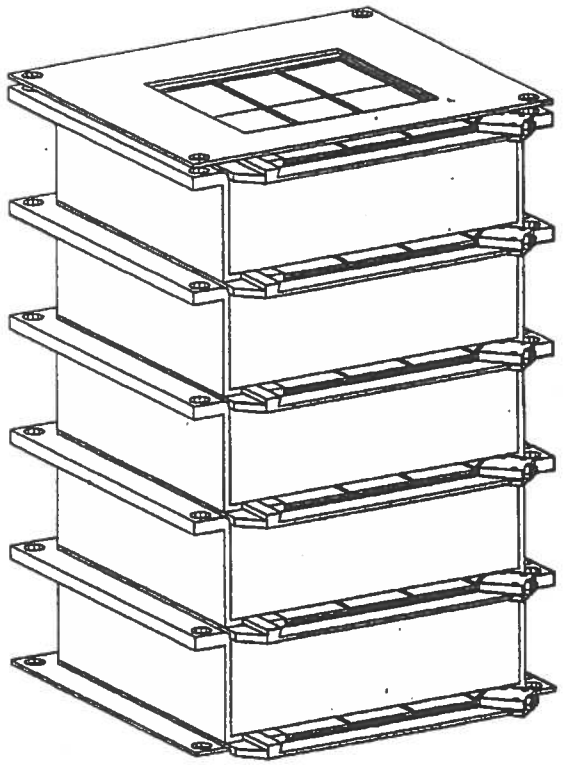

Fig. 2: The PAMELA spectrometer.

The silicon sensors are double sided double metal AC coupled, to avoid the use of external decoupling capacitors and kapton fanout. The p^+ strips are used to measure the X coordinate to have the best spatial resolution on the bending plane; the implantation pitch is 25 μm, and the readout pitch 50 μm, taking advantage of the capacitive coupling between adjacent strips. On the ohmic side the implant pitch is 67 μm with the double metal strips parallel to the junction's ones. The total number of readout lines in one ladder is 2048 and, for the whole tracker, we have 2048×3×6=36864 channels.

As a preliminary study, during november 1996, a system composed of three ladders completed by their electronics was exposed into a beam test at the PSI using MIP pions and non–MIP protons. The observed performances are well inside the requirement of the PAMELA experiment. In particular the signal to noise ratio is about 30 in the bending view and 20 in the non–bending view. With these detector characteristics the spatial resolution in the bending view will be equal or better than 7 μm (value required by the PAMELA project) resulting in a MDR larger than 400 GV/c.

The Transition Radiation Detector

The TRD consists of 9 layers of straw tube modules interleaving carbon fiber radiators which fill completely the gaps between the tubes. The whole detector is 270 mm high with 1024 total number of channels. The carbon fiber density is fixed to 60 g/l and the straw tubes are 300 mm long, with a di-

TRD results better than 30.

The calorimeter

It is a sampling calorimeter made of silicon sensor planes interleaved with tungsten absorbers. In Figure 3 is shown the modularity configuration of the PAMELA calorimeter. The external calorimeter dimensions are 484×483×204 mm^3. The sensitive area of one detector plane is 240×240 mm^2 and it consists of a 3×3 matrix of single sided silicon detector 80×80 mm^2, each one divided in strips with a pitch of 3.6 mm. This high granularity permits a very good path reconstruction of the particle energy released in the calorimetric volume. The thickness of the silicon sensors is 380 μm and that of the absorber tungsten layers is 2.3 mm corresponding to 0.7 X_0. The whole calorimeter is made of 46 detector layers (23 for the X view and 23 for the Y view) and 22 absorber layers. The performances of this kind of calorimeter in particle identification and energy measurement have been well studied using both beam test and balloon flights experiments in the context of the WIZARD balloon program (Bocciolini, 1996). An accurate simulation of the described calorimeter has been performed by tuning the simulated parameters with the real data. The main results of this simulation are a resolution in the electron and positron energy measurement better than 5% in the range 20–100 GeV (and ~6.5% at 250 GeV) and a rejection power of protons and electrons in the positron and antiproton identification better than 10^4.

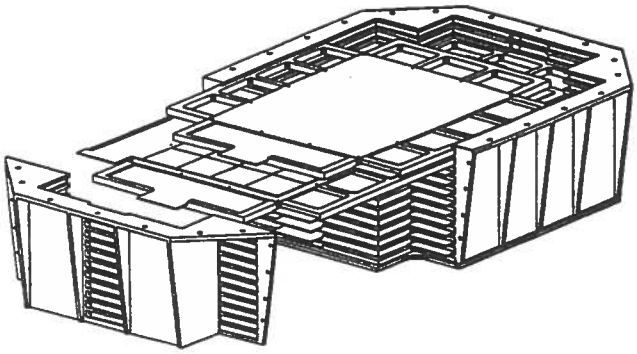

Fig. 3: Main structure of the calorimeter

CONCLUSIONS

The work for the PAMELA telescope construction is in progress and the flight is already scheduled and guaranteed by agreement. The characteristics of the experiment and of its orbit give a good opportunity to study many items of cosmic rays physics and in particular to study accurately the positron and antiproton fluxes in a large energy range. In Figure 4, as an example, is shown the antiproton identification capability of PAMELA compared with the main background duo to electrons. Analogous situation exist for the rejection of protons in the positron identification. The 3 years flight duration foreseen for the Resurs–Arktika satellite will allow to gather enough statistics to measure the antiproton and positron fluxes up to energies larger than 100 GeV.

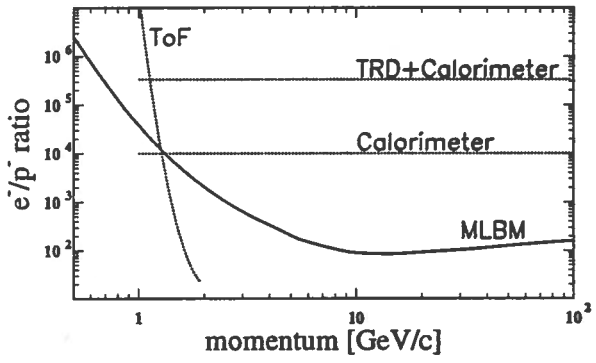

Fig. 4: PAMELA electron rejection power in the $\bar{p}$ measurement compared with the expected cosmic ray ratio of $e^-/\bar{p}$ from the Modified Leaky Box Model. The PAMELA apparatus is enable to well discriminate the antiproton component in all the energy range.

REFERENCES

Adriani, O., Alpat, B., Barbiellini, G. et al., Proc. 24th ICRC, 3, 591 (1995).

Durban 1997 XXV ICRC OG 10.5.8, Vol.5

ON BOARD NEURAL NETWORKS FOR PAMELA COSMIC RAY SPACE EXPERIMENT ON SATELLITE

M.Castellano for the PAMELA Collaboration

Istituto Nazionale di Fisica Nucleare, Sezione di Bari, Bari, Italy

ABSTRACT

Intelligent systems are required to make more reliable scientific and technological payloads carried on board of space facilities like balloons, spacecraft and satellites.

The PAMELA cosmic ray space experiment is the second and central step of the Russian Italian Mission program which will fly on board of a Resource series satellite to study the antimatter component of cosmic rays.

From one years ago has been activated a working group for the study of a PAMELA intelligent system based on neural network paradigms.

Its aim is to provide an high performance computing to both real-time event classification for the second level trigger and on board data filtering for scaling event rate to match the communication channel bandwidth.

In this paper the level-2 trigger organization for the PAMELA experiment is addressed.

The classification model based on the feed-forward neural network or CMNN is taken into account and some neural network technological solutions are investigated.

Finally, results about the CMNN simulation using physics data and generated pattern are shown.

INTRODUCTION

The measurement of cosmic ray p^- or e^+ requires that each singly-ionized particle result in a trigger. Further, it requires that either on-board particle identification be implemented or vast amount of data be taken for later analysis. The last case means that every particle that traverses the instrument results in transmission of data to the ground. The background of charged particles is high (proton of inner radiation belt, electrons of outer radiation belt). The second level trigger will be organized on the basis of fast handling of data from the detectors. It serves for rejection of part of detected protons, decreasing the dead time of the instrument and saving the useful volume of memory against storing uninteresting events. The main goals of the second level trigger of Pamela (L2) are to reject with very high efficiency a large amount of the background as no interacting protons, define a priority stream of event types (software second level trigger) for the transmission of the event to the ground.

Pamela experiment proposes an on-board particle identification system based on artificial neural network. After the L2 trigger, the data are all read out into the data acquisition system. Further event filtering and/or data reduction can be performed after event building.

The ability of artificial neural network (ANN) to perform a real-time classification with high background rejection has led to explore the ANN-based technology in high energy physics experiments (Lindsey, 1992, Denby, 1995, Balbanza, 1995). The ANN-based technology take advantage by the highly parallel processing architecture of the system which permits to carry out the tag of the incoming event in a very short time.

The idea of developing signatures for the dominant background (mainly protons and

applied for signal/background discrimination in the TS93 (Bellotti and Castellano et al. 1995) and CAPRICE flights (Bellotti and Castellano et al. 1996).
For both experiments has been used strictly feed forward NNs that are suitable for hardware implementations. Nowadays several ANN hardware are available, based both on analog and digital chips, with computational time of about nsec and μsec, respectively. It enables the ANN technological solutions to operate in trigger mode in HEP experiments.

The second level trigger for PAMELA experiment using ANN is addressed in the follows introducing some neural network trigger hardware solutions and the trigger organization.

NEURAL NETWORK TRIGGER HARDWARE

The ANNs analog implementation increased of a considerable factor the speed with respect to the digital ones. However we prefer the digital implementation because both of their intrinsic stability and the time-scale suitable for the PAMELA second level trigger. At the aim we propose to take into account two digital solutions, both of them supported by specific INFN R&D experiments and currently under test at the NN Laboratory of INFN-BARI.

MA16 solution

The MA16 is a digital microprocessor of systolic type supplied by Siemens as a prototype. It has 16-bit precision for the input and output and has an internal precision of 48 bits. Its clock frequency can reach up to 70 MHz. It requires external storage for the neural weights, the transfer function and the controller. A MA16 board, accommodating 16 input variables and a 2-layer feed-forward neural network with a maximum of 16 hidden nodes, can have a response time of 5.2 μsec at 50 MHz. The number of the input variables and of the weights can be increased, with a corresponding increase of the response time.

TOTEM solution

TOTEM is a digital VLSI parallel processor for fast learning and recognition with artificial neural networks. Its architecture is optimized for the implementation of the Reactive Tabu Search learning algorithm, a competitive alternative to back-propagation suited for VLSI implementation.
The main characteristics are:
-) Digital data stream, single-instruction multiple-data (SIMD) architecture;
-) 32 fixed-point fully-parallel multiply-and-accumulate processor (MACs)
operating in parallel with 3-stage pipeline;
-) Limited word width for econimical layout:
16-bit data, 8-bit weights, 32-bit results;
-) Simple interface with input data, output data, memory address and control buses. The chip can operate as a coprocessor in microprocessor systems;
-) Performance of 1000 million multiply-and-accumulate operation per second with 32 MHz clock. A multi-layer perceptron with 16-16-1 topology can be evaluated in about 2μsec. Higher performance can be achieved by paralleling up to four chips per network level to implement neurons with up to 128 inputs.

TRIGGER ORGANIZATION

The organization of the L2 must take into account the overall trigger rates (table 1) and physical information carry out by the detectors of the PAMELA experiments (table 2).

Table 1. Overall trigger rate of the PAMELA experiment

Level	Maximum Input Rate	Maximum Output Rate	Max. Decision Time
1	100 Hz	10 Hz	~ 50 nsec
2	10 Hz	1 Hz	~ 1 msec

Table 2. Features carry out by the detectors of PAMELA to be used for the neural network second level trigger

Detector	p	p^-	nuclei	e^-	e^+
TRACKER	posit. curv.	negat. Curv.	posit. curv.	negat. curv.	posit. curv.
CALORIM.	had.sh.-str.tr.	had.sh.-str.tr.	$dE/dx \propto Z^2$	el.mag.sh.	el.mag.sh
TRD	few hits	few hits	few hits	many hits	many hits

TEST RESULTS

Signals by the main detectors to be employed in PAMELA experiment have been taken into account for the study of the PAMELA L2: the tracker. the transition radiation detector (Barbarito et al. 1995) and the silicon-tungsten calorimeter (Bocciolini et al., 1996). Results here presented has been computed on data sets available by MC simulation codes, test beam and TS93 experimental data.

Tracker trigger

The output produced by the tracker detector can be seen as a grey-level image which record the energy released in each silicon strip. This data structure, with geometrical information inside can be efficently handled with a NN to speed up the rigidity recognition task.

The design strategy of the recognition algorithm is based on the template matching techniques. The neural network technological solution here proposed consists of the adaptive linear threshold units, organized in an input and output layer with feed-forward interconnection between them. The first layer is the incoming image while the last one is splitted in several template planes to provide the rigidity of the particle (Castellano, 1991). The performance of the algorithm is currently under study, using simulated data.

TRD trigger

A NN algorithm has been applied in order to distinguish positrons from protons in the TRD. In this approach several different representation of the TRD data has been introduced and their application in the L2 has been considered (Bellotti and Castellano et al. 1993, 1994). In our approach two novel representations of the TRD data are introduced, using spatial and energy information as input to the NN simultaneously. The first representation produces a structural description of the TRD data in a N-dimensional information space (Bellotti and Castellano et al. 1993) consisting of the total number of hits detected by each TRD's plane. The second one describes the TRD data by means a suitable template matrix which locates, using a cross-correlation algorithm (Rosenfeld and Kak, 1989) the spatial window where the event falls into.

TRD L2 trigger algorithm is based on the set of TRD information which consists of the total number of hits (or the total charge) detected by each TRD plane. This description ensures a good

Calorimeter trigger

The main goal of the calorimeter trigger is to reject the large portion of background protons. It mainly consists of no interacting protons which produce straight tracks. Moreover a signature of the interacting protons could be carried out using the recognition of the hadronic showers.

The set of calorimeter information selected for the L2 consists of the total number of fired strips and the total energy, released by each calorimeter plane. This description ensures a good degree of accuracy to identify and reject no interacting proton events, a very simple pre-processing phase to build up the variables to fed as input to the L2, a dimensionality of the calorimeter pattern space suitable to be handled by the neural network trigger. The recognition of hadronic shower could be achieved by exploiting the different longitudinal and lateral energy deposit profiles of the showers using variables as the total energy released in the whole calorimeter, the total number of fired strips in the whole calorimeter, the total number of fired strips inside a cylinder of radius equal to 4 Moliere radius around the track, the total number of fired strips inside a cylinder of radius equal to 1 Moliere radius around the track, the total energy released in a cylinder of radius equal to 1 Moliere radius around the track, the maximum energy released in a single strip, the total energy released in the two plane of maximun interaction, the medium distance between the most separated strips in each plane. The performance of the algorithm (Bellotti and Castellano et al. 1994, 1995, 1995a) are shown in table 3.

Table 3. Performances obtained in the selection of signal events using NNs

Experiment	Detector	S	B	Energy Range	Variables	Rejection (ε=90%)
Test Beam	TRD	e^-	π	1-5 GeV	10	~250
Test Beam	TRD	e^-	π	1-5 GeV	50	~500
TS93	TRD	e^-,e^+	p	5-50 GeV	10	~20
TS93	SiCal	e^-,e^+	p	5-50 GeV	10	~200
CAPRICE	SiCal	p^-	e^-	1.2-4 GeV	10	~900

REFERENCES

Baldanza, C. et al., NIM, A361, 506, (1995).
Barbarito, E. et al., NIM, A357, 588, (1995).
Bellotti, R., Castellano, M., De Marzo, C. et al., CPC, 78, 17, (1993).
Bellotti, R.; Castellano, M., De Marzo, C. et al., NIM, A350, 556, (1994).
Bellotti, R., Castellano, M., Candusso, et al., in Proc. of 24th ICRC, ed. Argalia, 3, 730, (1995).
Bellotti, R., Boezio, M., Castellano, M. et al., NIM, A381, 413, (1996).
Bocciolini, M. et al., NIM, A370, 403, (1996)
Castellano, M. et al., in Computing in High Energy Physics, ed. Univ. Acad Press, Tokyo, (1991).
Denby, B. et al., NIM, A356, 485, (1995).
Lindsey, C.S. et al., NIM, A317, 346 (1992).
Rosenfeld, A., and Kak,A.C., in Digital Picture Processing, ed. Accademic Press, (1989).

OG 10.5.10

NEURAL NETWORK IDENTIFICATION OF COSMIC RAY ANTIPROTONS IN THE WIZARD/CAPRICE EXPERIMENT

R. Bellotti for the WIZARD/CAPRICE Collaboration

Dipartimento Interateneo di Fisica dell'Università di Bari and INFN, Sezione di Bari, Italy

ABSTRACT

A data analysis based on an artificial neural network classifier is proposed to identify cosmic ray antiprotons detected with the CAPRICE silicon-tungsten imaging calorimeter against electron background in the energy range 1.2-4.0 GeV. A set of new physical variables, describing the events inside the calorimeter on the base of their different patterns, are introduced in order to discriminate between hadronic and electomagnetic showers. The ability of the artificial neural network classifier to perform a careful multidimensional analysis gives the possibility to identify antiprotons with an electron rejection 408 ± 85(stat) at 95.0 ± 0.2 (stat)% of signal detection efficiency. The high accuracy achieved by this method can improve substantially the efficiency in the evaluation of the cosmic ray antiproton spectrum.

INTRODUCTION

The study of cosmic ray antiprotons ($\bar{p}$) is of fundamental astrophysical interest. Detailed measurements of the $\bar{p}$ energy spectrum provide a crucial test of models describing $\bar{p}$ origin and propagation in the interstellar medium (Stephens and Golden, 1987). Since their discovery in 1979, by two independent balloon-borne experiments (Golden et al., 1979 - Bogomolov et al., 1979), the cosmic ray $\bar{p}$ measurement remains a difficult experimental task (De Marzo,1986). The energy region explored so far, which spans the interval from 0.2 to 20 GeV approximately, is limited and the statistical significance of the flux and $\bar{p}/p$ ratio needs futher improvements.

The CAPRICE balloon-borne experiment (Golden et al., 1992) has been devoted to measure the flux of low-energy antiprotons, positrons and light isotopes in the cosmic radiation. It was flown by a stratospheric balloon on 8-9 august 1994 over northen Canada and it collected data during more than 21 hours at a floating altitude less than 5 g/cm^2. The detector system employed consists of: (1) a superconducting magnet, equipped with multiwire proportional chambers and drift chambers, used as spectrometer; (2) a set of plastic scintillators providing trigger, time-of-flight and absolute charge measurements; (3) a Ring Imaging Cherenkov (RICH) as a β selector and (4) a silicon-tungsten imaging calorimeter to identify different particles according to the topological and energetic patterns of their interactions.

Nowadays many procedures currently used in high energy physics - from off-line data analysis to real time pattern recognition (triggering) - are performed applying neural network (NN) techniques. In particular, the Wizard Collaboration use neural network techniques to classify particles observed with balloon-borne cosmic ray experiments (Bellotti et al., 1995 - Wizard Coll., 1996). NNs are particularly apt to classify complex phenomena and provide robust and reliable methods to design efficient and fast systems for particle identification systems.

In this paper we study the antiproton/electron discrimination capability of the CAPRICE silicon-

and electromagnetic showers, several discriminating variables have been introduced. The ability of NN algorithms to perform a careful multidimensional analysis allows to take into account a large number of discriminating variables in order to exploit the difference between hadronic and electromagnetic showers. As a result a very high antiproton identification efficiency has been achieved.

DISCRIMINATING VARIABLES

The CAPRICE silicon-tungsten calorimeter, positioned at the bottom of the balloon payload, is composed of 8 silicon planes, sensitive both in the X and Y coordinates, each interleaved with one radiation lenght (=3.5 mm) of tungsten, for a total calorimeter thickness of seven radiation lengths. The sampling layer of the calorimeter is an array of 8 x 8 pairs (X-Y) of detectors (6 x 6 cm^2, divided in 16 strips, each 3.6 mm wide). Each sampling layer consists of two arrays having 128+128 readout channels. A built-in system equipped with ADCs and digital processors accomplishes the data acquisition.

An electromagnetic shower developing in tungsten consists of a cascade of photons producing $e^{\pm}$ pairs producing photons in turn. Due to the pair production threshold of order a few MeV, even photons or electrons of energy quite less than 1 GeV can initiate such a shower. As a rule, all massive particles in the e.m. shower ($e^{\pm}$) are relativistic and the general shape of the shower volume is a well defined cone with vertex in the first interaction point and a small aperture angle. The transversal development of an e.m. shower is quite regular and is well described by the Molière theory: the 99% of an e.m. shower, at any energy, is contained in a cylindrus of ratio R=3,5 RM, where RM is the Molière radius whose value is fixed for each material (0.69 cm for tungsten). Quite different is the behaviour of the particles inside a hadronic shower, usually initiated by a proton or an antiproton. Here the cascade is mainly due to strong interactions with tungsten nuclei; its volume is not so well defined and secondary particles at large angles may be present.

In the CAPRICE calorimeter the antiproton/electron recognition is achieved by exploiting the different longitudinal and lateral energy deposit profile of electromagnetic and hadronic showers. To this end, some discriminating variables have been defined for the detected events describing their energy and the number of hits along with other information on the shower development patterns.

These variables are as follows:

(1) The total energy released in the whole calorimeter.
(2) The total number of fired strips in the whole calorimeter.
(3) The total number of fired strips inside a cylinder of radius equal to 4 Molière radii, around the track direction.
(4) The total number of fired strips inside a cylinder of radius equal to 1 Molière radius, around the track direction.
(5) The total energy released in a cylinder of radius equal to 1 Molière radius, around the track direction.
(6) The maximum energy released in a single strip in the whole calorimeter.
(7) The total energy released in the two plane of maximun interaction, i.e. having the higher energy deposit.
(8) The medium distance between the most separated fired strips in each plane.

Even though other possible variables could be introduced, our experience and the results here presented show that the 8 variables defined above rappresent a set particularly good for a multidimensional analysis of the event patterns in the CAPRICE calorimeter.

EXPERIMENTAL RESULTS

To evaluate the antiproton/electron discrimination capability of the CAPRICE calorimeter, using the

the real silicon-tungsten detector.

The calorimeter response has been studied for electrons and antiprotons at momenta of 1.2, 1.6, 2.0, 2.1, 2.6, 3.0, 3.1, 3.6, 4.0 GeV/c; particles (samples of 1000 events for each energy) hit the calorimeter orthogonally, at the center of the first plane. After a number of optimisations, the GEANT energy cut has been fixed at 10 keV; this means that GEANT follows a secondary particle until its energy is above or equal this value, then drops it out. For each active silicon strip, a threshold corresponding to an energy of 0.7 mips (minimum ionising particle energy, fixed to 95 keV) has been imposed to reproduce the real data analysis procedure that separates the noise of the electronics from the signal and eliminates it.

For the multidimensional analysis of the calorimeter events a three-layered feed-forward neural network has been considered (Hertz et al., 1991). It consists of units (formal neurons) arranged in contiguous layers. Each neuron k ($k = 1, \ldots, N_h$) belonging to the hidden layer receives as input the output X_l ($l = 1, \ldots, N_i$) of all the l neurons of the input layer, to which it is connected by $w_{lk}^{(1)}$ synaptic strengths. On the other hand, the neuron k is also connected, with strengths $w_{ki}^{(2)}$, to the neuron of the output layer. The transfer function of the neurons is the sigmoid funtion.

The synaptic matrix $W^{(old)}$ is trained by showing to the network a data set of examples (training data set) and updating the weights according to the delta rule, which minimizes the mean squared error function E of the classification system (Hertz et al., 1991). After each training epoch, the quality of the new model $W^{(new)}$ is estimated by means of an independent data set (test data set). The learning session is stopped when the error function E, evaluated on the test set, reaches its lowest value. The training and stopping procedures are unbiased general criteria to build up a classification system in an accurate way.

From the point of view of data analysis each input neuron is associated with a physical variable. Therefore the NN enables one to explore a multidimensional input space by taking into account several complex information about the physical event. The set of discriminating variables introduced are fed to the artificial NN described, together with the rigidity of the event measured by the spectrometer. Moreover this procedure enables to correlate automatically the rigidity of the particle with the different behaviour of the discriminating variables in different parts of the energy spectrum.

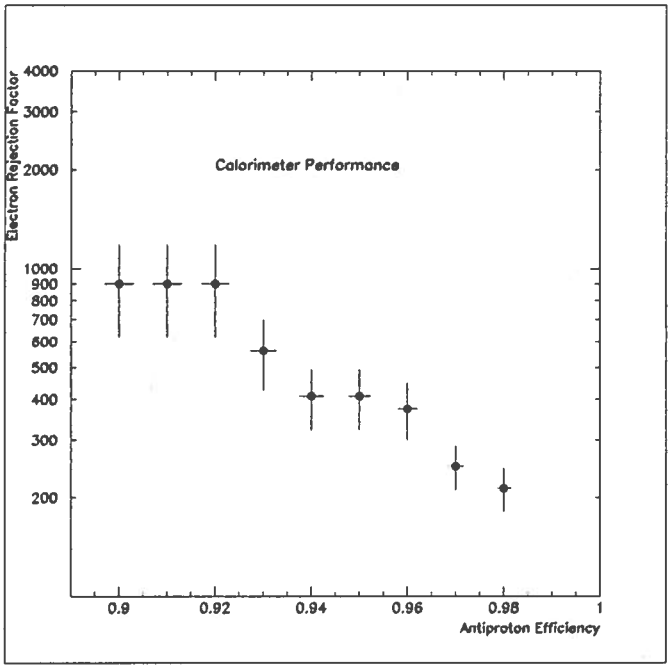

Fig. 1: Electron rejection factor evaluated for different antiproton signal efficiency by the neural network on simulated data.

For the purpose of evaluating the discrimination capability of the CAPRICE calorimeter its performance has been investigated in simulation using the multidimensional classifier above described. Per

A critical step has been to find the best NN architecture, where the number of hidden neurons is considered optimal when it is large enough to ensure a high degree of classification and small enough to ensure a high degree of generalization. The experimental evidence on the independent test set has shown that the best performance are obtained with five hidden neurons, even though a difference of a few percent only is obtained using a number of hidden neurons ranging from 3 to 20. The electron rejection as a function of antiproton efficiency is shown in fig. 1. This result is one order of magnitude better than those achived by means of mono- and bi-dimensional cuts on the chosen discriminating variables (Bocciolini et al., 1991).

CONCLUSIONS

In this paper a classification system based on a neural network is proposed to identify antiprotons detected by the CAPRICE calorimeter. Results show that the neural network classifier is capable of discriminating between antiprotons and electrons with very high efficiency. Specifically, the data analysis method here proposed permits to identify antiprotons with an electron background rejection of 408 $\pm$ 85(stat) at the efficiency of 95.0 $\pm$ 0.2 (stat)%. This result is particularly useful in the context of balloon-borne experiments where, in searching rare events with the constraint of short exposure time, a detection efficiency as large as possible is required. The neural network based analysis presented here will be used to improve the evaluation of the energy spectra of cosmic ray antiprotons in the CAPRICE experiment.

REFERENCES

Bellotti, R. et al., Proc. of 24th International Cosmic Ray Conference, 3, 730 (1995).

Bocciolini, M et al., Nucl. Instr. and Meth. A, 370, 403 (1996).

Bogomolov, E.A. et al., Proc. of 16th International Cosmic Ray Conference, 1, 330 (1979).

Brun et al., Detector description and simulation tool, CERN program library.

De Marzo, C.N., "Antiproton measurements and antinuclei search", Proc. of Workshop on Frontier objects in astrophysics and particle physics; Vulcano, Italy, june 1996, in press.

Golden, R.L. et al., Phys. Rev. Lett. 43, 1264 (1979).

Golden, R.L. et al., Proposal to NASA NRA-92-OSSA-10.

Hertz, J. et al., Introduction to the Theory of the Neural Computation, Addison-Wesley, (1991).

Stephens, S.A. and Golden R.L., Space Science Rev., 46, 31 (1987).

Wizard Collaboration, Astroparticle Physics, 5, 111 (1996).

HE 3.1.1

A MEASUREMENT OF THE μ^+/μ^- RATIO AT THE TOP OF THE ATMOSPHERE WITH THE CAPRICE EXPERIMENT

G. Barbiellini[12], G. Basini[4], R. Bellotti[1], M. Bocciolini[3], M. Boezio[10], U. Bravar[12], F. Cafagna[1], P. Carlson[10], M. Casolino[8], M. Castellano[1], M. Circella[1], A. Codino[7], G. De Cataldo[1], C. De Marzo[1], M.P. De Pascale[8], N. Finetti[7], T. Francke[10], N. Giglietto[1], R.L. Golden[0,6], C. Grimani[7], M. Hof[9], W. Menn[9], J.W. Mitchell[5], A. Morselli[8], J.F. Ormes[5], P. Papini[3], A. Perego[3], S. Piccardi[3], P. Picozza[8], M. Ricci[4], P. Schiavon[12], M. Simon[9], R. Sparvoli[8], P. Spillantini[3], P. Spinelli[1], S.A. Stephens[2], S.J. Stochaj[6], R.E. Streitmatter[5], M. Suffert[11], A. Vacchi[12], N. Weber[10], N. Zampa[12]

[0] *Deceased*

[1] *Dipartimento di Fisica dell'Università and Sezione INFN di Bari, Bari, Italy,* [2] *Tata Institute of Fundamental Research, Bombay, India,* [3] *Dipartimento di Fisica dell'Università and Sezione INFN di Firenze, Firenze, Italy,* [4] *Laboratori Nazionali INFN, Frascati, Italy,* [5] *NASA/Goddard Space Flight Center, Greenbelt, Maryland, USA,* [6] *New Mexico State University, Las Cruces, New Mexico, USA,* [7] *Dipartimento di Fisica dell'Università and Sezione INFN di Perugia, Perugia, Italy,* [8] *Dip. di Fisica dell'Università and Sezione INFN di Roma, Tor Vergata, Roma, Italy,* [9] *Universität Siegen, Siegen, Germany,* [10] *Royal Institute of Technology, Stockholm, Sweden,* [11] *Centre des Recherches Nucléaires, Strasbourg, France,* [12] *Dipartimento di Fisica dell'Università and Sezione INFN di Trieste, Trieste, Italy*

ABSTRACT

We report on a new measurement of the μ^+/μ^- ratio R at the top of the atmosphere in the momentum range 0.2-2.3 GeV/c using the NMSU-WIZARD/CAPRICE balloon-borne magnetic spectrometer. Data was collected on 8-9 August 1994 following a launch from Lynn Lake, Canada. We find a constant value R=1.64±0.08 over the measured momentum range. This value is significantly higher than the corresponding value at ground and is in agreement with results of simulations. The result is of importance for the understanding of the production of neutrinos in the atmosphere and for the atmospheric neutrino anomaly.

INTRODUCTION

Data on atmospheric muons is an important tool for understanding the production of atmospheric neutrinos and also as a general constraint on simulation of hadronic air showers. Of particular interest is the recently much discussed atmospheric neutrino anomaly (Gaisser 1994, Gaisser et al., 1996), which refers to the observations, in some underground neutrino detectors, of either too many ν_e or too few ν_μ interactions as compared to simulations of the hadronic interactions in the atmosphere (Aglietta et al., 1989, Becker-Szendy et al., 1992, Fukuda et al., 1994, Daum et al., 1995, Allison et al., 1997). The ob-

is only about one third of that for neutrinos, the determination of the ratio of the production spectra of π^+ and π^- is very important. At small atmospheric depths, almost all pions decay and the observed charge ratio μ^+/μ^-, corrected for the decay kinematics, also represents the π^+/π^- ratio. We report in this paper on a new measurement of the μ^+/μ^- ratio at the top of the atmosphere in the energy range 0.2-2.3 GeV.

THE NMSU-WIZARD/CAPRICE EXPERIMENT AND EVENT SELECTION

The CAPRICE experiment used the NMSU-WIZARD/CAPRICE balloon-borne magnet spectrometer. It was designed to give excellent particle identification properties and the spectrometer was equipped with a solid radiator Ring Imaging Cherenkov (RICH) detector (Carlson et al., 1994, Barbiellini et al., 1996), a time-of flight (ToF) system, a tracking magnetic spectrometer (Golden et al., 1991, Hof et al., 1994) and a silicon-tungsten calorimeter (Bocciolini et al., 1996). The launch took place on 8-9 August 1994 from Lynn Lake, Canada (Lat. 56.5°N, Long 101.0°W) with a low geomagnetic cut off of 0.4 GV/c. Results on the e^+/e^- and the $\overline{p}/p$ ratios as well as on fluxes have been reported elsewhere (Barbiellini et al., 1996b, Boezio et al., 1997).

Data was collected during the 23 h float at an altitude corresponding to 3.9 g/cm^2 residual atmosphere. The combination of the RICH and the calorimeter made it possible to identify muons with very small background of other particles in the energy range 0.2-2.3 GeV. Since muons constitute a very small part of the flux of particles at the top of the atmosphere, it is very important to be able to discriminate against background particles with high rejection power. The identification of positive muons is particularly difficult due to the large flux of protons and two independent rejection methods are necessary. The time-of-flight scintillator system (ToF) has a resolution of about 280 ps which, with a particle trajectory of about 1.1 m, gives a good rejection of protons against lighter particles for momenta less than about 1.3 GeV/c. The ToF system scintillators were also used to reject higher charged particles, mainly alphas. Positive and negative muons were selected with the same criteria.

The Ring Imaging Cherenkov counter (RICH) rejects protons and higher mass particles from pions, muons and electrons over the range 0.1-2.5 GeV/c. We conservatively choose 2.3 GeV/c as the upper limit for the data reported in this paper.The RICH rejection power depends on the applied cuts (Weber 1997) and on the particle momentum. We estimate the rejection to be about 10^3 at 1.5 GeV/c, increasing with decreasing momentum. The proton threshold in the RICH is 1 GeV/c and below this the RICH is used as a threshold device. The threshold for muons and pions is about 0.1 GeV/c. The performance of the RICH is illustrated in Figure 1, where the Cherenkov angle is shown as a function of rigidity for positive particles.

The silicon-tungsten calorimeter is used in several ways. The thickness corresponds to 7 radiation lengths and it is an excellent electromagnetic shower detector. Above 500 MeV/c muons can be selected with an efficiency close to 100% with nearly no contamination from $e^{\pm}$ (Weber 1997). Protons below 0.4 GeV/c are unable to reach the calorimeter and to cross the full calorimeter a proton must have a momentum above about 0.8 GeV/c. For strongly interacting particles the thickness corresponds to about 0.3 interaction lengths.

RESULTS AND DISCUSSION

The measured μ^+/μ^- ratio is shown in Figure 2 as a function of the muon momentum. A total number of 1900 muons were observed in the range 0.2-2.3 GeV/c. Within errors the ratio is constant with an average value of 1.64 ± 0.08. This is significantly higher than the value of the ratio measured at ground

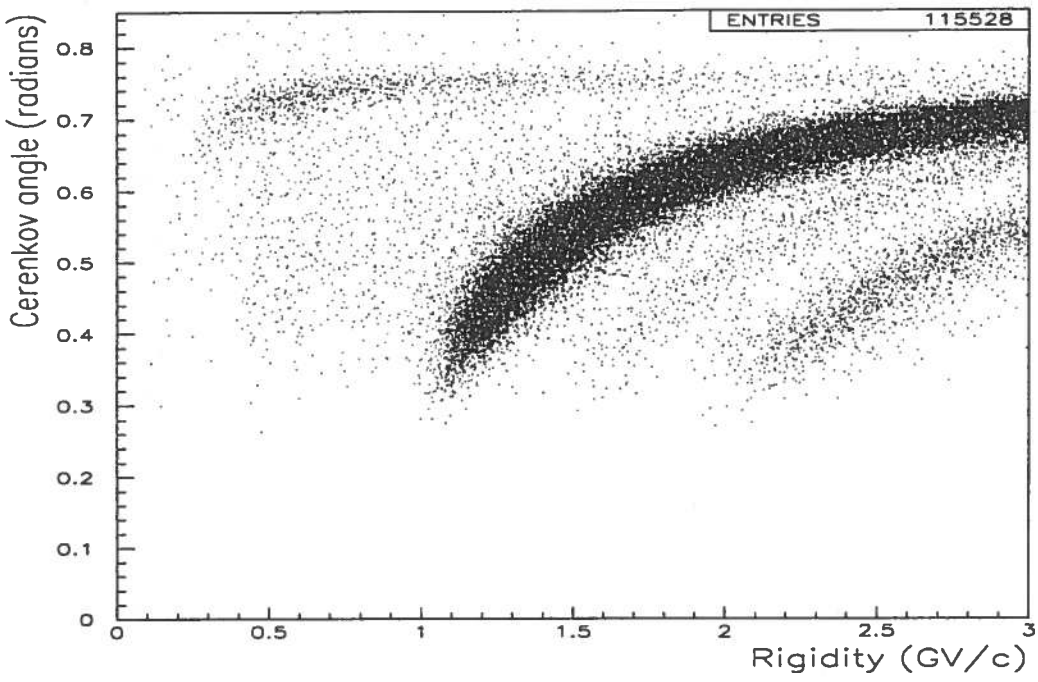

Fig. 1: Cherenkov angle as function of rigidity for positive particles. The calorimeter cut to eliminate positrons has been applied to the data and also a basic quality cut on the tracking and RICH data. 95% of the events are protons. Bands corresponding to muons and heavier particles (helium) are clearly visible.

for 0.42-0.47 GeV/c muons at a residual atmospheric depth of 3 g/cm^2 and an earlier magnetic spectrometer experiment (Bogolomov et al., 1979) gave 1.26±0.12 for the momentum range 0.4-1.4 GeV/c at an atmospheric depth of 11 g/cm^2.
New data from the MASS experiment (Brunetti et al., 1996) give an approximately constant value 1.27±0.05 of the μ^+/μ^- ratio over the momentum range 0.15-2 GeV/c. The data was taken at an atmospheric depth of 5.8 g/cm^2 from Ft. Sumner, New Mexico in 1991 (geomagnetic cut-off 4.5 GV/c).

The low energy μ^+/μ^- ratio is expected to depend on the geomagnetic latitude for the measurement. From the observed energy spectra of p, He and heavier nuclei (see Papini et al., 1996) one finds that the fraction of hadrons produced by He and heavier nuclei at 2 GeV/nucleon kinetic energy is about 29% during solar minimum rising to 35% at solar maximum. Above about 20 GeV this fraction decreases asymptotically to 23%. Thus, for a given geomagnetic cut-off, the contribution to hadron production from He and nuclei will increase below the proton cut-off energy. Since hadronic interactions of He and heavier nuclei on average give more π^- than protons, the μ^+/μ^- ratio will decrease with increased geomagnetic cut-off. The variation in the μ^+/μ^- ratio with solar activity, however, is expected to be less than 2.5% which is small compared to the measurement errors.

The μ^+/μ^- ratio observed in this experiment, 1.64±0.08, is in agreement with the calculations of Stephens (1981), who gives a value of the μ^+/μ^- ratio in the range 1.6-1.8 at 4.5 g/cm^2 of residual atmosphere. Finally we note that the ratio of the spectrum weighted moments for proton-air collisions,

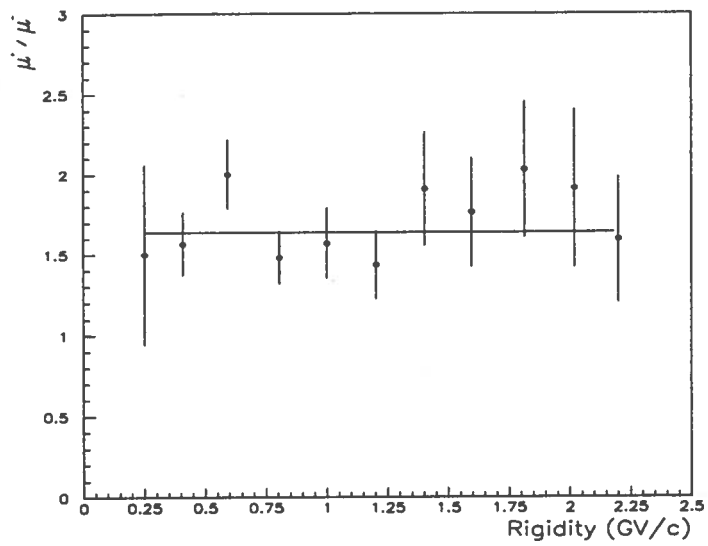

Fig. 2: The μ^+/μ^- ratio as a function of the rigidity. The straight line is a fit assuming a constant value for the ratio.

REFERENCES

Aglietta, M., et al., *Europhys. Lett.*, **8**, 611 (1989)
Allison, W.W.M., et al., *Phys. Lett.*, **B391**, 491 (1997)
Barbiellini, G. et al., *Nucl. Instr. Meth*, **A371**, 169 (1996a)
Barbiellini, G. et al., *Astr. Astrophys.*, **309**, L15(1996b)
Boezio, M. et al., *ApJ*, to appear Sept 97
Becker-Szendy, R. et al., *Phys. Rev.*, **D46**, 3720 (1992)
Bocciolini, M. et al., *Nucl.Instr.Meth.*, **A370**, 403 (1996)
Bogolomov, E. A. et al., *Proc. of the 16th ICRC* , **1**, 330 (1979)
Carlson, P. et al., *Nucl. Instr. Meth.*, **A349**, 577 (1994)
Brunetti, M.T. et al., *J. Phys. G*, **22**, 145 (1996)
Daum, K. et al., *Z. Phys. C*, **66**, 417 (1995)
Fukuda, Y. et al., *Phys. Lett*, **B335**, 237 (1994)
Gaisser, T.K., *Nucl. Phys. B Proc. Suppl*, **35**, 209 (1994)
Gaisser, T.K. et al., *hep-ph/9608253*
Golden, R. et al., *Nucl.Instr.Meth.*, **A306**, 366 (1991)
Hof, M., et al., *Nucl. Instr. Meth.*, **A345**, 561 (1994)
Krizmanic, J. F. et al., *Proc. of the 24th ICRC*, **1**, 690 (1995)
Papini, P., Grimani, C., & Stephens, S. A., *Il Nuovo Cimento*, **19**, 367 (1996)
Stephens, S.A., *Proc. 17th ICRC*, **4** , 282 (1981)
Weber, N., "A measurement of the antiproton and proton fluxes in the cosmic rays by the CAPRICE

HE 3.1.18

MEASUREMENTS OF THE COSMIC RAY MUON COMPONENT IN THE ATMOSPHERE FROM GROUND LEVEL TO BALLOON ALTITUDES

G. Basini[1], R. Bellotti[2], M. T. Brunetti[3], F. Cafagna[2], M. Circella[2], A. Codino[3], G. De Cataldo[2], C. N. De Marzo[2], M. P. De Pascale[4], N. Finetti[3], N. Giglietto[2], R. L. Golden[5], C. Grimani[3], M. Hof[6], J. W. Mitchell[8], A. Morselli[4], J. F. Ormes[8], P. Papini[7], S. Piccardi[7], P. Picozza[4], M. Ricci[1], M. Simon[6], P. Spillantini[7], P. Spinelli[2], S. A. Stephens[9], S. J. Stochaj[5], and R. E. Streittmatter[8]

[1]*INFN - Laboratori Nazionali di Frascati, Frascati, Italy.* [2]*Università di Bari and INFN, Bari, Italy.* [3]*Università di Perugia and INFN, Perugia, Italy.* [4]*Università di Roma "Tor Vergata" and INFN, Rome, Italy.* [5]*Particle Astrophysics Lab, New Mexico State University, Las Cruces, NM, USA.* [6]*Universität Siegen, Fachbereik Physik, Siegen, Germany.* [7]*Università di Firenze and INFN, Florence, Italy.* [8]*NASA - Goddard Space Flight Center, Greenbelt, MD, USA.* [9]*Tata Institute of Fundamental Research, Bombay, India.*

ABSTRACT

We have used the data collected by the NMSU/WIZARD balloon borne magnet spectrometer during the ascent phases of two flights to study the momentum spectrum and charge ratio of muons produced in cosmic ray showers in the atmosphere. The experiments were performed during the same maximum of solar activity in different conditions of geomagnetic cutoff. We have exploited the discrimination capabilities of the detector to select high purity samples of muons. The two analyses are here reviewed together, in order to illustrate the experimental approach and the data analysis procedures. A comparison of the two sets of results allows us to check the accuracy of the overall normalization of the measurements and to point out the effects of the different experimental conditions.

INTRODUCTION

The cosmic ray muon component has been long investigated in the past, even though the observations have mainly been performed at ground or at low altitude. The muon spectrum has been measured over a large interval of energy at ground and in underground experiments in an attempt to get clues both on the primary cosmic ray flux and on the particle interaction mechanisms in the atmosphere. Recently, the increasing evidence of the atmospheric neutrino anomaly has raised a renewed interest in cosmic ray muon measurements, which have been proposed by several authors as a powerful crosscheck for the neutrino flux calculations (e.g., Perkins, 1993; Gaisser, 1994).

Since muons continuously lose energy while propagating in the atmosphere and their probability of decay per unit atmospheric depth is a function of the altitude, it is important that such comparisons be performed on as wide a depth range as possible.

There have been very few attempts in the past to perform muon measurements at balloon altitudes. (Bogomolov et al., 1979; Basini et al., 1995; Krizmanic et al., 1995; Schneider et al., 1995; Bellotti et al., 1996; Brunetti et al., 1996; Circella, 1997). Out of these, the WIZARD collaboration has extensively studied the muon component in the atmosphere: We have used the data collected by our magnet spectrometer during the ascents of two balloon experiments to get detailed information on the altitude dependence of the muon momentum spectrum and charge ratio. Both these experiments were devoted to measurements of the primary antiparticle components of cosmic rays at different geomagnetic cutoffs, and neither the ascent profiles nor the instrumentations had been optimized for the

magnet spectrometer, which has been succesfully deployed by the WIZARD collaboration in several balloon flights. The spectrometer consisted of a single coil superconducting magnet and of a gas chamber tracking device. The magnet was operated at a current of 120 A and was able to produce a field of intensity 0.1–2 T in the region of the chambers. The tracking device was equipped with eight multiwire proportional chambers in the 1989 configuration; it was improved for the 1991 flight by adding two modules of drift chambers. The maximum detectable rigidity was about 120 and 170 GV, respectively for the 1989 and 1991 configurations. The spectrometer was complemented in both flights with a scintillator system, which gave the trigger for data acquisition and was used as well for time of flight and pulse height measurements. An additional layer of scintillator, of larger thickness, was provided in the 1989 flight. The particle identification was performed by means of a threshold gas Cherenkov detector and a streamer tube imaging calorimeter. The detector configuration was therefore basically the same in the two experiments, even though some improvements in the 1991 setup allowed to get higher event statistics and better particle discrimination capabilities at the same time. These improvements included: an increased geometric factor, higher reconstruction performances of the spectrometer, a higher efficiency of the calorimeter tubes and an improved light collection of the Cherenkov detector.

Table 1: Main sources of background for the muon measurements in the two experiments. TOF stands for time of flight. Spillover is relevant only for the 1989 flight; the correction was performed in the interval 8–40 GV. Rejection of protons, as well as of secondary pions from interactions in the apparatus, is relevant only for the 1991 flight.

Background	Selection	Residual contamination
e^-/e^+	no Cherenkov signal at less than 0.8 GV	$\leq 1\%$
albedo	$1/\beta$ from TOF ≥ 0.5	none
spillover	spillover subtraction	negligible
protons	TOF measurement at less than 1.5 GV	$\leq 1\%$
	Cherenkov selection in 5–15 GV	$\leq 1\%$ above 100 g/cm^2
atmospheric pions	–	$\leq 1\%$
atmospheric kaons	–	negligible
pions from interactions	consistency checks on the reconstructed tracks	negligible

MUON SELECTION AND BACKGROUND REJECTION

Muons were identified in both flights as singly charged particles, traversing downward the whole stack of detectors without interacting in the calorimeter. We used the spectrometer to measure the rigidity of the particles and to discriminate between particles of opposite charge. Even though the spectrometer in the 1991 configuration had multitrack capabilities, we only analyzed single muon events. Albedo particles were rejected by means of the time of flight measurement. We used the pulse height information from the scintillators to select singly charge minimum ionizing particles as well as to reject events caused by interactions in the apparatus. Muon events were also required to show a single clean track in the calorimeter, aligned with the extrapolated track from the spectrometer.

Further requirements were introduced to get rid of possible sources of contamination, as shown

than 100 g/cm^2. Table 1 shows the main sources of background for the muon measurements, along with the most effective rejection criteria and the estimated level of residual contamination. The good quality of the data is apparent.

Redundancy of the measurements is crucial both for a cross-check of the event selection and for the evaluation of the selection efficiencies. Figure 1 gives an illustration of this issue. More details on the selection of events and data analysis are reported elsewhere (Bellotti et al., 1996; Circella, 1997).

RESULTS AND DISCUSSION

Using the events selected in each flight, we have reconstructed the growth curves of negative muons in the momentum range 0.3–40 GeV/*c* with atmospheric depth ranging from the float altitude of 5 g/cm^2 down to the ground level and have studied the altitude dependence of the momentum spectrum. We have also explored the muon charge ratio at low energy in the 1991 flight (Basini et al., 1995). In Figure 2 we show the results on the altitude variation of the negative muon flux in different momentum intervals. These data illustrate one of the main conclusion of this study: Such curves do not scale with changing muon momentum. Lower energy muons are produced relatively higher in the atmosphere, and attenuate faster at atmospheric depths larger than the level of maximum flux. The momentum spectra at different heights are affected accordingly.

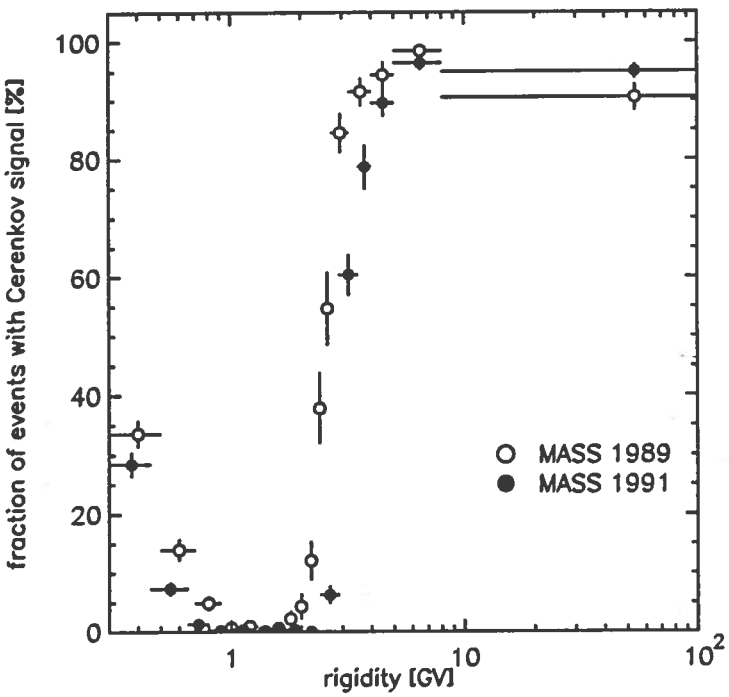

Fig. 1: Fraction of events with a Cherenkov signal from the sample of negative muon-like events selected by means of the calorimeter and the scintillators in the two experiments. The low-energy events showing a signal are interpreted as electrons misidentified in the calorimeter and removed from the analysis. Their number tends rapidly to vanish with increasing energy. Muons start to emit when their rigidity approaches the threshold for emission. The results in the figure show the effect of the different thresholds in the two experiments as well as the increased rejection capabilities for low-energy electrons in the 1991 flight. The dip at high rigidity in the 1989 data is interpreted as due to spillover events, subsequently removed from the sample.

As mentioned, the two experiments took place during the same maximum of solar activity at different geomagnetic locations, the vertical rigidity cutoff being about 0.65 GV in the 1989 flight and about 4.5 GV in 1991. The latter occurrence should be visible in Figure 2, in the sense that it should decrease in some way the low energy muon flux measured in the second experiment, especially at high altitude. The comparison of the data from the two flights shows in fact a deficit of very low energy muons, amounting to about 20% in the 0.3–0.53 GeV/*c* interval for atmospheric depths less than 100 g/cm^2, which may be interpreted as due to the higher suppression of low energy primaries in the second flight. In addition to this low

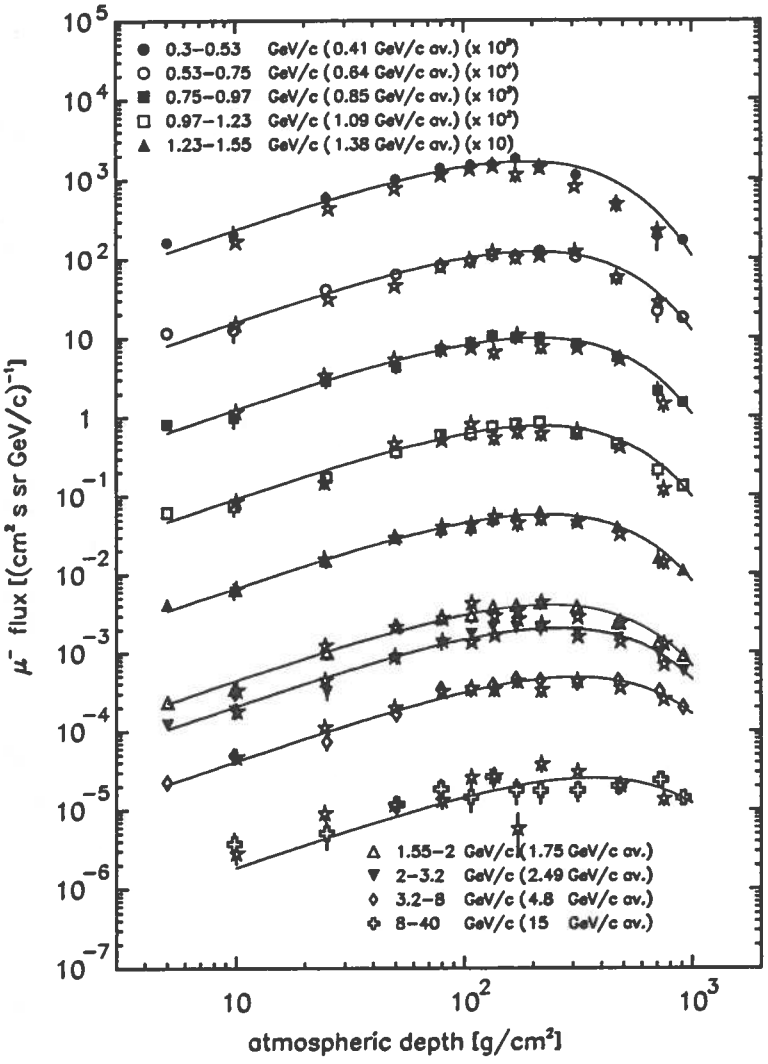

Fig. 2: Growth curves of the flux of negative muons in the atmosphere in the momentum interval 0.3–40 GeV/c. Results are shown from both flights, separately for the momentum bins indicated. The 1989 symbol code is as indicated. The 1991 measurements are marked by stars, and refer to the same momentum bin as for the closest set of the 1989 measurements. Some of the measurements have been scaled, as indicated. The measurements at the highest and lowest atmospheric depth are taken from De Pascale et al. (1993) and Brunetti et al. (1996), respectively.

REFERENCES

Basini, G., et al. (MASS collaboration), *Proc. 24th ICRC*, **1**, 585 (1996).
Bellotti, R., et al. (MASS collaboration), *Phys. Rev. D*, **53**, 35 (1996).
Bogomolov, E. A., et al., *Proc. 16th ICRC*, **1**, 330 (1979).
Brunetti, M. T., et al. (MASS collaboration), *J. Phys. G*, **22**, 145 (1996).
Circella, M., *Tesi di Dottorato*, Università di Bari, Italy (1997), in Italian.
De Pascale, M. P., et al. (MASS collaboration), *J. Geophys. Res.*, **98**, 3501 (1993).
Gaisser, T. K., *Phil. Trans. Roy. Soc. London*, **A346**, 75 (1994).
Golden, R. L., et al., *Nucl. Instr. Meth. A*, **306**, 366 (1991).

Durban 1997 XXV ICRC OG 7.2.1, Vol.4

ANTIHELIUM FLUX ATTENUATION FROM THE INTERGALACTIC SPACE TO THE SOLAR CAVITY

A, Codino[1], and M. Lanfranchi[1]

[1] *Dipartimento di Fisica dell'Università di Perugia and INFN, sezione di Perugia, Italy*

ABSTRACT

The search for cosmic antinuclei initiated in 1961 is presently pursued in various experiments. Some symmetric models of the Universe postulate the existence of antinuclei sources in macroscopic antimatter conglomerates made of antigalaxies. During the propagation from the parent antigalaxy to the Milky Way, antihelium experiences energy losses in the ambient matter due to ionization, nuclear interactions and galactic wind. The attenuation of the $\bar{\alpha}$ flux with respect to that postulated to exist in the intergalactic space has been calculated by a simulation program. The parametrization of the $\bar{\alpha}$ flux attenuation as a function of $\bar{\alpha}$ momentum and galactic thickness is given. The results indicate a depression of the $\bar{\alpha}$ flux at low momenta, below 5 GeV/c, where the most significant experimental data have been collected. A momentum cutoff in the antihelium flux is present below 2 GeV/c. This implies that upper limits to the antihelium-to-helium flux ratios measured in past experiments at low rigidities should be reconsidered.

INTRODUCTION

Antinuclei of the cosmic radiation leaked out from antigalaxies may reach the solar cavity and signal the existence of macroscopic antimatter conglomerates. Antihelium out of other antinuclides coming from antigalaxies is believed to be the most abundant species besides antiprotons. Many experiments have been performed to determine a finite flux of antinuclei in the primary cosmic radiation, though the experimental evidence is still lacking. Historically, the most sensitive antihelium searches (Buffington et al. 1981; Ormes et al. 1995) have been accomplished at low rigidity, where the ordinary cosmic ray flux is at its highest level.

ANTIHELIUM FLUX REDUCTIONOBSERVABLE IN THE SOLAR CAVITY

Extragalactic antihelium arriving close to the Earth will experience ionization energy losses and nuclear interactions both in the intergalactic space and in the interstellar medium of the parent antigalaxy and the Milky Way. These processes have been taken into account by the simulation program LEASA (Low Energy Antinucleus Simulation Algorithms) developed in the past years (Codino et al. 1989; Brunetti 1991). The parameters of the $\bar{\alpha}$ projectile in LEASA are the initial energy, position and direction. A parallelepiped of external dimensions $10 \times 10 \times 1.1$ km^3 made of 100 equal matter layers of gaseous hydrogen of dimensions $10 \times 10 \times 0.011$ km^3 is appropriate for this calculation, as justified elsewhere (Codino and Lanfranchi 1997). The matter thickness encountered by the $\bar{\alpha}$ projectiles, in the range 10-30 g/cm^2 (Webber 1995, Ginzburg and Ptuskin 1976), is treated as a parameter that may be varied by changing the hydrogen density. Energy losses due only to ionization and nuclear elastic scattering are given in another paper (Codino and Lanfranchi 1996).

The $\bar{\alpha}$ flux attenuation as a function of the momentum in the range 1-15 GeV/c for 4 different grammages is shown in Figure 1. These results have been represented by the following parametrization:

$$T(p) = A + Be^{\alpha p} + Ce^{\beta p^2} + De^{\gamma/p} \qquad (1)$$

Table 1: Numerical values of the constants appearing in the equation (1).

Grammages (g/cm^2)	A	B	C	D	α	β	γ
5	0.46	-0.3	-10	0.3	-0.77	-1.2	-0.8
10	0.02	-0.51	-8	0.55	-0.68	-0.79	-0.5
15	0.006	-3.4	-5	0.43	-1.5	-0.5	-1.18
30	-0.078	-1120	-5.1	0.28	-3.6	-0.43	-1.88

in Ahlen et al. 1982. The effect of the galactic wind is included in the subsequent results.

ANTIHELIUM RIGIDITY SPECTRA

The results on $\bar{\alpha}$ flux attenuation described in the previous section ignore the energy spectrum of intergalactic antihelium. The analytical representation of the $\bar{\alpha}$ flux attenuation given by the function (1) allows one to determine the $\bar{\alpha}$ rigidity spectra, once that of the intergalactic space surrounding our Galaxy is known. However, the flux level and rigidity spectrum of cosmic antihelium in the intergalactic space are totally unknown. In these circumstances, only conjectures may be formulated in order to delimit the range of possibilities for calculating the $\bar{\alpha}$ spectrum. Assuming the $\bar{\alpha}$ rigidity spectrum in the parent antigalaxy analogous to that of α observed in our Galaxy, the resulting $\bar{\alpha}$ rigidity spectra in the intergalactic space (dashed lines) surrounding the Milky Way are shown in Figure 2.

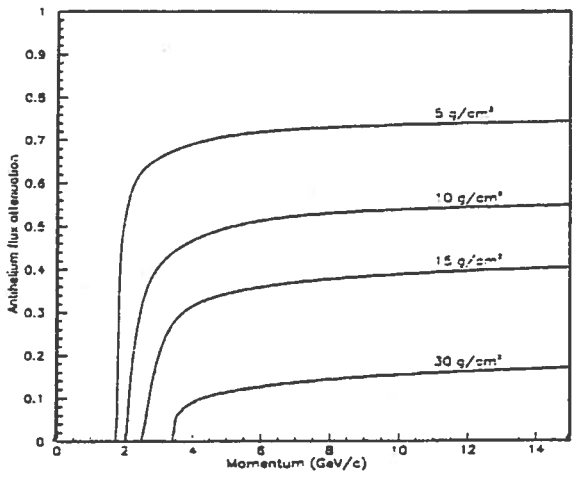

Fig. 1: Antihelium flux attenuation observable in the galactic disk plane as a function of momentum for various grammages. The antihelium flux has been arbitrarily normalized to 1 in the intergalactic space.

Following the experimental data giving the upper limits to the antihelium-to-helium flux ratios, it is plausible to envisage that at least 6 orders of magnitude separate the helium and antihelium rigidity spectra in the proximity of the solar cavity. The number of $\bar{\alpha}$, $N_{\bar{\alpha}}$, with rigidities greater than a specified value, R_{min}, has been computed from the curves shown in Figure 2. by the expression:

$$N_{\bar{\alpha}} = C \int_{R_{min}}^{+\infty} J_{\bar{\alpha}}(R)\, dR \qquad (2)$$

where $J_{\bar{\alpha}}(R)$ is the rigidity spectrum of $\bar{\alpha}$ displayed in Figure 2, and C is a constant related to the experiment which takes into account the observing time, the geometrical factor, the α and $\bar{\alpha}$ detection efficiencies and similar empirical parameters of the instrument. In the subsequent results, we put $C = 1$. The number of helium events, N_{α}, is computed in a similar way. The computed $N_{\bar{\alpha}}/N_{\alpha}$ ratio versus R_{min} for the three different grammages of 10, 15 and 30 g/cm^2 is shown in Figure 3.

CONCLUSIONS

The critical importance of the results shown in Figure 3 related to experiments searching for cos-

the same confidence level of 95% in two different rigidity bands. The experiment A collected events with rigidities greater than 1 GV/c and the experiment B with rigidities greater than 5 GV/c. From the curves of Figure 3, the $N_{\bar{\alpha}}/N_{\alpha}$ ratio is 0.014 ($y_A = 0.014$) for the experiment A and 0.074 ($y_B = 0.074$) for the experiment B. A grammage of 30 g/cm^2 has been assumed in both experiments. As a consequence, the upper limit to the $\bar{\alpha}/\alpha$ flux ratio or the sensitivity of the experiment A is reduced by a factor $y_B/y_A = 5.3$ compared to that of the experiment B. For comparison, a grammage of 15 g/cm^2 would result in a $y_B/y_A = 4.1$.

Note that $^3\overline{\text{He}}$ is abundantly produced by $^4\overline{\text{He}}$ fragmentation and the resulting $^3\overline{\text{He}}$ flux might even dominate that of the $^4\overline{\text{He}}$ for large grammages (Codino and Lanfranchi 1997). However, the inclusion of the $^3\overline{\text{He}}$ fragment in this calculation does not significantly alter the relative sensitivities of the experiments A and B. In fact, the $^3\overline{\text{He}}$ spectrum, shown in Figure 4, like that of $^4\overline{\text{He}}$ shown in Figure 3, is also depleted at low rigidities (below 1.3 GV/c). At high rigidities (i. e. $R \geq 1.7$ GV/c) the $^3\overline{\text{He}}$ spectrum is reminescent of that of the parent $^4\overline{\text{He}}$.

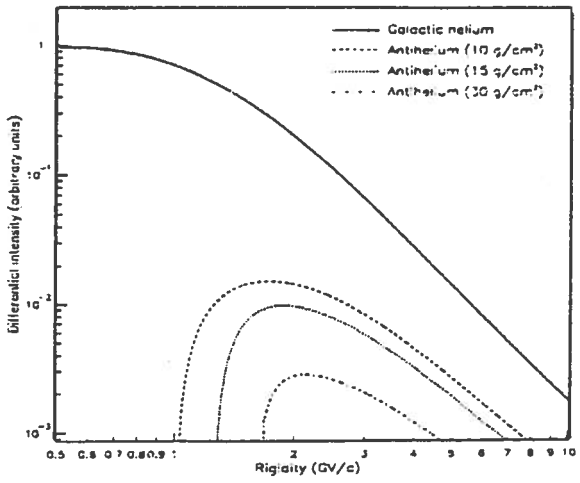

Fig. 2: Helium rigidity spectrum in the interstellar space of our Galaxy (solid line). Antihelium rigidity spectrum observable in the solar cavity (dashed and dotted lines) shaped by the galactic wind. The $\bar{\alpha}$ spectrum in the parent antigalaxy has been arbitrarily normalized to that of helium observed in the interstellar medium of our Galaxy.

REFERENCES

Ahlen S. P. et al. 1982, the The Astrophysical Journal, **260**, 20.
Brunetti M. T. 1991, "Rivelazione di antielio cosmico in un calorimetro al silicio", Thesis, University of Perugia, Italy.
Buffington A. et al. 1981, The Astrophysical Journal, **248**, 1179.
Codino A. and Lanfranchi M. 1996, INFN/AE-96/42, december 1996.
Codino A. and Lanfranchi M. 1997, to appear in The Astrophysical Journal.
Codino A. et al. 1989, Il Nuovo Cimento, **103B**, 319-331.
Ginzburg V. L. and Ptuskin V. S. 1976, Review of Modern Physics, **48**, 161.
Ormes J. F. et al. 1995, Proceedings of the XXIV ICRC Rome **Vol. 3**, page 92.
Webber W. R. 1995, The Astrophysical Journal, **457**, 435.

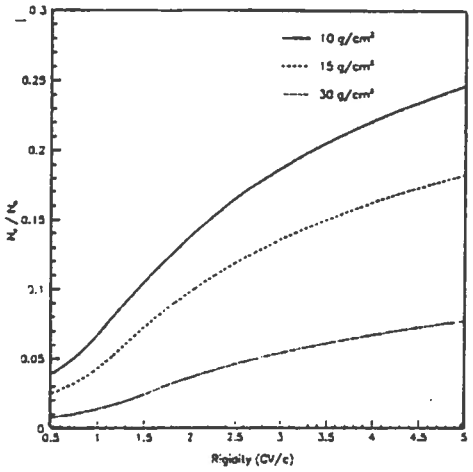

Fig. 3: Computed ratio of the number of antihelium-to-helium events as a function of the rigidity. The $N_{\bar{\alpha}}/N_{\alpha}$ ratio at a given rigidity, R, is calculated by taking all the α and $\bar{\alpha}$ events having rigidities greater than R. The effect of the galactic wind is included in these results.

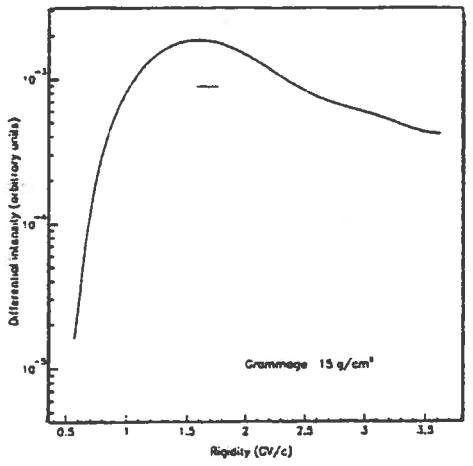

Fig. 4: $^{3}\overline{\mathrm{He}}$ rigidity spectrum observable in the solar cavity shaped by the galactic wind. The $^{3}\overline{\mathrm{He}}$ is produced by $^{4}\overline{\mathrm{He}}$ fragmentation. A grammage of 15 g/cm² has been considered.

OG 11.1.1

PHYSICS OBJECTIVES FOR A SUPERCONDUCTING MAGNETIC FACILITY ON ISSA

M.P. De Pascale[1], P. Papini[2], S. Piccardi[2], M. Ricci[3], P. Spillantini[1]

[1] *II University and INFN, Roma–Tor Vergata (Italy).*
[2] *University and INFN, Firenze (Italy).*
[3] *Laboratori Nazionali INFN, Frascati (Italy).*

ABSTRACT

Most of the important items on very high energy cosmic rays research in space can be afforded by means of a "Magnetic facility" based on a superconducting coils system equipped with a very precise microstrip silicon tracker, complemented with different ancillary detectors as required by the specific experiments. The performance that can be obtained by a magnetic facility of about 1 t is discussed for several experiments: composition at the knee, element and isotope spectra, particle and antiparticle spectra, antinuclei search, medium and high Z element fluxes, high energy gamma ray sources and spectra.

INTRODUCTION

In early eighties, the NASA of USA tried to complement the preparation of the big observatories program by an adequate effort in the study of Cosmic Rays (CR) (NASA report, 1979). NASA convened an international study group, that gathered most of the active CR physicists, and it produced a research program in CR physics for the decade 85–95 (NASA report, 1985). The program was indeed implemented in the following years, but the difficulties following the Challenger disaster slowed it considerably. In particular, the most challenging pillar of the program, the superconducting magnet facility ASTROMAG (NASA report, 1988) for the study of very high energy (VHE) CR, was canceled due to the "vanishing" of its spacecraft, the Freedom Space Station. Its supporters and potential users had to continue their activity by ballooning, waiting to recover their original and more ambitious projects in space. In fact, also the two CR experiments to be conducted in orbit in the next future will partially cover only one of the foreseen items, i.e. the study of the antiparticle component in CR by PAMELA experiment (Adriani, 1995) and the search for antinuclei by PAMELA and AMS (Alhen, 1994) experiments.

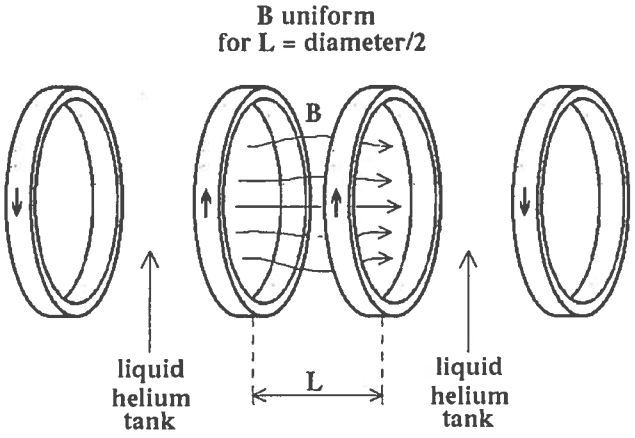

Fig. 1: The conceptual SPACEMAG scheme.

THE SUPERCONDUCTING MAGNETIC SPECTROMETER FOR THE STUDY OF VHE–CR

With the beginning of the International Space Station Alpha (ISSA) construction the time to resume the previous space projects is finally arrived. In order to guarantee a significative progress on all the

Physics problems	Needed measurements	Needed energy	Needed acceptance
Limit of acceleration and Trapping mechanism	Composition	up to $> 10^{14}$ eV/n	$\sim$1 m^2 sr
Galactic magnetosphere and winds	Radioactive isotopes	up to 10^9 eV/n	0.1 m^2 sr
Primary sources and WIMP's	$\bar{p}$ and e^+	up to 10^{12} eV	0.1 m^2 sr
Identify near sources	e^-: energy and directions	behind 10^{12} eV	0.1 m^2 sr
Matter/Antimatter symmetry	$\bar{N}$ search	behind 10^{11} eV/n	$\sim$1 m^2 sr
Probe regions of nucleosynthesis	Isotopes Z>28	$\leq 10^9$ eV/n	>1 m^2 sr
Time scale of nucleosynthesis	Elements Z$\longrightarrow$96	$\leq 10^9$ eV/n	>10 m^2 sr
Very high energy γ–ray sources, IR background, Hubble constant	Energy γ–ray spectra and directions	up to 10^{12} eV	$\sim$10 m^2 sr

Table 1: *Direct detection of high energy cosmic rays: perspectives for future experiments.*

committee recommendations (NASA report, 1995) updating them in the light of the ISSA potentialities and creating the occasions to merge all the now separated potentialities to afford adequately large and complex experimental enterprises. The time is favorable, also because the organizational effort that one decade ago was mainly supported by NASA can be now helped by the effort of other organizations either in USA or in Europe (ESA, CERN and several national agencies) and possibly in Russia and Japan.

PHYSICS ITEMS REQUIRING A LARGE MAGNETIC FIELD

Some of the most relevant items in CR research is reported in Table 1, with the requirements for an apparatus that could allow a significant progress for them. This table intends to show the opportunity of a "long range" planning in CR research (a "road–mapping plan" in the NASA jargon). It appears that most of the proposed items could profit of a magnetic spectrometer with a field of at least 2 T and a Geometry Factor (GF) approaching 1 m^2 sr. These parameters are similar to those of the above mentioned ASTROMAG facility. This was a huge instrument, whose magnetic core had a mass of 5 t and other 5 t were foreseen for the served experiments. Ten years after the study of that project many technological progresses were made, both in superconducting magnet performance and in particle detection techniques. For what concern the magnetic field intensity the present technology allows to gain a factor 1.5 (with the same mass and dimension) whereas more dramatic progresses have been done in tracker precision with the introduction of the silicon microstrip detectors.

THE SPACEMAG PROJECT

In the following, as a simple quantitative example, we consider a scheme based on the ASTROMAG concept, but smaller in geometrical dimensions and much lighter than ASTROMAG. It could be the

MAGNETIC COILS	SPACEMAG	(ASTROMAG)
number	4	2
field intensity (max in the S.C.)	6.5 T	7 T
size (diameter)	1.2 m	1.7 m
S.C. matrix current density	245 A/mm^2	405 A/mm^2
mass	113 kg	440 kg

CRYOSTAT (L.He tank + vacuum shell)	SPACEMAG	(ASTROMAG)
number	2	1
tank capacity	1070 l	3500 l
size (diameter)	1.4 m	2.1 m
size (length)	1.07 m	2.6 m
mass	65 kg	1350 kg

MASS: basic elements, without mechanical structure and services	SPACEMAG (kg)
coils	4×113=452
L.He tanks	2×65=130
L.He	2×134=268
vacuum shells	2×101=202
TOTAL	1052

Table 2: *Main parameters of the SPACEMAG spectrometer.*

distance between them should be considerably less than their diameter. Aiming to have a GF exceeding 0.5 m^2 sr for an apparatus located in the center, the coil diameter must be about 1 m and their mass 113 kg each, producing 3 T averaged field in the experimental volume. The total mass of the four coil system, including the two liquid helium tanks, the vacuum tanks and the mechanical structure, is about 1 t. In Table 2 a breakdown and a comparison between SPACEMAG and ASTROMAG is shown.

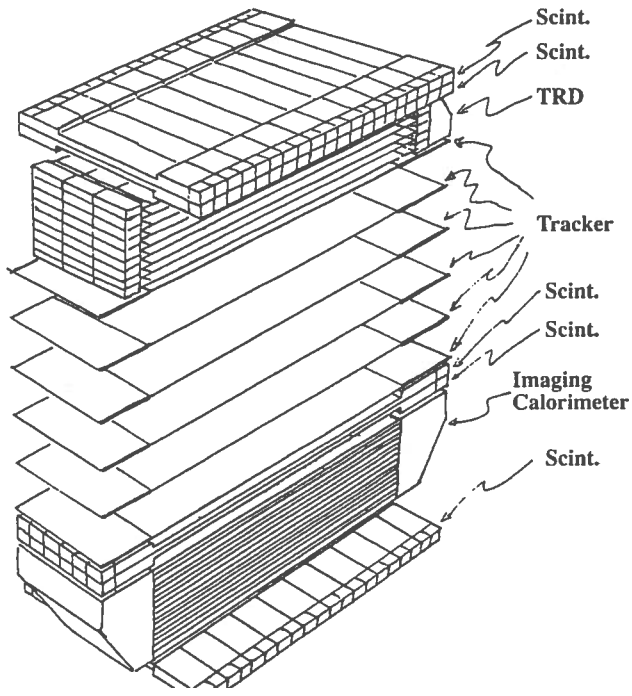

SCHEMES FOR DIFFERENT EXPERIMENTS

In order to get a high Maximum Detectable Rigidity (MDR), several silicon microstrip planes must track the going through particle with a 10 μm precision per each point. Using 8 planes inside the uniform field volume the MDR results 12 TV/c, with a multiple scattering con-

given in Figure 2. Different arrangements of further tracker planes and ancillary detectors would specialize the spectrometer for different measurements (see Figure 3). For example, the addition of further planes on top and bottom of the magnetic field region could considerably increase the MDR. Adding 4 plane at 1 m on the top and 4 planes, on a similar path, under the magnetic field region the MDR could result up to 90 TV/c. Also the two "end cup" regions, where the magnetic field intensity is lower than in the center but the geometry is open and suitable for covering several m^2 sr, could be used. They could be equipped either with very wide acceptance γ–ray spectrometers or with large area JACEE-like passive detectors to reach the 10^{15} eV/n region in the measurement of CR composition (see Figure 4).

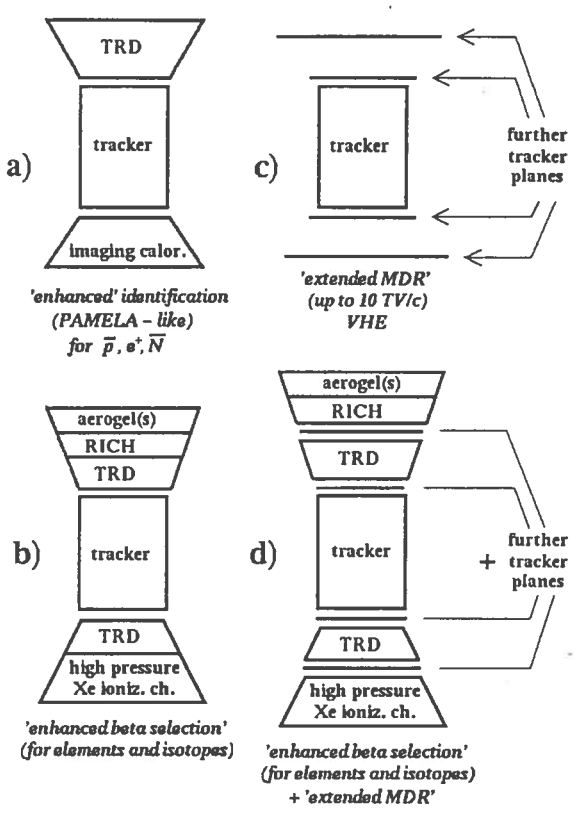

Fig. 3: Different experimental schemes for different measurements

CONCLUSIONS

The proposed SPACEMAG scheme could be conceived as a "multipurpose" experiment to be flown on board of a free–flyer. However, the location on board of a serviceable platform allows to use the spectrometer as a facility. The concept of magnetic facility implies that it could be served for refurbishing consumables and alternate detectors, or recovering passive sensors for off line analysis. The most natural location would be the ISSA, or a free-flyer serviceable from it. The presented four coils configuration (Figure 1) intends to be an example, the most straightforward one, introduced to open a discussion on the possible physics. It is not the only possible configuration and perhaps not the most efficient. Other configurations, already studied for ASTROMAG, could allow a larger magnetic field without loss of performance.

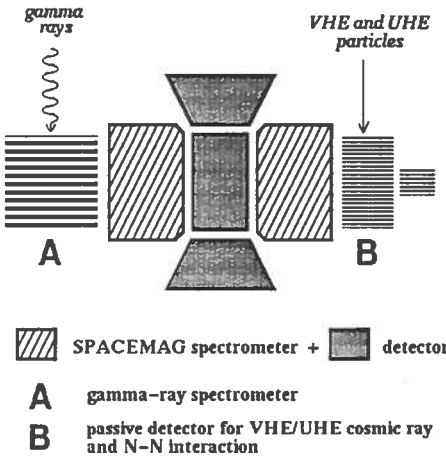

Fig. 4: Possible experiments in the "end cup" regions.

REFERENCES

NASA report, 1979, Committee on Space Astronomy and Astrophysics, "A strategy for Space Astronomy and Astrophysics for the 1980's", (1979).

NASA report, 1985, Cosmic Ray Program Working Group, "The Particle Astrophysics Program for 1985–1995", (1985).

NASA report, 1988, Astromag Definition Team, "The Particle Astrophysics Magnet Facility ASTRO-MAG", (1988).

HE 4.2.6

GeV MUONS IN THE ATMOSPHERE

M. Circella [1], C. N. De Marzo [1], T.K. Gaisser [2] and Todor Stanev [2]

[1] *Dipartimento di Fisica dell'Università and INFN, I-70126 Bari, ITALY*
[2] *Bartol Research Institute, University of Delaware, Newark, DE 19716 USA*

ABSTRACT

We compare calculations with measurements of the flux of 0.3–10 GeV muons at various depths in the atmosphere and at different geomagnetic locations. The comparison serves both to check calculations of atmospheric muons and neutrinos and to study the systematics of measurements of muons in the atmosphere. In addition, it provides an independent check of the normalization of the flux of primary nucleons in the energy range from a few GeV up to ~ 100 GeV.

1. THE CALCULATION

The calculation is an updated version (Gaisser & Stanev 1995) of the work of Barr, Gaisser and Stanev (1989) – BGS. The major improvement over BGS is the use a detailed model of the geomagnetic field. The same codes have been used (Agrawal *et al.* 1996) to extend the calculation of atmospheric neutrinos up to 10^4 GeV. In (Agrawal *et al.* 1996) a survey was made of measurements of the primary spectrum in order to obtain the best possible guess at the normalization of the primary spectrum of nucleons and the fraction of nuclei. The latter is especially important for the muon charge ratio as well as the ratio of $\bar{\nu}_e/\nu_e$. Because of the close genetic relation between fluxes of muons and neutrinos, comparison with the measured muon fluxes high in the atmosphere is the most direct experimental check on calculations used to interpret the measurements of atmospheric neutrinos, which show indications of an anomaly in the ratio of neutrino flavors (the atmospheric neutrino anomaly).

2. THE DATA

In the past few years there have been several measurements of the intensity of muons during the ascent of balloon-borne payloads through the atmosphere (Bellotti *et al.* 1996; Basini *et al.* 1995; De Nolfo *et al.* 1995: Krizmanic *et al.* 1995). Here we use the results from two flights of the MASS spectrometer (Bellotti *et al.* 1996; Basini *et al.* 1995) in similar, but not identical, configurations and under similar, but not identical, conditions of solar modulation. The 1989 flight was from Prince Albert, Canada with a geomagnetic cutoff below the effective threshold for pion production, whereas the 1991 flight was from Fort Sumner, NM, with a vertical cutoff of 4.5 GV, which is high enough to reduce somewhat the flux of low energy muons and neutrinos. This difference is in principle sensitive to the production of pions and their decay products by low energy nucleons, including both free protons and nuclei, especially helium. The two experiments are described and compared in detail in Circella (1997).

3. COMPARISON TO CALCULATION

Most muons and neutrinos in the GeV range are produced between the altitudes of 10 and

fluxes of protons and helium adopted in Agrawal *et al.* (1996). The comparison with the MASS 1989 measurement supports the results of the flux survey of Agrawal *et al* (1996), which practically averages the fluxes of Seo *et al.* (1991) and Webber, Golden & Stephens (1987) in the GeV region. For comparisons with muons of lower momentum we will use the flux of Seo *et al.* (1991) which appears to be closer to the experimental data.

Figure 2 shows the μ^- measurements (Bellotti *et al.* 1996) at selected depths. The comparison at float altitude ($\approx$ 5 g/cm^2) (Brunetti *et al.* 1996) does not depend on treatment of cascading in the atmosphere, but only on the assumed primary spectra of protons and nuclei, the treatment of the geomagnetic cutoffs and the representation of pion production. Similarly, cascading is negligible at 9 g/cm^2, so the comparison of the first two panels serves as a check on the systematics of the data taken at float and that taken (during a much shorter time interval) during the last phase of the ascent. The middle two panels are at depths in the most important region for production of muons and neutrinos. Finally, the measurements at the beginning of the ascent (736 g/cm^2) and at the ground depend predominantly on the treatment of cascading, including the approximation in the present calculation that all secondaries propagate exactly forward along the direction of the beam. The last two panels also serve as a check of possible systematic differences between measurements early in the ascent and a longer exposure on the ground, which was reported in a separate publication (De Pascale *et al.* 1993).

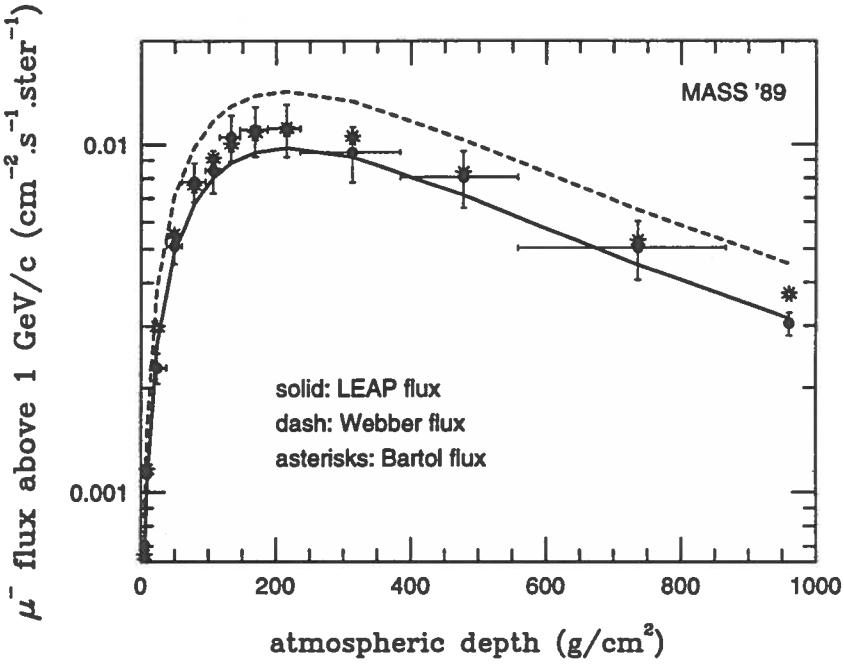

Fig. 1: Comparison of the flux of negative muons with momenta above 1 GeV/c to calculations with the primary flux derived by LEAP (Seo et al 1991) – solid line, Webber, Golden & Stephens (1987) – dashed line, and from the survey of Agrawal et al (1996).

The calculation is slightly lower than the experimental data at floating altitude in the whole momentum range. The agreement at momenta above 1 GeV/c is quite good at all altitudes, while a discrepancy seems to develop with increasing atmospheric depth for sub–GeV muons. A comparison between the 1989 and 1991 flights would be of interest because of the different geomagnetic cutoffs. Both flights occurred during the last solar maximum, but the 1989 flight occurred on Sept. 5 during a very significant Forbush decrease (Webber *et al.* 1991). Clem *et al.* (1993) have compared the helium spectrum measured four days earlier by the SMILI experiment with the helium spectrum measurement from the MASS flight. We have used Fig. 3 of Clem *et al.* (1993) to scale the interstellar rigidity spectra of protons and nuclei from

of the parent charged pions. Results at the smallest atmospheric depths are not yet available for both flights, even though they have been discussed by Circella (1997).

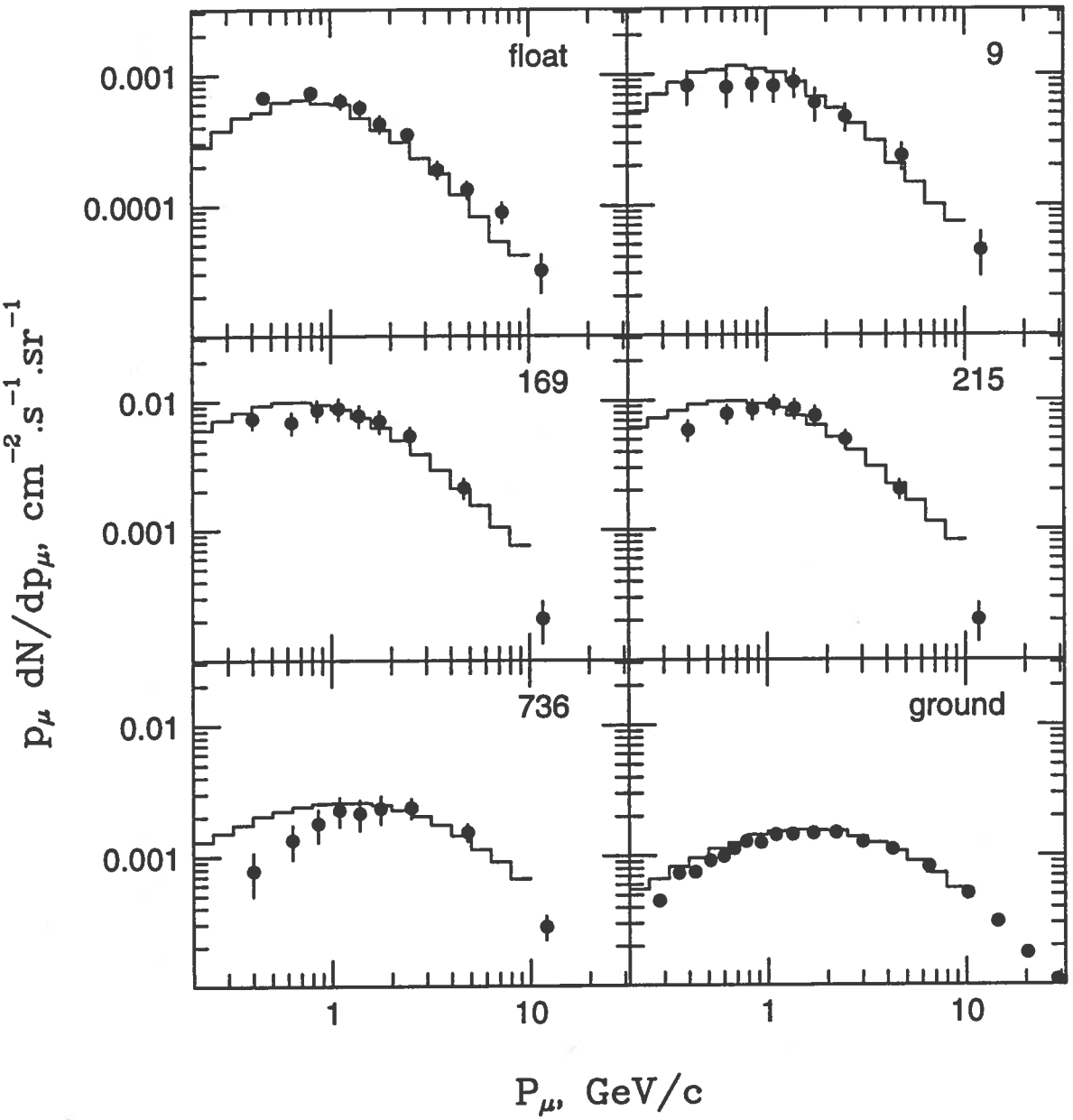

Fig. 2: Comparison of the negative muon fluxes detected by MASS '89 to calculations with the LEAP flux (histogram) as a function of the muon momentum at different altitudes. The primary flux is corrected for the Forbush decrease on September 5 1989 (see text). The altitude in g/cm^2 is indicated in the right upper corner of each panel.

Finally, in Fig. 3 we show the charge ratio as a function of depth for three different bands of muon momentum, 0.30 – 0.65, 0.65 – 1.0 and 1.0 – 1.5 GeV/c. The errors of the experimental points are too high to allow us to draw any conclusion on the proton to neutron ratio in the primary cosmic ray flux. It is not obvious that the ratio of positive to negative muons could be

muon momentum and with altitude. In the lowest muon momentum bin (0.3 – 0.65 GeV/c) the charge ratio is the lowest at high altitude, where it is governed by the lower cutoff (higher rigidity per nucleon) of the helium and heavier nuclei component of the cosmic ray flux. As the altitude increases, higher energy cosmic rays, that are not affected by the geomagnetic cutoff, become responsible for the muon production and the charge ratio increases. The altitude dependence of the charge ratio of muons with momenta above 1 GeV/c is very weak, although it shows the same trend.

Acknowledgements. The authors thank John Clem for helpful discussions and for sharing his unpublished results.

4. REFERENCES

Agrawal, V., T.K. Gaisser, Paolo Lipari and Todor Stanev 1996, Phys. Rev. D53, 1314.

Barr, G., T.K. Gaisser and Todor Stanev 1989, Phys. Rev. D39, 3532.

Basini, G., *et al.* 1995, Proc. 24th Int. Cosmic Ray Conf. (Roma) 1, 585. See also Circella (1997) for a fuller discussion.

Bellotti, R., *et al.* 1996, (MASS collaboration), Phys. Rev. D53, 35.

Brunetti, M.T., *et al.* 1996, J. Phys. G, 22 145.

Circella, M. 1997, Tesi di Dottorato, Università di Bari, Italy, in Italian.

Clem, J.M., *et al.* 1993, Geophys. Research Letters 20, 1743.

de Nolfo, G., *et al.* 1995, Proc. 24th Int. Cosmic Ray Conf. (Roma) 1, 589.

De Pascale, M.P., *et al.* 1993, J. Geophys. Res. 98, 3501.

Gaisser, T.K. & Todor Stanev 1995, Proc. 24th Int. Cosmic Conf. (Roma) 1, 694.

Krizmanic, J.F., *et al.* 1995, Proc. 24th Int. Cosmic Ray Conf. (Roma) 1, 593.

Seo, E.–S., *et al.* 1991, Ap. J. 378, 763.

Webber, W.R., R.L. Golden & S.A. Stephens 1987, in Proc. 20th Int. Cosmic Rays Conf.

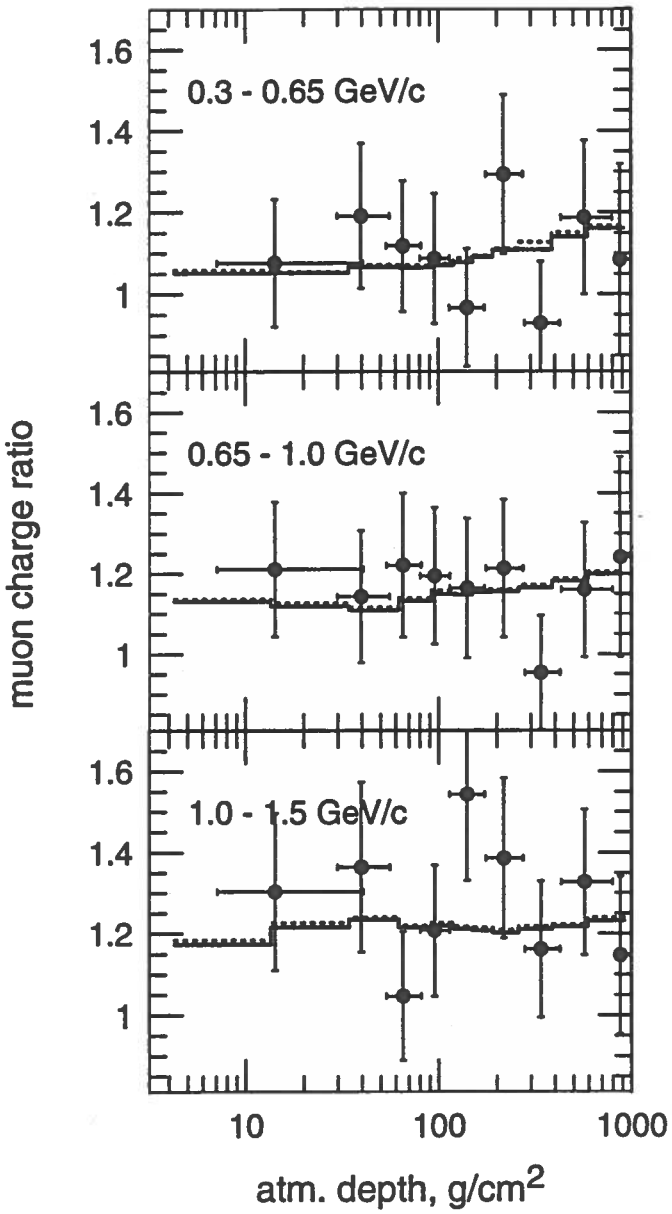

Fig. 3: Comparison of the charge ratio derived from the MASS '91 flight (Basini et al. 1995) in three momentum bins (0.30 – 0.65, 0.65 – 1.0 and 1.0 – 1.5 GeV/c) to calculations using the LEAP (solid histogram) and Webber, Gold & Stephens (dots) primary flux parametrizations

The Wizard-NINA Collaboration

A.Bakaldin[1], G.Barbiellini[2], S.Bartalucci[3], R.Bellotti[4], V.Bidoli[5], M.Boezio[2], W.Bonvicini[2], F.Cafagna[4], M.Casolino[5], M.Castellano[4], M.Circella[4], C.De Marzo[4], M.P.De Pascale[5], A.M.Galper[1], S.Giuntoli[5], S.Koldashov[1], M.Korotkov[1], V.Mikhailov[1], A.Moiseev[1], A.Morselli[5], A.M. Murashov[1], Y.Ozerov[1], P.Papini[6], S.Piccardi[6], P.Picozza[5], A.V.Popov[1], M.Ricci[3], R.Sparvoli[5], P.Spillantini[6], P.Spinellli[4], A.Vacchi[2], S.Voronov[1], N.Zampa[2]
1 Moscow Engineering Physics Institute, Moscow, Russia
2 Department of Physics, Univ. of Trieste and INFN, Italy
3 INFN Laboratori Nazionali di Frascati, Italy
4 Department of Physics, Univ. of Bari and INFN, Italy
5 Department of Physics, Univ. of Rome "Tor Vergata" and INFN, Italy
6 Department of Physics, Univ. of Firenze and INFN, Italy

The Wizard-SilEye Collaboration

V.Bidoli[1], M. Casolino[1], M. De Pascale[1], G.Furano[1], A.Morselli[1], P.Picozza[1], E.Reali[1], R.Sparvoli[1], A.Galper[2], Yu.Ozerov[2], A.Popov[2], V.Zemskov[2], V.Zverev[2], A.Alexandrov[3], S.Avdeev[3], V.Shabelnikov[3] M.Boezio[4], P.Carlson[4], C.Fuglesang[4] G.Barbellini[5], W.Bonvicini[5], A.Vacchi[5], N.Zampa[5], S.Giuntoli[6] G.Mazzenga[6], M. Ricci[6] G.Castellini[7], O.Adriani[7], P.Spillantini[7]
1 Department of Physics, II Univ. of Rome "Tor Vergata" and INFN, Italy
2 Moscow State Engineering Physics Institute, Moscow, Russia
3 Russian space corporation "Energia" Kaliningrad, Moscow , Russia
4 Royal institute of Technology, Stockholm, Sweden
5 Department of Physics, Univ. of Trieste and INFN, Italy
6 I.N.F.N Laboratori Nazionali, Frascati, Italy
7 Department of Physics, Univ. of Firenze and INFN, Italy

The Wizard-Caprice Collaboration

G.Barbiellini[1], *G.Basini*[2], *R.Bellotti*[3], *M.Bocciolini*[4], *M.Boezio*[5], *U.Bravar*[1], *F.Cafagna*[3], *P.Carlson*[5], *M.Casolino*[6], *M.Castellano*[3], *M.Circella*[3], *A.Codino*[7], *G.De Cataldo*[3], *C.De Marzo*[3], *M.P.De Pascale*[6], *N.Finetti*[7], *T.Francke*[5], *N.Giglietto*[3], *R.Golden*[8], *C.Grimani*[7], *M.Hof*[9], *W.Menn*[9], *J.W.Mitchell*[10], *A.Morselli*[6], *J.F.Ormes*[10], *P.Papini*[4], *A.Perego*[4], *S.Piccardi*[4], *P.Picozza*[6], *M.Ricci*[2], *P.Schiavon*[1], *M.Simon*[9], *R.Sparvoli*[6], *P.Spillantini*[4], *P.Spinelli*[3], *S.Stephens*[11], *S.Stochaj*[8], *R.E.Streitmatter*[10], *M.Suffert*[12], *A. Vacchi*[1], *N.Weber*[5], *N.Zampa*[1]
1 Department of Physics, University of Trieste and INFN, Italy
2 Laboratori Nazionali di Frascati INFN, Frascati, Italy
3 Department of Physics, University of Bari and INFN, Italy
4 Department of Physics, Univ. of Firenze and INFN, Italy
5 Royal institute of Technology, Stockholm, Sweden
6 Department of Physics, University of Roma "Tor Vergata" and INFN, Italy
7 Department of Physics, University of Perugia, Perugia, Italy
8 New Mexico State University, Las Cruces, USA
9 Department of Physics, Siegen University , Siegen, Germany
10 NASA/Goddard Space Flight Center, Greenbelt, USA
11 Tata Institute of Fundamental Research, Bombay. India
12 Centre des Recherches Nucleaires, Strasbourg-Cedex, France

The Wizard-PAMELA Collaboration

O.Adriani[1], *M.Ambriola*[2], *G.Barbiellini*[3], *L.Barbier*[4], *S.Bartalucci*[5], *G.Basini*[5], *R.Bellotti*[2], *D.Bergstrom*[6], *M.Boezio*[3], *W. Bonvicini*[3], *F.M.Brancaccio*[1], *U.Bravar*[3], *F.Cafagna*[2], *R.Cardarelli*[7], *P.Carlson*[6], *M.Casolino*[7], *M.Castellano*[2], *G.Castellini*[11], *E.Christian*[4], *F.Ciacio*[2], *M.Circella*[2], *R. D'Alessandro*[1], *A.Davis*[8], *G.De Cataldo*[2], *C.De Marzo*[2], *M.P.De Pascale*[7], *T.Francke*[6], *C.Fuglesang*[6], *A.Galper*[14], *F.Giannini*[7], *N.Giglietto*[2], *M.Hof*[10], *S.Koldashov*[9], *M.Korotkov*[9], *J.Krizmanic*[4], *B.Marangelli*[2], *W. Menn*[10], *R.Mewaldt*[8], *V.Mikhailov*[9], *N. Mirizzi*[2], *J.Mitchell*[4], *A.Moiseev*[9], *A.Morselli*[7], *J.F.Ormes*[4], *J.Ozerov*[9], *P.Papini*[1], *A.Perego*[1], *S.Piccardi*[1], *P.Picozza*[7], *M.Ricci*[5], *P.Schiavon*[3], *S.Schindler*[8], *M.Simon*[10], *R.Sparvoli*[7], *P. Spillantini*[1], *P.Spinelli*[2], *S. Stephens*[11], *D. Stilwell*[4], *S.Stochaj*[12], *R.E.Streitmatter*[4] , *F. Taccetti*[1], *A. Vacchi*[3], *V.Vignoli*[1], *S.Voronov*[9], *N.Weber*[6], *N.Zampa*[3]

1 Department of Physics, University of Firenze and INFN, Italy
2 Department of Physics, University of Bari and INFN, Italy
3 Department of Physics, University of Trieste and INFN, Italy
4 Laboratori Nazionali di Frascati INFN, Frascati, Italy
5 NASA/Goddard Space Flight Center, Greenbelt, USA
6 Royal Institute of Technology, Stockholm, Sweden
6 New Mexico State University, Las Cruces, USA
7 Department of Physics, University of Roma "Tor Vergata" and INFN, Italy
8 Space Radiation Laboratory, California Institute of Technology, Pasadena, USA
9 Moscow Engineering Physics Institute, Moscow, Russia
10 Department of Physics, Siegen University , Siegen, Germany
11 Tata Institute of Fundamental Research, Bombay. India
12 New Mexico State University, Las Cruces, USA

The Wizard-ELFO Collaboration

O.Adriani[1], *G.Alberici*[2], *A.Alexandrov*[3], *S.Avdeev*[3], *G.Barbiellini*[4] *S.Bartalucci*[5], *C.Basar-Eroglu*[6], *I.Bodis-Wollner*[7], *A.P.Burlina*[8], *L.Casoli*[2], *M.Casolino*[10], *G.Castellini*[11], *C.Catena*[5], *S.Cerdonio*[2], *S.Conforto*[12], *D.Conti*[5], *M.Durante*[13], *A.Galper*[14], *G.Gialanella*[13], *G.Grossi*[13], *A.Lenti*[2], *L.Lopez*[15], *Yu.Ozerov*[14], *M.Peresson*[16], *A.Popov*[14], *M.Pugliese*[13], *P.Renzi*[17], *M.Ricci*[5], *E.Righi*[5], *W.G.Sannita*[18], *V.Shabelnikov*[3], *B.Spataro*[5], *P.Spillantini*[1], *C.Tanzarella*[9], *G.Trenta*[5], *A.Vacchi*[4], *N.Zampa*[4], *V.Zemskov*[14], *V.Zverev*[14]

1 Department of Physics of Univ. and Sez. INFN of Florence, Italy
2 Laben S.p.a.,Milan, Italy
3 Russian Space Corporation Energia, Kaliningrad, Moscow region, Russia
4 Departmentof Physics, Univ. of Trieste and INFN, Italy
5 LNF-INFN, Frascati (Rome), Italy
6 Institute of Psychology and Cognitive Research, University of Bremen, Bremen, Germany
7 Department of Neurology,SUNY, HSCB, Brooklin, NY, USA
8 Div. of Neurology, Hospital of Castelfranco Veneto, Italy
9 Department of Biology, Univ. of Rome3, Rome, Italy
10 Department of Physics, Univ. of Rome "Tor Vergata" and INFN, Italy
11 IROE of CNR, Florence, Italy
12 Department INFOCOM, Univ. of Roma "La Sapienza" and Roma3, Rome, Italy
13 Department of Physics of Univ."Federico II", Naples, Italy
14 Moscow Engineering and Physics Institute, Moscow, Russia
15 Consultant neurophysiologist - ITAB - University "G.D'Annunzio", Chieti, Italy
16 Div. of Neurology, Hospital Fatebenefratelli -S.Pietro, Roma, Italy
17 Department of Psychology, Univ. of Rome "La Sapienza", Rome, italy
18 Department of Motor Sciences/neurophysiopatology - Univ. of Genova, genova, Italy and Department of